EVALUATION OF HORIZONTAL RESISTANCE ON PRE-BORED PILE FOUNDATION SYSTEM DUE TO CYCLIC LATERAL LOADING

アディタヤ, ヨガ, プルナマ

https://doi.org/10.15017/2534437

EVALUATION OF HORIZONTAL RESISTANCE ON PRE-BORED PILE FOUNDATION SYSTEM DUE TO CYCLIC LATERAL LOADING

ADHITYA YOGA PURNAMA

SEPTEMBER 2019

EVALUATION OF HORIZONTAL RESISTANCE ON PRE-BORED PILE FOUNDATION SYSTEM DUE TO CYCLIC LATERAL LOADING

A THESIS SUBMITTED
IN PARTIAL FULFILLMENT OF THE REQUIREMENTS
FOR THE DEGREE OF
DOCTOR OF ENGINEERING

BY

ADHITYA YOGA PURNAMA

TO THE

DEPARTMENT OF CIVIL AND STRUCTURAL ENGINEERING
GRADUATE SCHOOL OF ENGINEERING
KYUSHU UNIVERSITY
FUKUOKA, JAPAN
2019

GEOTECHNICAL ENGINEERING LABORATORY
DEPARTMENT OF CIVIL AND STRUCTURAL ENGINEERING
GRADUATE SCHOOL OF ENGINEERING
KYUSHU UNIVERSITY
FUKUOKA, JAPAN

CERTIFICATE

*The undersigned hereby certify that they have read and recommended to the Graduate School of Engineering for the acceptance of this dissertation entitled, "**EVALUATION OF HORIZONTAL RESISTANCE ON PRE-BORED PILE FOUNDATION SYSTEM DUE TO CYCLIC LATERAL LOADING**" by **ADHITYA YOGA PURNAMA** in partial fulfillment of the requirements for the degree of **DOCTOR OF ENGINEERING**.*

Dated: July 2019

Supervisor:

Professor Noriyuki YASUFUKU, Dr. Eng

Examining committee:

Professor Taiji MATSUDA, Dr. Eng

Professor Hideki SHIMADA, Dr. Eng

ACKNOWLEDGMENTS

After an intensive period of three years, today is the day, writing this note of thanks is the finishing touch on my dissertation. It has been a period of intense learning for me, not only in the scientific area but also on a personal level. Writing this dissertation has had a big impact on me. I would like to reflect on the people who have supported and helped me so much throughout this period.

My first and last gratitude is to the Almighty "Allah", the God of all mankind, for giving me the health, strength, patient, and faith to undertake this work. Alhamdulillah, all praises to Allah for His blessing in completing this dissertation.

I would like to express my special appreciation and sincere gratitude to my supervisor Prof. Noriyuki YASUFUKU, for his patience, motivation, enthusiasm, endless encouragement, immense knowledge and guide throughout my three years of research. He has always been available to advise me even he is busy with his daily routine work, make him a great mentor. He inspired me about the art of research in long-term performance. Thank you for your kindness and for accepting me three years ago to experience your extensive knowledge in Geotechnical Engineering.

My thousands of appreciation also goes to Examining Committee Prof. Taiji MATSUDA and Prof. Hideki SHIMADA for their precious suggestions and insightful comments with regard to improve this research work. Thank you also for letting my defense be a memorable moment.

I would also like to address my thanks to Assoc. Prof. Ryohei ISHIKURA for his worth guidance and valuable advice during my research and writing of this dissertation.

My grateful appreciation is also addressed to Assoc. Prof. Ahmad RIFA'I for patient and kindness in guiding me and precious advice during my research works.

My thanks also go to Mr. Michio Nakashima for his tremendous help, precious friendship during my study and his non-stop help throughout my experimental tests and instruments for this research. His wonderful skills really lighten the arising problem.

I would also like to extend my sincere appreciation to other academic and technical staffs in the Geotechnical Engineering Laboratory, both past, and present, Mrs. Aki ITO and Mrs. Shinobu SATO.

My special gratitude also is dedicated to the Japan Government for providing the opportunity to study and financial study assistance during my doctoral program in Kyushu University through the MEXT scholarship.

Special thanks are given to present and past research colleges members in Geotechnical Engineering Laboratory for their friendship and support throughout my time at Kyushu University. Thank you for the memorable technical site visit and laboratory party, great work environment and fun chat.

I would also like to take this opportunity to express the profound gratitude from my deep heart to my beloved parents for their love, wise counsel and sympathetic ear, patience and continuous support during my study in Japan. All of you always there for me.

Finally, there are my friends. We were not only able to support each other by deliberating over our problems and findings, but also happily by talking about things other than just our papers.

Thank you very much, everyone!

ADHITYA YOGA PURNAMA

Fukuoka, September 2019

ABSTRACT

Conventional bridges are designed with elastomeric bearing and other structural releases that allow the girder to expand or shrink freely due to environmental thermal forces. These bearings have a limited ductility and durability that need to be maintained every year. In order to maintain the performance of this bearing, it requires high cost for construction and maintenance works. Integral abutment bridges are becoming popular because the elastomeric bearings are eliminated, which can reduce construction and maintenance costs. However, because of the bearing elimination, the girder displacement due to environmental thermal forces is directly supported by the pile foundation, which can increase the pile stresses and pile bending moment. Pile foundation need to become more flexible because there is no expansion joint like in conventional bridges. Pre-bored pile foundation system can be used to reduce the pile stresses on integral abutment bridge foundation using a pre-bored hole covered with steel ring and filled with elastic materials. However, the behavior of soil and soil response due to the attachment of pre-bored pile foundation system is still rarely explained. The proposed design refers to the previous researcher to conduct a new system foundation that can maintain the flexibility of the pile. The characteristic of filler material and standard design of this system also developed in this research.

The specific objectives are mentioned as follows. The first is to investigate the influence of pre-bored ring and filler material on the pre-bored pile foundation system under cyclic lateral loading. The appropriate filler properties and the dimension of this system are expected to reduce the bending moment along the pile body due to lateral displacement loading, which can solve the problem on the integral abutment bridge foundation. The second is to evaluate the failure pattern of soil on the pre-bored pile foundation system under cyclic lateral loading. This failure pattern can affect on determining the effective dimension of pre-bored ring system based on the failure zone during the cyclic lateral loading. The third is to introduce the simplified model for predicting the lateral pile capacities on the pre-bored

pile foundation system which consider the soil-pile interaction during the lateral loading. Thus, in order to achieve these goals, this research consists of 7 chapters, as follows.

Chapter 1 describes the background of this research. The necessity of this research is to investigate the soil-pile behavior of pre-bored pile foundation system, which is explained in this chapter. The objectives of this research are briefly outlined, and the original contributions of this research are presented.

Chapter 2 provides a summary of the previous research on integral abutment bridge foundation system subjected to lateral loading. It reviews the following aspects: integral abutment bridge structure, loading mechanism, failure mechanism of the laterally loaded pile, and methods for predicting the lateral resistance of pile under lateral loading. Furthermore, a summary of the previous experiments performed by previous researchers on a single pile under static and cyclic lateral loading is shown in this chapter.

Chapter 3 shows a comprehensive description of the experimental works that carried out in the laboratory (1g model). Five types of sand were used with different geotechnical properties (e.g., particle size distribution, relative density, internal friction angle) to evaluate the appropriate filler material properties on pre-bored pile foundation system under cyclic lateral loading. The effective depth of pre-bored ring system also evaluated using single pile embedded in two-layered ground soil under cyclic lateral loading. A clear description of the experimental setup, instrumentations, scale factors, ground soil material preparation, loading mechanism, and pile model used in this research are explained.

In Chapter 4, a parametric study was carried out using 1g laboratory model test to evaluate the filler material properties and pre-bored ring dimension under static and cyclic lateral loading. The effectiveness of filler material properties such as soil uniformity and density were evaluated to reduce the pile bending moment. The effective dimension of the pre-bored hole that can maintain the bending moment of the pile foundation also evaluated in this chapter. Filler material with low uniformity coefficient and medium or high density provide a stable pile performance during the cyclic loading. The effective diameter of the ring is recommended more than the plastic deformation area of the soil for a shallow depth of the ring.

Chapter 5 evaluates the stress and strain distribution on pre-bored pile foundation system under cyclic lateral loading. Image analysis using Particle Image Velocimetry method was used to evaluate the strain distribution on the system under cyclic lateral loading. Three different diameters of the pre-bored ring were used to evaluate the effect of ring dimension on this system. Placement of pre-bored ring system can reduce the potential increase of pile stress during the cyclic loading. The optimum diameter of the ring is between 3 to 5 time of pile diameter that can provide more stable results of pile stress and soil behavior. The smaller diameter of the ring provides a higher pressure on the ring structure that causes ring movement during cyclic loading. Influence of pre-bored ring with ring diameter ratio more than 5 is not significant.

Chapter 6 introduces the simplified model for the design of pre-bored pile foundation to estimate static lateral pile capacity developed in the previous chapters. An analytic closed-form solution is proposed for estimating the ultimate lateral resistance of piles in sandy soils considering the soil-pile interaction. Furthermore, to evaluate the accuracy and to verify the proposed model, a statistical analysis was conducted using three statistical criteria; (a) best fit line criterion, (b) cumulative probability, and (c) statistical parameter criterion and were compared with the previous methods. The proposed closed-form solution can reduce average error percentages compared to values resulted from other methods, and the estimation of lateral pile resistance for both rigid and flexible pile can be represented using the proposed method.

Chapter 7 shows the conclusions, the main outcomes of the study, and the recommendations for future research target.

Table of Contents

List of Figures

List of Tables

List of Notations

Ap	cross-sectional area of pile
COV	coefficient of variation
CP_i	cumulative probability
D	pile diameter
D_r	relative density of soil
D_{50}	mass median diameter
E	Young's modulus
EI	flexural stiffness of pile
E_s	Young's modulus of soil material
E_p	Young's modulus of pile material
E_p/E_s	pile/soil relative stiffness
F	side shear resistance factor
Gs	specific gravity of soil
H_1	lateral static pile capacity at 1st cycle
H_N	lateral cyclic pile capacity at Nth cycles
$(H_u)_m$	ultimate measured lateral pile capacity
$(H_u)_p$	ultimate predicted lateral pile capacity
I_m	moment of inertia of pile modeling laboratory
I_p	moment of inertia of pile prototype in field
K	earth pressure coefficient
K_a	active earth pressure coefficient
K_h	modulus of subgrade reaction of soil
Ko	coefficient of lateral earth pressure at rest
K_p	passive earth pressure coefficient

K_q	Brinch-Hansen lateral soil pressure coefficient
K_{rs}	stiffness factor
K_s	lateral earth pressure coefficient
L	embedment length of pile
M_m	measured bending moment of pile
M_y	yielding bending moment of pile
N	number of cycles
Nu	ultimate lateral shear drag
P	lateral load per unit length of pile
P_u	ultimate lateral load per unit length of pile
P_{50}	value of $(H_u)_p/(H_u)_m$ 50% cumulative probability percent
P_{90}	value of $(H_u)_p/(H_u)_m$ 90% cumulative probability percent
Qu	ultimate net frontal soil force
R	ranking index
$R1$	ranking based on best fit regression analysis criterion
$R2$	ranking based on cumulative probability criterion
$R3$	ranking based on arithmetic mean and COV criteria
S	slope of pile
U_c	uniformity coefficient
V	shear force of pile
c	soil cohesion
d	pre-bored ring diameter
e	lateral load eccentricity
f	loading frequency
n	numbers of case studies

nh	coefficient of subgrade reaction
p	soil lateral resistance
p_{max}	maximum frontal passive earth pressure
p_u	ultimate soil lateral resistance
p_1 *and* p_N	soil reactions for 1st and for the Nth cycle, respectively
r	degradation and magnification factor
r^2	coefficient of determination
s	standard deviation
t	time
y	lateral displacement of pile
z	depth below ground soil level
z_0	embedment length of pile up to the point of rotation
γ	unit weight of soil
γ_d	dry unit weight of soil
γ_{max}	maximum dry weight of soil
γ_{min}	minimum dry unit weight of soil
Δu	generated pore water pressure
δ	interface friction angle between pile wall and soil
ε	bending strain in pile shaft
ε_s	lateral strain of soil due to lateral pile movement
ζ *and* χ	degradation factors
η *and* ξ	shape factors
θ	radial angle of pile
λ	parameter for the residual soil strength
μ	arithmetic mean
σ_n	normal stress

σ_h	horizontal soil stresses
σ_v	total overburden stress of soil
τ	side shear stress
τ_{max}	maximum side shear resistance of soil at pile shaft
υ	Poisson's ratio
φ	internal friction angle of soil
ψ	Dilatancy angel of sand

CHAPTER I

INTRODUCTION

1.1 BACKGROUND

Most of the bridge construction in Indonesia used a simple beam system. In general, a simple beam bridge structures need an expansion joint and dilatation between the superstructure and substructure. The bridge structure is a building that needs to be maintained, especially for the girder bearing and expansion joint. If there is no proper maintenance, it can cause damage to the bridge structure such as cracks around the expansion and damage on the bearing. Furthermore, it can result in the inconvenience for bridge users due to the damage of the expansion joint. Maintenance of infrastructure in Indonesia is still the main issue because of the infrastructure maintenance costs are continually increasing, especially for bridge structure that needs to maintain continuously. So many infrastructures were built, but long-term consideration about the maintenance of infrastructure is still neglected. It caused much damage to the bridge structure, as shown in Figure 1-1.

Figure 1-1 Condition of a bridge in Indonesia

Indonesia is a tropical country that consists of 17,000 small islands and five major islands and has so many large and small rivers. Indonesia is currently estimated to have 88 thousand bridges or equivalent to approximately 1,000 km. Most of the bridges built on the main road that supports economic system. Almost all of the bridge in Indonesia still using traditional bridge joint support that needs to maintain every year and most of the bridges (small bridge) in Indonesia are not in good condition due to the poor maintenance. The total amount of bridge based on its conditions in Indonesia are shown in Figure 1-2.

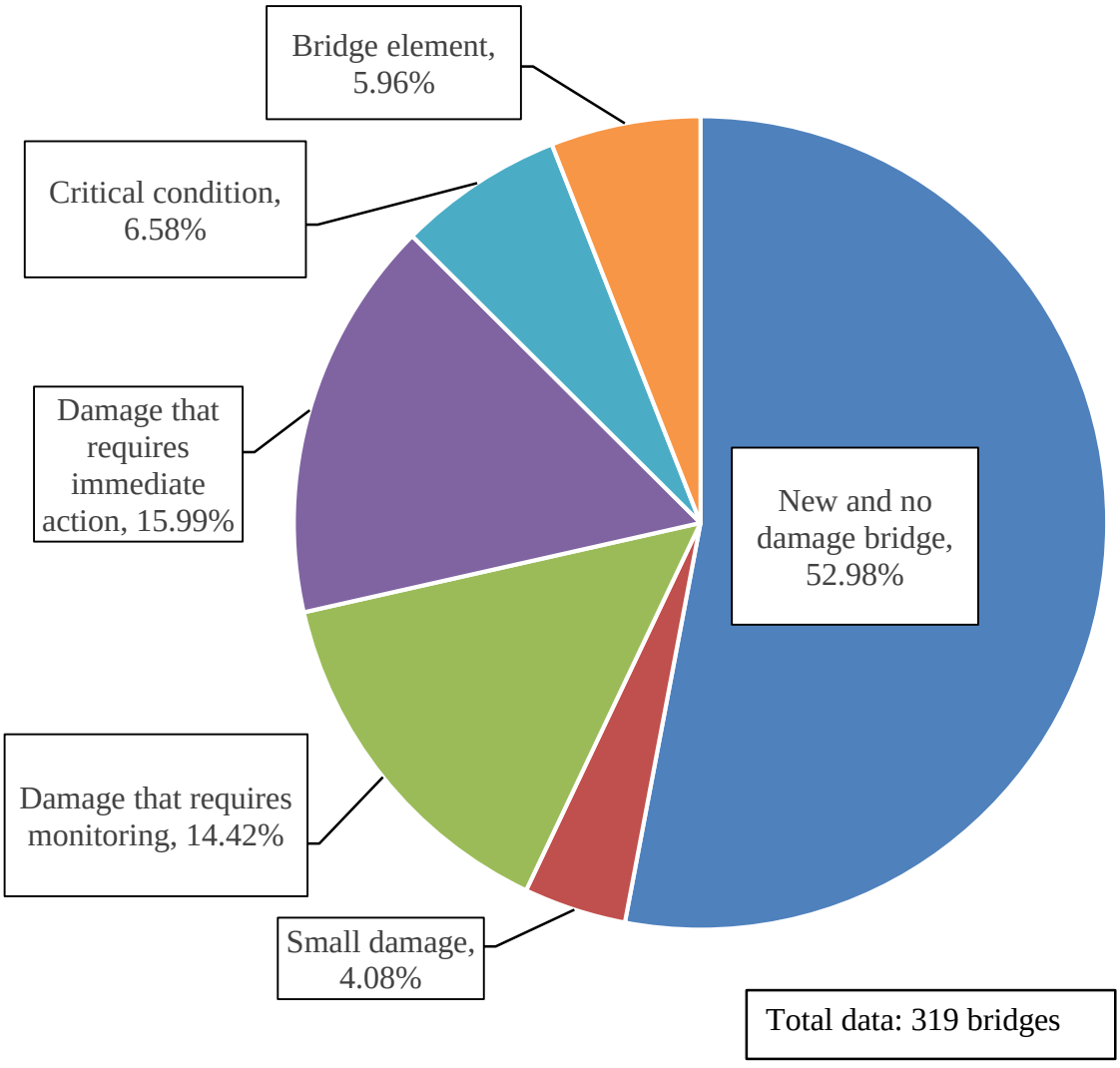

Figure 1-2 Data of total bridge in Indonesia based on bridges condition (http://www.datajembatan.com)

1.2 INTEGRAL ABUTMENT BRIDGE SYSTEM

Nowadays, integral abutment bridges are becoming popular because the elastomeric bearings are eliminated, which reduce the construction cost and maintenance costs. Conventional bridges are designed with expansion joints and other structural releases that allow the superstructure to expand and contract freely with changing temperatures. The integral-abutment bridge is less expensive because elastomeric bearings are eliminated in the bridge deck, which reduces the initial construction and maintenance costs (Girton et al., 1991). However, when the elastomeric bearing and other structural releases are eliminated, thermal forces are followed into the bridge, and it needs to be considered in the design approach. The schematic picture of an Integral Abutment Bridge system is shown in Figure 1-3

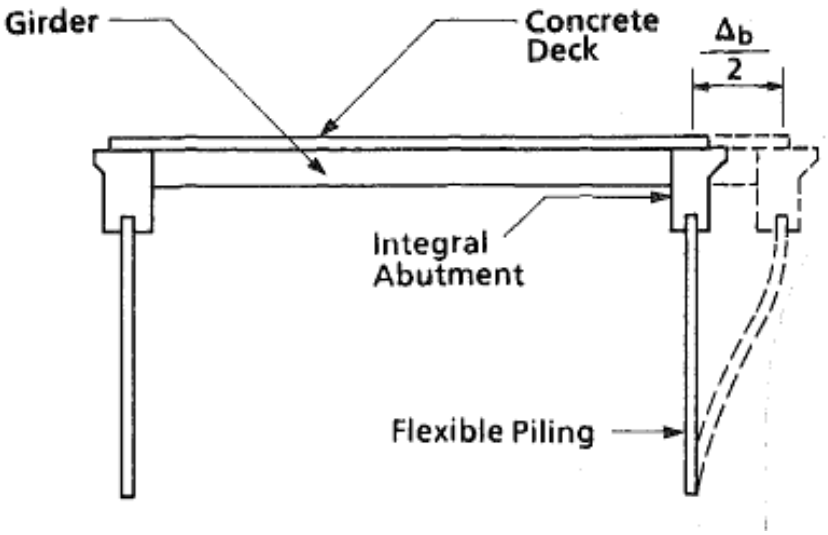

Figure 1-3 Integral abutment bridge (Girton et al., 1991).

However, when expansion joints and other structural releases are eliminated, thermal forces are introduced into the bridge and must be accounted for in the design. More than half of the state highway agencies in the United States of America have accepted the design of integral abutment bridges, but all have limitations on a safe length for such bridges (Greimann et al. 1986, 1987; Wolde-Tinsae et al. 1988). In the American Association of State Highway Officials (AAHSTO), the integral abutment bridge is not mentioned clearly, but it mentioned that all bridge design should be considered for the thermal movements of the girder. The foundation system of the integral bridge needs to consider on the girder displacement due to the thermal expansion that allowed in this system. Pile foundation needs to be more flexible

because there is no elastomeric bearing, which is provided in a conventional bridge. There is no general standard design to analyze the foundation system of the integral bridge, and it is still in development.

The integral abutment bridge causes the pile foundation connection to become fixed. However, it will cause relatively high pile stresses and bending moment due to lateral displacement of the bridge. In order to reduce the stresses, the connection between abutment and girder can be design as a pinned-head or create a hinge connection. The other method is attaching the piles in pre-bored holes (also called predrilled or pre-excavated) as shown in Figure 1-4. Based on Dunker and Liu (2007), it shows that the Iowa Department of Transportation in 2006 proposed the pre-bored hole diameter is twice of the pile diameter with 3.05 m of depth. The depth of the holes can be changed for the special condition. The pile was installed on the pre-drilled hole followed by inserting the ring in the hole. The area between pile and ring was filled with the elastic filler material to maintain the displacement of the pile due to lateral loads. A steel or concrete ring should be placed in the hole to separate the filler material and ground soil. This ring is expected to maintain the filler material properties inside the hole in long-term conditions due to cyclic loading.

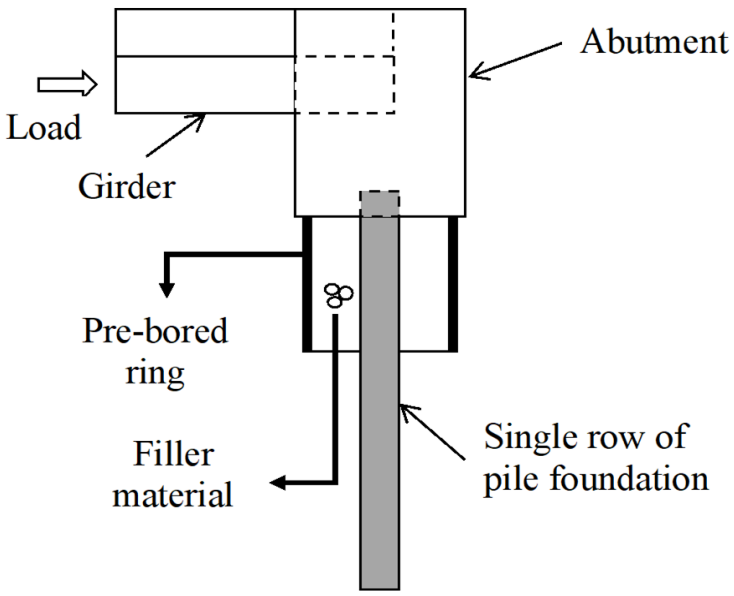

Figure 1-4 Typical design of integral abutment bridge with a pre-bored hole system.

The previous researchers only focus on the structural system, but the behavior of soil and soil response due to the flexible piling design is still rarely. Foundation system of the integral

bridge needs to withstand strain load/ displacement load due to the thermal expansion that allowed in this system. Pile foundation needs to be more flexible because there is no expansion joint like a standard bridge. There is no standard procedure to analyze the foundation system of the integral bridge, and it was still developing by researchers. The proposed design refers to the previous researcher that conduct a new system foundation to maintain the flexibility of the pile. Characteristic of filler material and standard design of this proposed foundation still in development.

1.3 **OBJECTIVES AND SCOPES**

The main objective of this research is to evaluate the appropriate filler properties and the dimension of a pre-bored pile foundation system that expected to reduce the pile stress and bending moment along the pile due to cyclic lateral displacement loading that can solve the problem on the integral abutment bridge foundation. The effective system will be evaluated by considering the soil behavior due to cyclic lateral loading on the pile foundation. To achieve this objective, the mechanism of soil behavior due to this system under static and cyclic lateral loading has been investigated by experimental and numerical approaches. The specific objective is mentioned as follows:

1. To Investigate the influence of pre-bored ring and filler material on the pre-bored pile foundation system under cyclic lateral loading based on geotechnical point of view. The appropriate filler properties and the dimension of this system are expected to reduce the bending moment along with the pile due to lateral displacement loading, which can solve the problem on the integral abutment bridge foundation.
2. To evaluate the failure pattern of soil on the pre-bored pile foundation system under cyclic lateral loading. This failure pattern can effect on determining the effective dimension of pre-bored ring system based on the failure zone during the cyclic lateral loading.
3. To introduce the simplified model for predicting the lateral pile capacities on the pre-bored pile foundation system which consider the soil-pile interaction during the lateral loading, to reduce the error values between the actual measured value and estimated value.

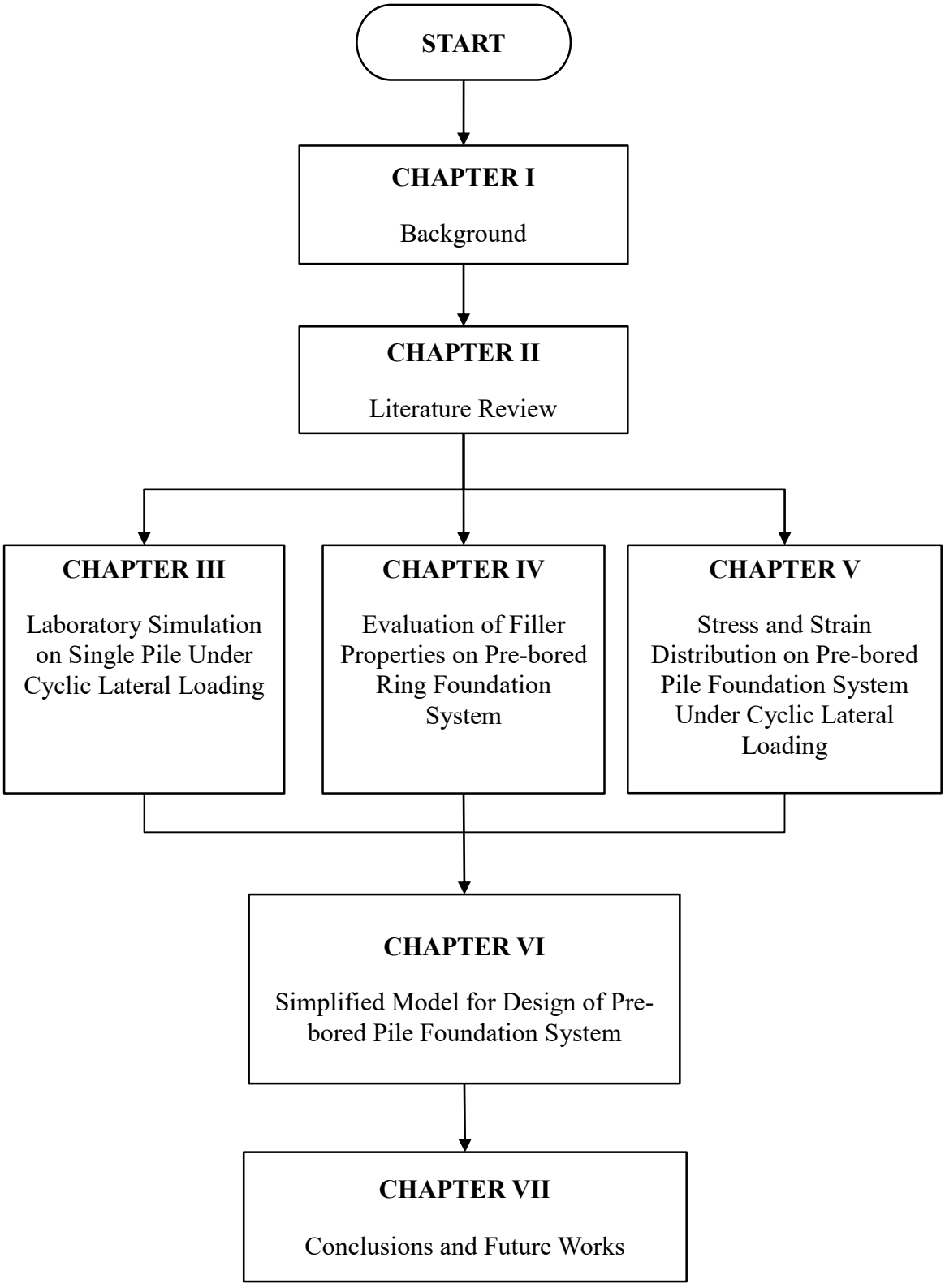

Figure 1-5 Flowchart of the research

1.4 FRAMEWORK AND OUTLINES

In order to achieve the objective of this research, this dissertation is consist of 8 chapters with a framework, as shown in Figure 1-5. The outlines of each chapter are described as follows:

Chapter 1 describes the background of this research. The necessity of investigating the soil-pile behavior of pre-bored pile foundation system also explained in this chapter. The objectives of this research are briefly outlined, and the original contribution of this research is presented.

Chapter 2 provides a summary of the previous research on single pile and integral abutment bridge foundation system subjected to static and cyclic lateral loading. It reviews the following aspects: integral abutment bridge structure, loading mechanism, the failure mechanism of the laterally loaded pile, and methods for predicting the lateral resistance of pile under lateral loading. Furthermore, a summary of the previous experiments performed by previous researchers on a single pile under lateral loading is shown.

Chapter 3 shows a comprehensive description of the experimental works that carried out in the laboratory (1g model). Kumamoto sand and Toyoura sand were used with different geotechnical properties (e.g., particle size distribution, relative density, internal friction angle, etc.) to evaluate the appropriate filler material properties for pre-bored pile foundation system on single pile under cyclic lateral loading. Effective depth of pre-bored ring system also evaluated using single pile under cyclic lateral loading in two-layered ground system. A clear description of the experimental setup, instrumentations, scale factors, ground soil material preparation, loading mechanism, and pile model used in this research are explained.

In Chapter 4, the evaluation of filler material properties on pre-bored pile foundation system using 1g model was evaluated under static and cyclic lateral loading. A parametric study using the laboratory test results to evaluate the filler material properties (e.g. relative density, soil uniformity) and pre-bored ring dimension under static and cyclic lateral loading on a single pile in terms of: (1) cyclic lateral capacity of single pile and (2) mobilized bending moment due to cyclic lateral loading. The effect of soil type also evaluated to determine the effect of filler material properties that can maintain the pile bending moment during the lateral cyclic loading.

Chapter 5 introduces the stress and strain distribution on pre-bored pile foundation system under cyclic lateral loading. Image analysis using Particle Image Velocimetry (PIV) method was used to evaluate the strain distribution of the system under cyclic lateral loading. GeoPIV-RG program was used to measure the deformation of soil due to the lateral cyclic loading on the pile. The failure pattern of the soil inside the pre-bored ring was investigated to determine the point of pile rotation and the soil movement due to the pre-bored ring system. Three different diameters of the pre-bored ring were used to evaluate the effect of ring dimension on this system.

Chapter 6 proposed the simplified model for the design of pre-bored pile foundation to estimate static lateral pile capacity developed in the previous chapters. An analytic closed-form solution is proposed for estimating the ultimate lateral resistance of piles in sandy soils considering the soil-pile interaction. In this study, 31 cases of experimental laboratory small-scale model were carried out to evaluate the proposed equation. Furthermore, to evaluate the accuracy and verified the proposed model, a statistical analysis is conducted using three statistical criteria; (a) best fit line criterion, (b) cumulative probability, and (c) statistical parameter criterion. The proposed model also compared with the previous methods, including Prasad and Chari (1999), Zhang et al. (2002) and Awad-Allah and Yasufuku (2013).

Chapter 7 shows the summaries, conclusions, main outcomes of the study, and recommendations for future research target.

1.5 **ORIGINAL CONTRIBUTION**

This research investigates the performance of pre-bored pile foundation system for integral abutment bridge under static and cyclic lateral loading using experimental and analytical approaches. Some new findings are obtained to which are considered as the originality of this research, as follows:

1. Optimum properties of pre-bored pile foundation system due to lateral cyclic loading considering the geotechnical point of view. The behavior of filler material, pile, and the pre-bored ring have been evaluated to obtain the optimum properties of pre-bored pile foundation system on integral abutment bridge under cyclic lateral loading.

2. There is very little research that investigates the failure pattern of the pre-bore pile foundation system considering the geotechnical aspects. Therefore, one of the originalities of this research is investigating the failure pattern of filler material inside the ring system due to cyclic lateral loading. The failure pattern of soil might be changed due to the placement of pre-bored ring system, and it will effect on the determination of optimum dimension of this system.
3. A simplified model to estimate the ultimate lateral capacity of pre-bored pile foundation system is proposed using the concept of a beam on an elastic foundation model or Winkler's model. The ultimate lateral resistance of pile is predicted using the differential equation solution based on the basic equation and consider the effect of pile slenderness and the effect of the attached pre-bored ring system.

1.6 **REFERENCES**

Dunker K. F., and Liu D., Foundations for Integral Abutments. Pract. Period. Struct. Des. Constr., Vol 12, Issue 1, 2007, pp.22-30.

Girton D. D., Hawkinson T. R., and Greimann L. F., Validation of Design Recommendations for Integral-Abutment Piles. Journal of Structural Engineering, Vol 117, Issue 7, 1991, pp. 2117-2134.

Greimann L. F., Abendroth R. E., Jonshon D, E., and Ebner, P. B., Pile Design and Tests for Integral Abutment Bridges. Final Rep. Iowa DOT Project HR-273, Iowa State Univ., 1987, pp.3-6.

Greimann, L. F., Yang, P., and Wolde-Tinsae, A. M. Nonlinear Analysis of Integral Abutment Bridges. Journal of Structural Engineering, Vol. 112(10), 1986, pp. 2263–2280.

The American Association of State Highway Officials, Standard Specifications of Highway and Bridges. The Association of General Offices, Ed. 11, 1973, pp.108.

Wolde-Tinsae, A. M., Klinger, J. E., & White, E. J. Performance of Jointless Bridges. Journal of Performance of Constructed Facilities, Vol. 2(2), 1988, pp. 111–125.

http://www.datajembatan.com/index.php?g=guest_bridge&m=statistik.by_kondisi

CHAPTER II

LITERATURE REVIEW

2.1 INTRODUCTION

The bridge structure is a building that needs to be maintained, especially for the elastomeric bearing. The elastomeric bearing of a bridge was made from rubber combined with a steel plate. In order to maintain this elastomeric bearing, the girder of the bridge needs to be lifted upward using heavy equipment that needs a high cost. Integral abutment bridges are becoming popular around the world, but the standard design is different from one country to another. This causes a different technical approach design to solve the same problem in every country. Conventional bridges are designed with elastomeric bearing and other structural releases that allow the girder to expand or shrink freely due to environmental thermal force.

2.2 INTEGRAL ABUTMENT BRIDGE SYSTEM

2.2.1 Integral abutment bridge in the United States

Integral abutments eliminate the need to provide elastomeric bearings. In addition, it can save bridge costs, time, and reduce inconvenience compared to conventional bridges. Colorado was the first state to build integral abutments in 1920. Massachusetts, Kansas, Ohio, Oregon, Pennsylvania, and South Dakota followed in the 1930s and 1940s. California, New Mexico, and Wyoming built integral abutment bridges in the 1950s. With the National Interstate Highway System construction boom in the late 1950s and the middle of 1960s, Minnesota, Tennessee, North Dakota, Iowa, Wisconsin, and Washington start to use bridges with integral abutments, as standard construction practice (Kunin and Alampalli, 1999). A testament of their excellent performance over the years is the fact that the current policy of the vast majority of states is to build integral abutment bridges whenever possible. This is confirmed, which indicates that forty-one states are now using integral abutment bridges. The use of integral abutment bridges over the years is illustrated in Figure 2-1.

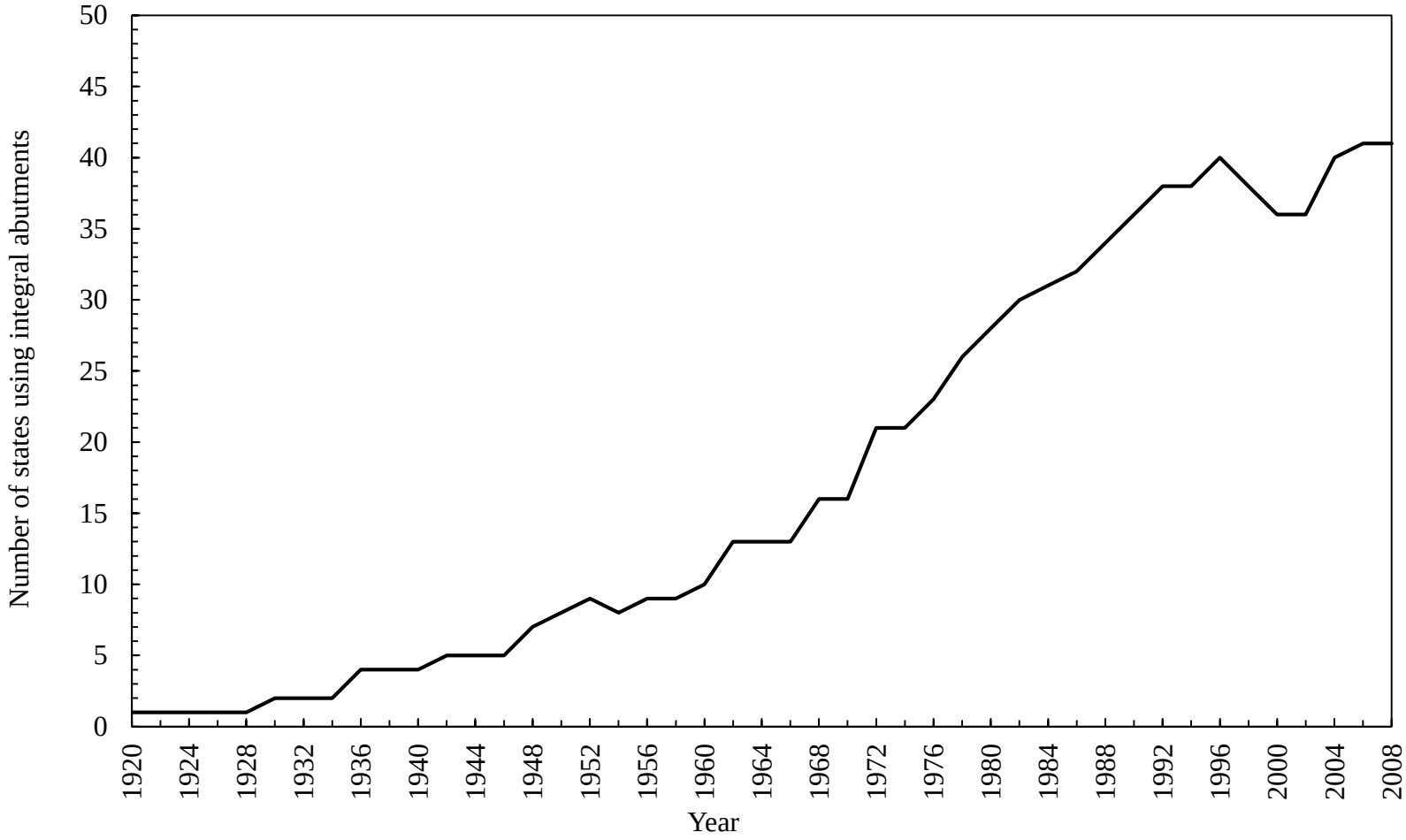

Figure 2-1 Number of states built integral abutment bridges in the United States (Paraschos and Made, 2011)

However, there are some problems with integral abutment bridges; the severity and cause of problems differ from state to state. One of the following issues is the standard design for an integral abutment bridge, especially on the pile foundation. The elimination of elastomeric bearing caused the lateral displacement directly induced the pile foundation. This conditions affected the behavior of soil around the pile and the pile stress.

2.2.2 Integral bridge in Asia

A modified type of semi-integral abutment was proposed in China by Jin et al. (2005). This improved abutment type has been used in many IABs (Integral Abutment Bridges) in China, not only the newly constructed IABs but also the retrofit of existing bridges, due to many advantages. The first retrofitting application by using the improved semi-integral abutment in China was the 'Longtan Bridge' (Tang et al., 2007). The existing supported bridge was constructed in 1966 and subjected to a large number of durability problems. The total length of the existing bridge is 109.2m with ten unequal spans, and the width of the deck slab is 6.7m. The superstructure of the existing bridge is composed of four reinforced concrete I-beams and one deck slab. Nine gravity piers and two gravity abutments with splayed wing walls were constructed in the existing bridge. The elevation layout of the "Longtan Bridge" is shown in Figure 2-2.

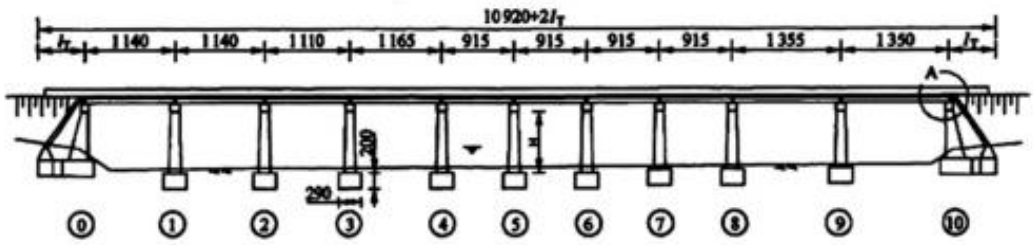

Figure 2-2 Layout of "Longtan Bridge" in China (Tang et al., 2007)

1. Demolish deck slabs and flange slabs of side girders. Cast concrete to new side girders and deck slabs. In this case, the deck slabs can be widened from 6.7m to 8m (Figure 2-3(a)).
2. Convert conventional abutments into improved semi-integral abutments (Figure 2-3(b)). Most parts of conventional abutments can be reused; however, the height of abutment back-walls should be shortened to provide the spaces for approach slabs. The approach slabs with the length of 5.5m are connected directly to girder ends

without expansion joints and supported by the abutment back-walls with sliding surfaces and backfill. Sliding bearings should be installed to replace existing bearings.

3. Position the reinforcements of new deck slabs, which should be connected to existing girders by post-embedded rebar. Install steel plates between the ribs of adjacent girders over piers. Add more longitudinal reinforcements for the deck slabs over piers. Position the reinforcements of pavements, which should be connected to approach slabs.
4. Cast concrete to complete the connections of adjacent girders, new deck slabs, and approach slabs.

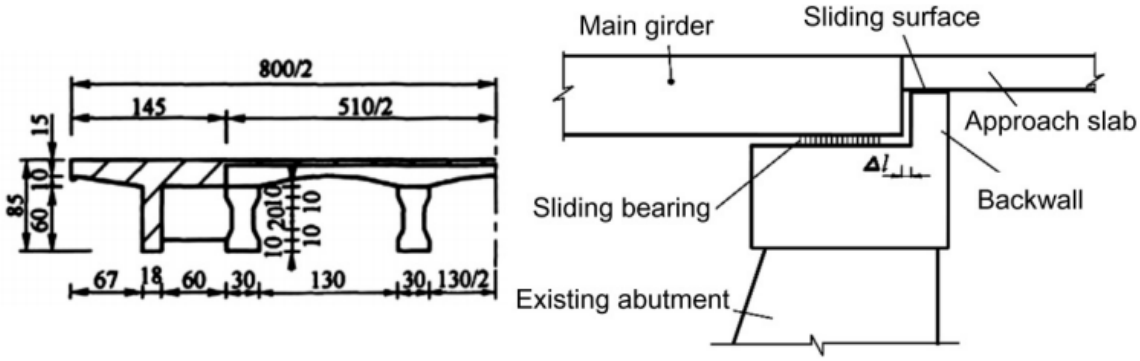

a. Superstructure widens b. Improved semi-integral abutment

Figure 2-3 Retrofitting procedure of 'Longtan Bridge' in China (Jin et al., 2005)

In Singapore, the retrofitting approach with the IAB concept was applied to an existing prestressed concrete bridge with a single span 18.16m constructed in 1968-70. It needed to be upgraded due to the enhanced vehicular load (Jayaraman & Merz, 2001). The total width of the superstructure is 18.8m, which is composed of 4-lane undivided carriageway with the clear width of 15.3m and two footpaths with the clear width of 1.5m each. The existing superstructure is made of 37 precast pre-tensioned inverted T-beams connected by casting in-situ reinforced concrete diaphragms and one deck slab. Elastomeric bearings were installed on reinforced concrete cantilever wall type abutments. Precast reinforced concrete square piles were used in the existing bridge.

Three retrofitting approaches were proposed initially, including installing externally bonded steel plates or composite materials, applying external prestressing and converting to the IAB.

The retrofitting method with the FIAB (Fully Integral Abutment Bridge) concept is found to be the best choice, compared with the other two retrofitting methods, which can suit the real conditions on-site where heavy vehicular and container traffic have to be maintained during retrofitting.

2.2.3 Integral bridge in Indonesia

Several studies about integral bridge were developed in Indonesia. Setiati (2015) explained that the application of an integral bridge in Indonesia has not been as popular in some countries such as the UK, USA, Australia, and other countries. This concept was beginning to study in 2007 by Directorate General of Highways in collaboration with some universities. That research was continued by the Institute of Road Engineering in 2009, finally, in 2012, the Institute of Road Engineering performed a full-scale experiment of reinforced concrete integral bridge girder with spans of 20 meters in Sumedang. The behavior of integral bridges in Indonesia would be very different from abroad, so during the construction, Sinapeul integral bridge was equipped with several sensors to detect and study the behavior of the bridge. This study aimed to analyze and evaluate the results of the data recorded in the monitoring system, which in turn, results of the analysis will be compared with the behavior of integral bridges abroad and analysis theory. Based on the analysis and discussion, some conclusions are obtained by abutment displacement of Sinapeul integral bridge with a span length of 20 meters as a result of temperature change was 2.88 mm, while for overseas conditions assuming the same span is 4.80 mm (greater of 60% of the displacement of integral bridge in Indonesia). Maximum strain displacement of the abutment and girder bridge, at 10.59 a JO6. Strain value is still less than strain obtained from analytical theory (150×10^{-6}) so that the Sinapeul integral bridge is still in a state of elastic.

2.3 LATERAL LOADING DUE TO THERMAL EXPANSION ON BRIDGE FOUNDATION

As a response of environmental influence such as environmental temperature and climate change a bridge structure will, the bridge will have experienced a change in temperature and bridge structures response to environmental influences varies depending on the material. It is becoming difficult to determine structure expansion and shrinkage accurately due to thermal induction. England et al. (2000) have developed the magnitude of thermal expansion

for different material, namely as EBT (Effective Bridge Temperature). However, this EBT only can be applied in the United Kingdom areas with four seasons condition. EBT is a parameter of the thermal parameter that changes throughout the year. The temperature change in the United Kingdom area is shown in Figure 2-4.

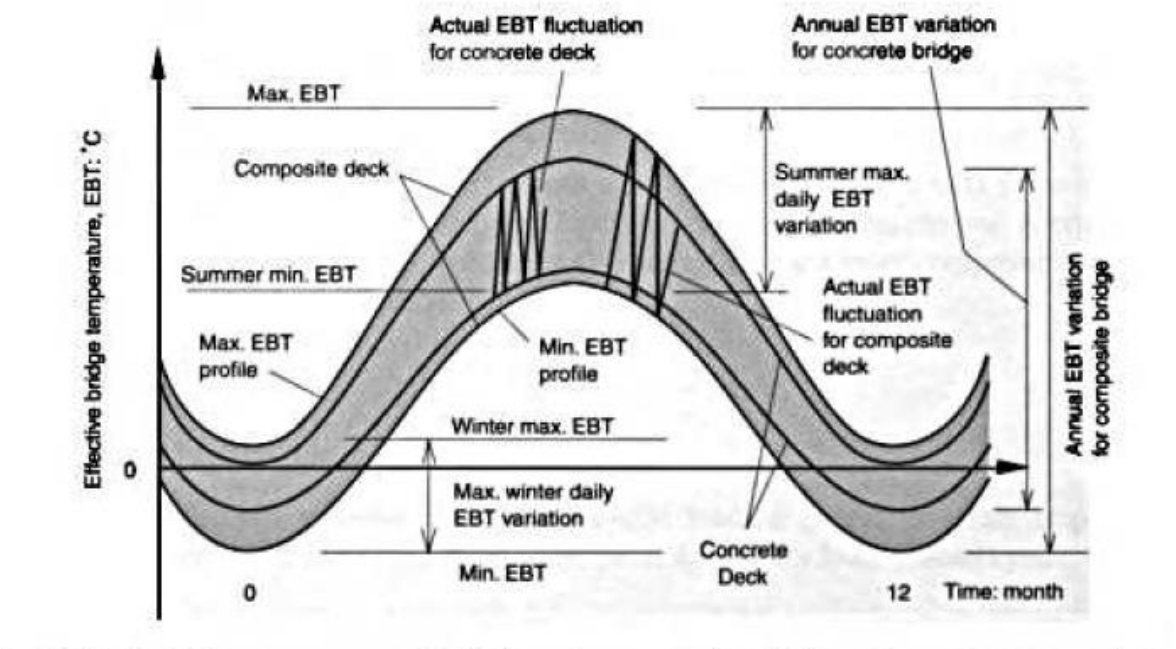

Figure 2-4 EBT throughout the year (England et al., 2000)

Two types of thermal actions need to be considered. First, a uniform temperature change, which means that the abutment is displaced horizontally. The magnitude of the bridge movement depends on the difference between the mean temperature of the structure at the time that the superstructure is locked to the abutments and in the design situation. Also, uneven temperature distribution across the depth of the superstructure causes movements of the piles as the end of the superstructure rotates and cause a horizontal displacement of the pile top. The mean bridge temperature is dependent mainly on the ambient air temperature but also on wind and rain effects and solar radiation. Temperature gradients through the depth of the bridge beams generate bending of the superstructure and rotation of the end. The maximum temperature differentials (with positive gradient) occurs when the concrete deck slab is exposed to solar radiation during the summer and winter, resulting in a concrete deck slab that is warmer than the steel beams and thus the rotation of the end of the superstructure will occur in the opposite direction to that due to the traffic load. The

minimum temperature differential (with negative gradient) occurs when the concrete deck slab is suddenly drenched with cold rain or snow, thus cooling the concrete deck slab at a faster rate than the steel beams. It will give rotation of the superstructure end in the same direction as the traffic load in the framed arrangement of an integral bridge. Sudden temperature changes will also affect the temperature in the lower flange faster than the concrete slab, thus creating a temperature gradient through the superstructure. It is not common to measure the bridge temperature, and it is thus valuable to have models to estimate the bridge temperature from the ambient temperature.

In Eurocode EN 1991-1-5 (CEN 2003b) the maximum and minimum temperatures are in Figure 7 based on daily temperature ranges of 10° C, which is 13% of the maximal annual temperature range. Measurements in the UK (Emerson 1977) showed that the daily temperature range in a composite bridge was at most about 25% of the annual. For integral abutment bridges, the bridge temperature variations will cause strain variation in the substantial piles. An estimate for fatigue calculations should aim to give a constant value for the amplitudes that gives the same fatigue damage as the real case. The previous researchers estimate the daily variations give the same fatigue effect of the material as if the daily variations were of constant amplitude and 10% of the annual ones. It is estimated that 80% of the values given in Eurocode EN 1991-1-5 (CEN 2003b) is sufficient to use to calculate annual temperature ranges for fatigue calculation.

2.4 **LOAD TRANSFER ON PILE FOUNDATION**

2.4.1 Elastomeric bearing on conventional bridge

An elastomeric bearing allows movements in all directions by elastic deformation and rotation around every direction, thereby allowing the transfer of forces from one component to another. The elastomeric block can be either rectangular or circular. An elastomeric block is made mainly of elastomer (natural rubber or synthetic rubber) which is capable of regaining its initial shape and dimension when subjected to loads within its elastic range, but when supporting high vertical loads, it deforms vertically, which then result in bulging of the rubber. The deformation of the rubber has to be controlled to keep it within the allowable elastic range. Excessive deformation can result in sliding; hence, there is a need for the rubber block to be reinforced by horizontal steel plates under high vertical loads. The steel

plates prevent the rubber from bulging; the thickness and number of steel plates depending on the magnitude of the vertical load the bearing will support. The steel plates are chemically bonded to the rubber in layers during vulcanization. In addition, to prevent sliding between the bearing, substructure, and superstructure friction has to be controlled. It was done by adding restraining steel plates added to the elastomer on top, bottom and sides of the bearing, which is then connected to the structures by studs, bolts or pins, as shown in Figure 2-5 below.

a. Elastomeric bearing with anchor plate b. with restraining plates

Figure 2-5 Elastomeric bearing (Fasheyi, 2012)

2.4.2 Fully integral abutment bridges

In the past years, some states in the USA preferred using a welded connection between piles and girders (Figure 2-6). However, the major disadvantage of this type of connection is that the piles have to be driven very close to their planned position, as the girders shall be welded on top of them. It means that piles often must be driven within a tolerance of 2-3 cm, and this can be hard to achieve in difficult pile driving condition (Conboy et al., 2005) (Yannotti et al., 2005).

Nowadays, another way of constructing a rigid connection between piles and girders is used. Initially, the driven piles are covered with a pile cap or a lower part of the abutment back-wall. The girders are mounted on top of the pile cap and fixed to the abutments on leveling bolts that are anchored in the pile cap (Figure 2-7). These leveling bolts may be replaced by

precisely leveled steel pressure plates which allow for a horizontal correction as well. However, a tilting of the steel beam needs to be avoided during construction in any case. The ends of the girders are later surrounded by concrete when the top of the abutment back-wall is cast. In particular, if settlement of the foundation has to be expected, a possibility of horizontal adjustment has to be provided, the height has to be controlled metrological during construction. It has been proven that constructions without welds between piles and girders are easier to construct, and no differences in performance have been detected (Conboy, et al., 2005).

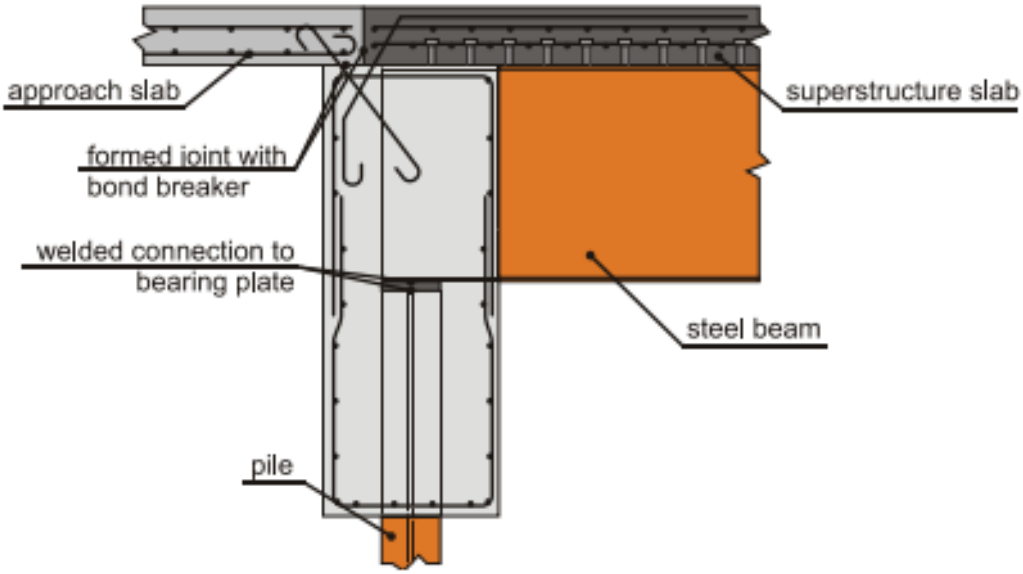

Figure 2-6 Connection between piles and girders (Feldmann et. al. ,2010)

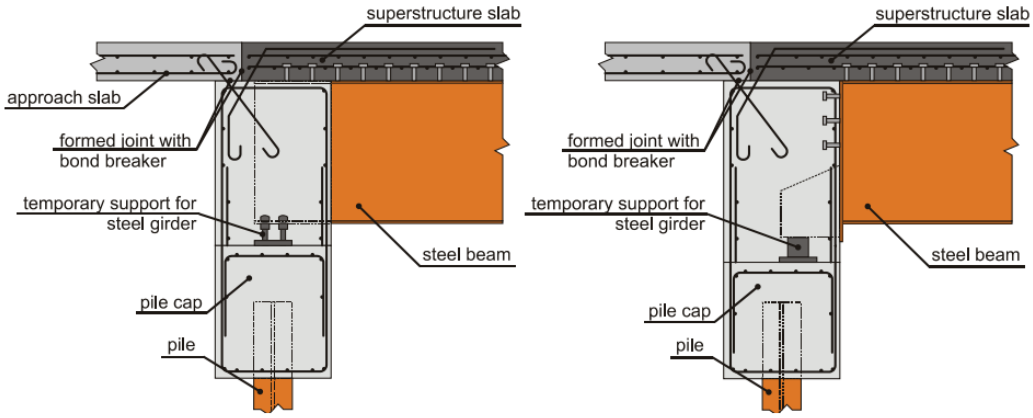

Figure 2-7 Girder mounted on the leveling bolts/pressure plate on top of a pile cap (Feldmann et al.,2010)

2.4.3 Semi-integral abutment bridges

The hinge connection might be placed between the pile cap and the abutment (Figure 2-8). Within the scope of the INTAB project (Feldmann et al., 2010), another type of hinged connection was developed and tested, as shown in Figure 2-8.

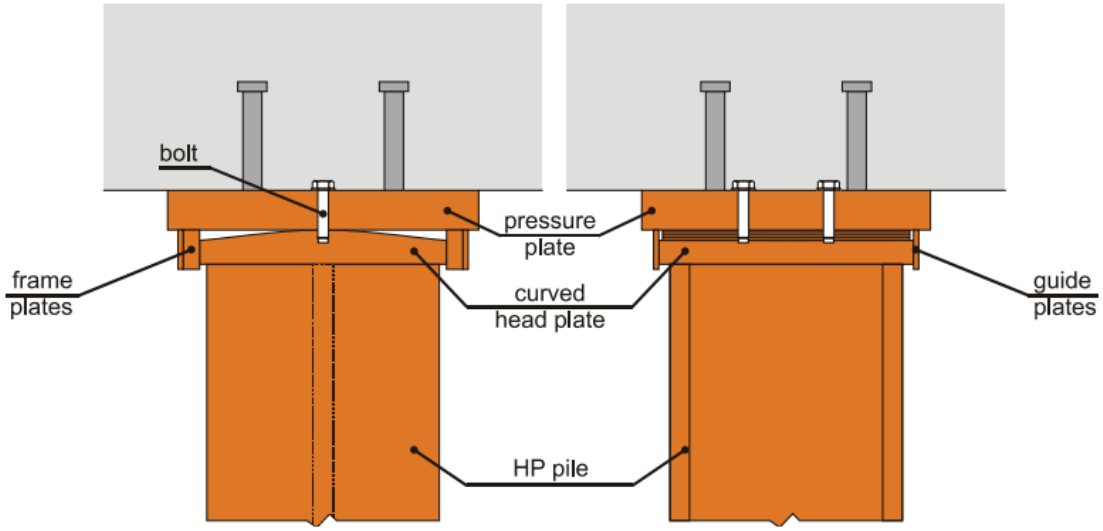

Figure 2-8 Hinged connection (Feldmann et al., 2010)

A curved head plate is welded on top of the piles, enclosed by a pressure plate with welded on frame plates. The shear forces are transferred by the fame plates, the bolt just serves as assembling aid.

2.5 FOUNDATION SYSTEM ON INTEGRAL ABUTMENT BRIDGE

The integral abutment bridge concept has been practiced for many years. However, with the more complex bridges being designed recently and efforts to minimize long-term bridge costs, it is important to consider concepts for extending the use of integral abutments to a typical bridge. For an integral abutment bridge, the primary concept is to accommodate the expansion and shrinkage of bridge structure due to annual temperature changes by flexibility in the foundations. An estimation of the thermal expansion on the bridge girder can be determined; creep and shrinkage may be added. Some states limit the total amount of movement to be taken by integral-abutment foundations in the range from 13 to 102 mm (Kunin and Alampalli 1999). Other states limit movements indirectly by limiting bridge length (Maruri and Petro 2005). Once movements and integral-abutment specifications are

known, the designer can use structural principles and detailing to design the structure, considering soil-structure interaction. If the abutments are founded on piles, the piles need to flex or otherwise provide for movement without excessive internal bending stresses or excessive axial stresses in the superstructure. In order to reduce these stresses, there are some design option as follows (Dunker and Liu, 2007): (1) use the most laterally flexible piles (although some states may disagree); (2) place the piles in pre-bored holes or sleeves; (3) hinge the tops of the piles; (4) detail the tops of the piles to slip; and/or (5) add compressible material to the regions directly behind the abutments. Using a hinged-abutment or pinned-pile head also has the effect of shifting the maximum bending stresses in a pile downward away from the pile head.

2.5.1 Fixed Head Pile

The fixed head pile system using the fixed connection on the top of pile connection to provide continuity between the pile and superstructure, as shown in Figure 2-9. The results computations show that 300 mm embedment is sufficient for fixity of an HP 250x62 oriented for strong axis bending (Wasserman and Walker 1996). In tests conducted by the University of Tennessee, a 300-mm embedment resulted in some cracking, but the adequate performance at large, lateral displacements. A 600-mm embedment increased moment development at the pile head (Burdette et al. 2000). The embedment is 600mm, with a reinforcing spiral. Larger embedment and reinforcement may be required for larger and stiffer piles.

2.5.2 Pinned-Head Pile

In order to reduce the maximum bending moment in a pile, the head of the pile may be design as a pin connection. Figure 2-10 illustrates the use of padding to create a pinned connection at the pile head. The detail had a plastic foam cap 50 mm thick, topped with an elastomeric pad and sliding bearing plate (Kamel et al. 1996).

2.5.3 Hinged Abutment

Some areas prefer to provide a hinge connection system on the abutment, rather than the rotating pile connection (Dunker and Liu, 2007) as illustrated in Figure 2-11. Researchers termed this system as a semi-integral, however, others consider as an integral abutment. In

each situation the superstructure is placed on a neoprene pad on the abutment and superstructure is dowelled to the abutment.

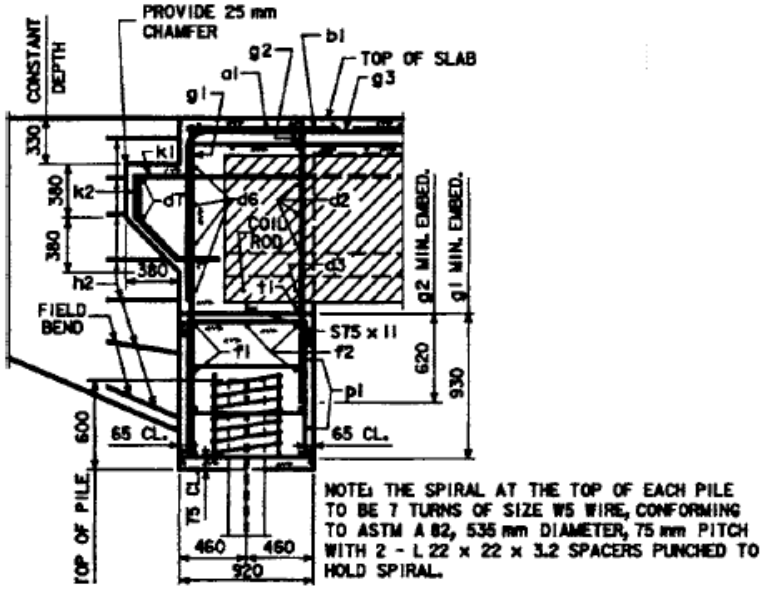

Figure 2-9 Fixed head pile used in Iowa state (Dunker and Liu, 2007)

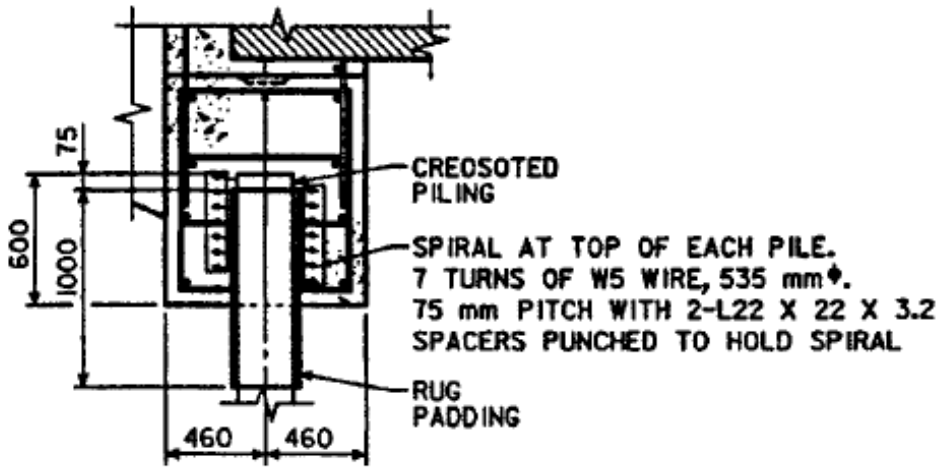

Figure 2-10 Pinned head details used in Iowa state (Dunker and Liu, 2007)

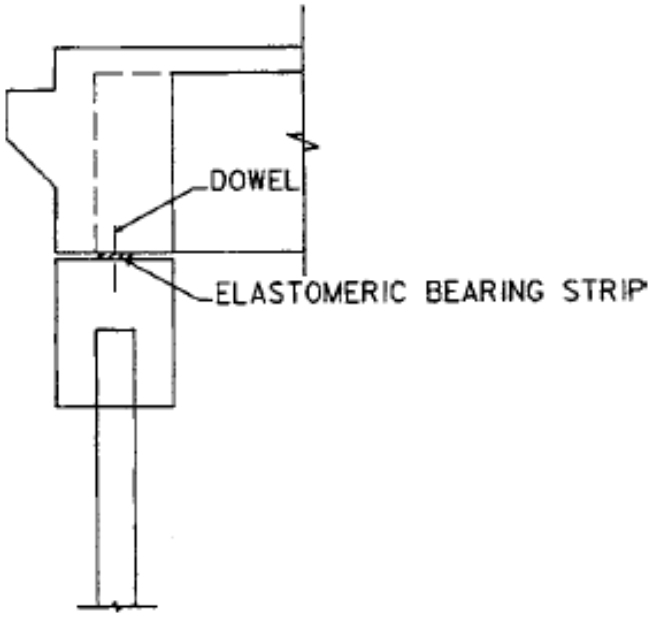

Figure 2-11 Hinge connection system (Dunker and Liu, 2007)

2.5.4 Fixed-Base Pile

Another system for pile analysis is to establish an equivalent cantilever by estimating the depth-to-pile fixity (Greimann et al. 1987). The designer has the opportunity to set the depth-to-fixity by design where bedrock is close to the surface. The rock can be cored to a predetermined depth and steel H piles anchored in concrete in the core holes, as shown in Figure 2-13. The elevation of the bottom of the holes was set to give the piles sufficient length to flex as the bridge expands and contracts (Dunker and Abu- Hawash 2005). With a relatively shallow depth to reach bedrock, the designer should check ductility to ensure that the pile can sustain plastic deformation (Greimann et al. 1987; Abendroth and Greimann 2005).

2.5.5 Pre-bored Hole

In case of pile foundation embedded in a stiff soil, piles will have small opportunity to displace because the lateral earth pressure of soil will create a fixed condition close to the top area of the pile, and it increases the pile stress which can be affected on the bridge length limit. In order to increase pile flexibility, the piles may be placed in pre-bored holes filled with flexible material, as shown in Figure 2-12. Iowa DOT (Department of Transportation) typically makes the holes twice the diameter of the pile and 3.05-m deep. Deeper holes may

be used for special conditions. Empty holes might affect the long-term maintenance problems, so the holes should be filled with a deformable material, such as bentonite slurry, loose sand, or pea gravel. In addition to increasing pile flexibility, pre-bored holes have the advantage of eliminating down drag from compressible fills.

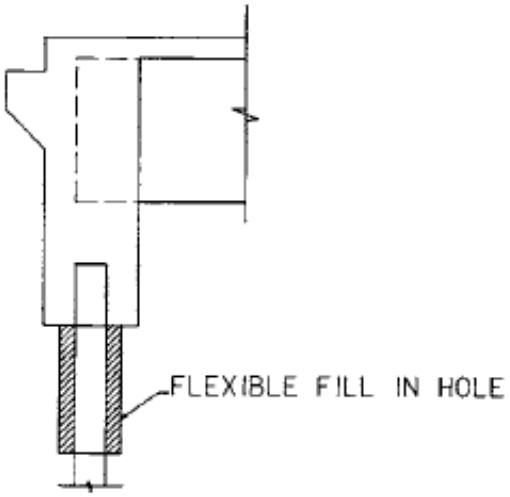

Figure 2-12 Pre-bored hole filled with material (Dunker and Liu, 2007)

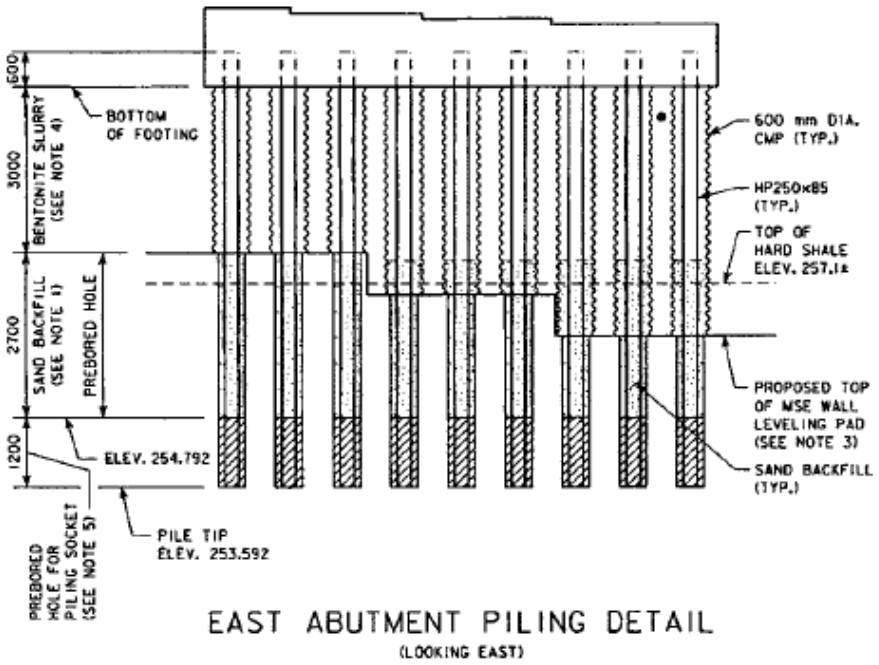

Figure 2-13 Fixed-base and sleeved-pile details for I-235 Ramp 5th Street in Des Moines, Iowa (Dunker and Liu, 2007)

2.5.6 Pile Sleeve

In the condition of a small construction area, there may not be room for the berms, as shown in Figure 2-13. Although the abutment might be extended downward to be a retaining wall, that configuration will not allow for a large amount of abutment movement. As a result, the designer may choose to place a separate retaining wall in front of the abutment. A mechanically stabilized earth (MSE) wall often provides the most economical solution (Dunker and Liu, 2007). Due to the construction sequence for the MSE wall, pre-bored holes are not feasible. Therefore, the piles should be placed in a corrugated-metal pipe (CMP) sleeves at least twice the diameter of the pile to avoid additional lateral pressure on the MSE wall (Dunker and Abu-Hawash 2005; Hassiotis et al. 2005). In Iowa, the sleeves are filled with saturated sand up to the elevation where a pre-bored hole would begin, as shown in Fig. 5. Above the top of the sand, the sleeves are filled with bentonite slurry. As with pre-bored holes, the sleeves can be used to eliminate down drag on the piles.

Table 2-1 Summary of Design Concepts

Design concept	Advantages	References
Fixed-head pile	A relatively high moment at pile head, fixity provided by 300 to 600 mm embedment	Wasserman and Walker (1996), Burdette et al. (2000)
Pinned-head pile	A negligible moment at pile head, usually detailed with padding	Kamel et al. (1996)
Hinged abutment	A negligible moment at pile head, usually detailed with elastomeric strip and dowels	Dunker and Abu-Hawash (2005), Greimann et al. (1987)
Fixed-base pile	Applicable for shallow bedrock, the potential for insufficient flexibility and ductility	Abendroth and Greimann (2005)
Pre-bored hole	Increased pile flexibility, reduction of down drag	Iowa DOT (2006)
Pile sleeve	Applicable for constructed fill especially adjacent to MSE walls, increased pile flexibility, reduction of down drag	Dunker and Abu-Hawash (2005), Hassiotis et al. (2005)

The integral abutment concepts described above and summarized in Table 1 are not all of the possibilities. Although the designer needs to consider unusual bridge configurations and site conditions, soil-structure interactions often are not easily quantified. Engineering judgment is important and must be part of the design process (Dunker and Liu, 2007).

2.6 SINGLE PILE UNDER STATIC AND CYCLIC LOADING

The lateral capacity of the pile is mobilized due to the interaction between the pile structure and the resistance of the soil also known as soil-pile interaction (Briaud et al., 1983; and Smith, 1987). The lateral pile resistance is carried out on the single pile as a combination of lateral soil pressures and skin friction acting on the pile. Mechanism of the pressures acting on a pile is shown in Figure 2-14. The pile is subjected to soil pressure and skin friction on the side of the pile. The lateral load per unit length of pile, (P) can be calculated by considering the effective stress at a certain depth (σ'_v), lateral earth pressure coefficient (K) and the pile diameter (D) as written in the following equation.

$$P = K\sigma_v D \tag{2-1}$$

where:

K = earth pressure coefficient;

σ_v = vertical effective stress; and

D = pile diameter.

In Figure 2-14, the actual stress distribution is shown on the left, whereas the simplification, which is used in the general approximation in Equation 2.1, is shown to the right. Then the total lateral pile capacity (H) is estimated by integration of above formula over the embedded length of the pile (L), as follows:

$$H = \int_0^L K\sigma'_v \, D dz \tag{2-2}$$

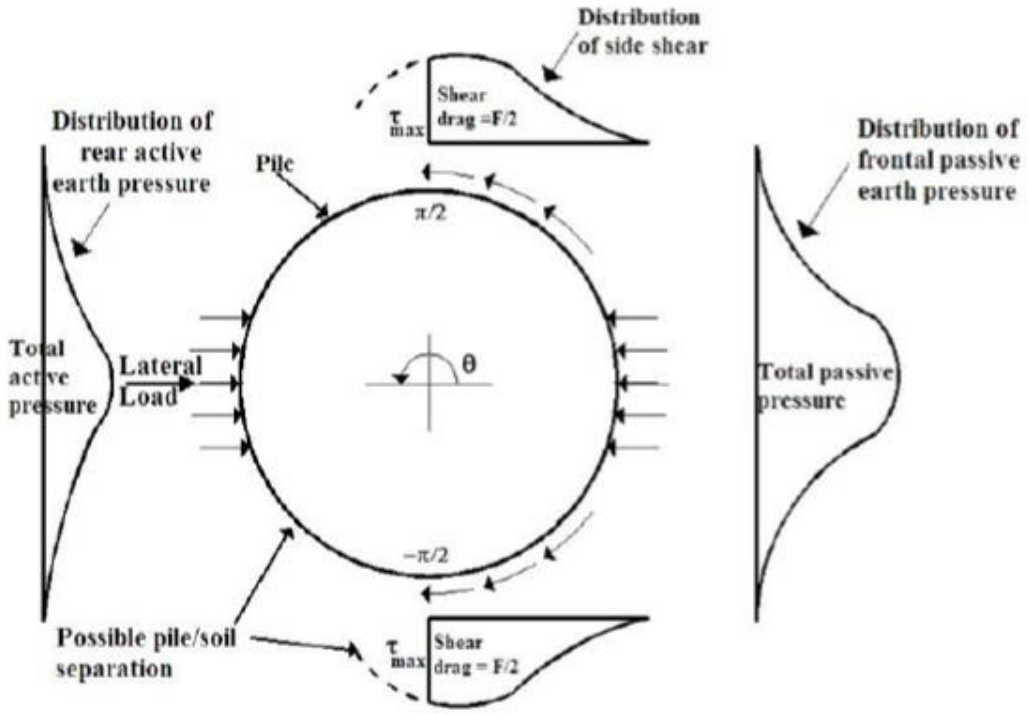

Figure 2-14 Illustration of soil pressure approximation in a cross-section of the pile (after Smith, 1987)

Previous researchers have developed the numerical and empirical approaches to estimate the static and cyclic lateral capacity of piles. Generally, it can be classified into three groups (Kim et al., 2011): (1) ultimate lateral strength methods (e.g., Brinch Hansen, 1961; Broms, 1964; Meyerhof et al., 1981; etc.), (2) subgrade reaction methods (Matlock, 1970; Reese et al., 1974; O'Neil et al., 1982; Kishida et al., 1985; Ashour et al., 1998; etc.) (3) elastic and finite element methods (Brown and Shie, 1991; Jeremic and Yang, 2002; etc.). In this research focuses on closed-form solutions and empirical techniques for piles subjected to lateral static and cyclic loading, so, the first and second approaches are introduced in this chapter.

2.6.1 Ultimate Lateral Strength Methods

Various methods of the literature to predict the ultimate lateral resistance to piles in cohesionless soils have been published (e.g., Brinch Hansen, 1961; Broms, 1964; Meyerhof et al., 1981; Prasad and Chari, 1999; etc.). The main difference between those methods is the assumption of lateral earth pressure distribution in front of the pile during loading (Figure 2-15); Each method gives a different value for ultimate horizontal load for the same soil

conditions. A key element in the design of laterally loaded piles is the determination of the ultimate lateral earth pressure that can be exerted by the soil against the pile movement (Awad-Allah and Yasufuku, 2013). Some approaches assumed that pile rotates at the pile base, such as Broms method (1964). However, other methods proposed by Petrasovits and Award (1972), Prasad and Chari (1999), Brinch Hansen (1961), and Meyerhof et al. (1981) consider that the point of pile rotation is at a certain depth below the ground level (z).

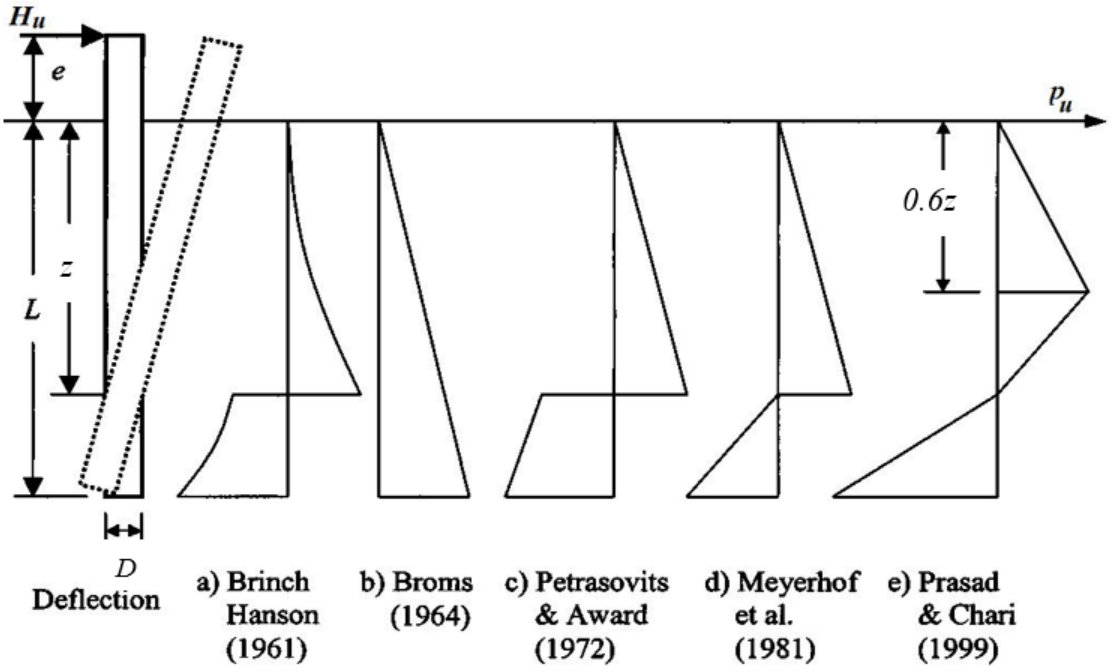

Figure 2-15 Assumed distributions of soil pressure patterns by several researchers

The most commonly used approaches are summarized, as follows:

a. Broms method (1964)

Broms's method (1964) is one of the most popular methods in practice for estimating ultimate lateral soil resistance. A simplified solution has been developed for laterally loaded piles based on the assumption of plastic yield resistance of the pile section on pile bending. It assumed that a lateral load acts at the pile base and therefore, the pile rotates according to the pile base. The ultimate lateral soil resistance, p_u, at fully mobilized passive state is given as follows:

$$p_u = 3K_p\sigma_v' \qquad (2\text{-}3)$$

where:

K_p= $\tan^2(45°+\varphi`/2)$ = passive earth pressure coefficient;

K_a= $\tan^2(45°-\varphi`/2) = 1/K_p$ = active earth pressure coefficient; $\varphi`$= internal friction angle of soil; and

σ_v' = vertical effective stress

b. Prasad and Chari method (1999)

Prasad and Chari (1999) proposed an estimation method for predicting ultimate soil resistance for laterally loaded pile in cohesionless soil, as shown in Equation 2.4.

$$p_u = 10^{(1.3\tan\phi'+0.3)}\sigma_v' \quad (2\text{-}4)$$

c. Zhang et al. method (2005)

Zhang et al. (2005) proposed a method for calculating the ultimate lateral soil resistance to piles in cohesionless soil, considering frontal soil resistance and side shear resistance, as given below:

$$p_u = \left(\eta p_{\max} - \zeta\tau_{\max}\right) \quad (2\text{-}5)$$

where,

$$p_{\max} = K_p^2\sigma_v' \quad (2\text{-}6)$$

$$\tau_{\max} = K_s\tan\delta\sigma_v' \quad (2\text{-}7)$$

where,

η = shape factor to account the non-uniform, distribution of earth pressure in front of the pile (Table 2-2);

ξ = shape factor to account for the non-uniform distribution of lateral shear drag (Table 2-2);

p_{max}= maximum frontal passive earth pressure of soil ahead of pile shaft; and and

τ_{max} = maximum side shear resistance of soil at pile shaft.

K_s = lateral earth pressure coefficient (ratio of horizontal to effective vertical stress); and

δ = interface friction angle between pile wall and soil (a function of soil type and density).

In order to estimate the values of K_s and δ, Kulhawy (1991) summarized in Tables 2.2 and 2.3, respectively. Consequently, ultimate lateral resistance that can be exerted by the soil against the pile lateral movement can be expressed.

The expressions for estimating (p_u) for laterally loaded pile in sand soils proposed by some researchers are summarized in Tables 2.4. These formulas

Table 2-2 Values of η and ξ (after Briaud and Smith, 1983)

Pile shape	η	ξ
Circular	0.8	1.0
Square	1.0	2.0

Table 2-3 Recommended values of δ by Kulhawy (1991)

Pile type	δ
Rough concrete	1.0 φ`
Smooth concrete(i.e., precast pile)	(0.8–1.0) φ`
Rough steel (i.e., step-taper pile)	(0.7–0.9) φ`
Smooth steel (i.e., pipe pile or H pile)	(0.5–0.7) φ`
Wood (i.e., timber pile)	(0.8–0.9) φ`
Drilled shaft built using a dry method or with temporary casing and good construction techniques	1.0 φ`
Drilled shaft built with a slurry method (higher values correspond to more careful construction methods)	(0.8–1.0) φ`

Table 2-4 Equations of p_u proposed by some researchers for sand soils

Method	Equation of p_u
Prasad and Chari (1999)	$p_u=10^{(1.3\tan\phi+0.3)}\gamma 0.6z$
Zhang et. al. (2002)	$p_u=\eta p_{max}+\zeta\tau_{max}$
Awad-Allah and Yasufuku (2013)	$p_u=\eta[(K_p^2-K_a)+\zeta K_s \tan\delta]\sigma_v'$

note:

K_p= $\tan^2$ (45°+φ'/2);

K_a= $\tan^2$ (45°-φ'/2);

φ' = internal friction angle of soil;

η and ξ = dimensionless shape factors;

p_{max} = maximum frontal passive earth pressure of soil ahead of pile shaft $P_{max} = K_p^2\sigma'_v$;

τ_{max} = maximum side shear resistance of soil at pile shaft $\tau_{max} = K_s\sigma'_v \tan\delta$

K_s = lateral earth pressure coefficient (ratio of horizontal to vertical effective stress);

δ = interface friction angle between pile wall and soil (a function of soil type and density);

σ'_v = vertical effective stress.

2.6.2 Subgrade reaction approach

The differential equation of the problem of a single laterally loaded pile formulated based on a beam on elastic foundation technique (Winker's model) as shown in Figure 2-16. The differential equation of laterally loaded piles in cohesionless soil is given by the following formula.

$$EI\frac{d^4y}{dz^4} + p_u z = 0 \qquad (2\text{-}8)$$

where,

$E_p I_p$ = flexural stiffness of pile; and

P = lateral pile resistance per unit length of the pile.

Vesic (1961) has shown that the error inherent in Winkler's hypothesis is not significant. In the Winkler soil model, lateral pile resistance per unit length of the pile (P) and lateral

displacement (y) at a point are assumed to be related through a modulus of subgrade reaction (K_h) (e.g., Reese and Matlock, 1956; and Davisson and Gill, 1963).

$$K_h = \frac{P}{yD} \tag{2-9}$$

$$K_h = n_h z \tag{2-10}$$

where,

K_h = modulus subgrade reaction,

D = diameter or width of pile (L); and

n_h = coefficient of subgrade reaction.

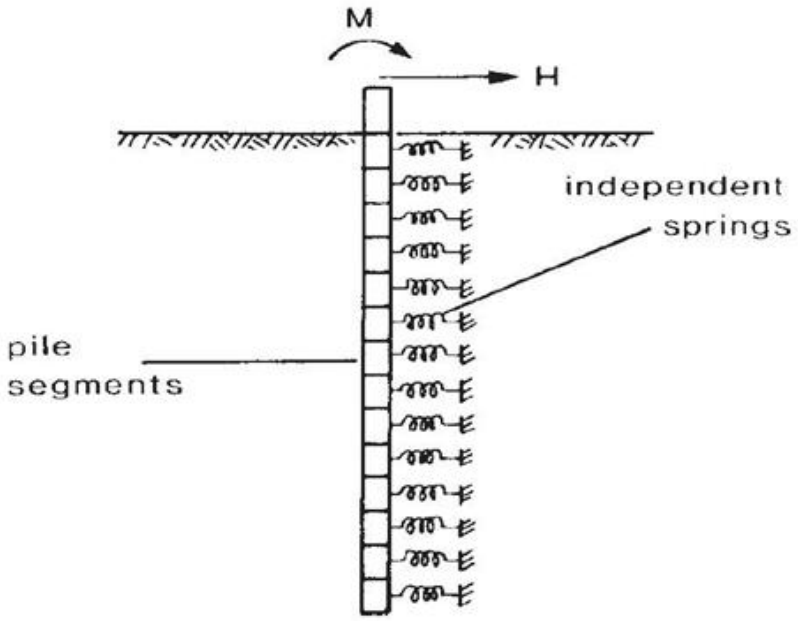

Figure 2-16 Subgrade reaction model of soil around based on pile Winkler's idealization of a beam on elastic foundation

This formula is known as the differential equation for the elastic curve of the laterally loaded pile. Within this framework, Reese (1977) proposed the well-known ‘p–y method’, as shown in Figure 2-17. This approach is based on fourth-order differential equation (Equation 2.8) for solving the problem of the laterally loaded pile, and it can be used for both free- and fixed-head single piles.

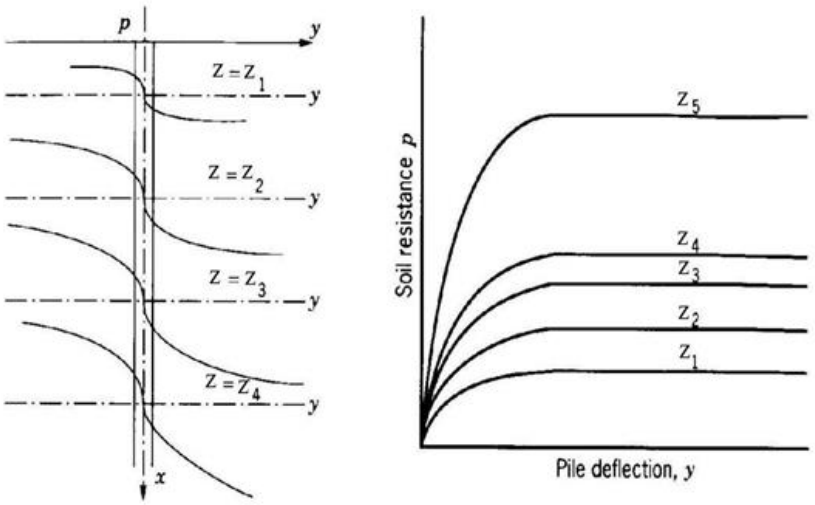

Figure 2-17 Sets of 'p-y'curves model

2.7 SUMMARY OF PROBLEM TO BE SOLVED

Integral abutments eliminate the need to provide elastomeric bearings. In addition, it can save bridge costs, time, and reduce inconvenience compared to conventional bridges. However, the previous researchers only focus on the structural system, but the behavior of soil and soil response due to the flexible piling design is still rarely explained. The characteristic of filler material and standard design of this foundation system is still in development. In this research, the authors conducted numerous research activity to evaluate the appropriate design for the pre-bored pile foundation system. The selection of this system than the other system is the pre-bored pile foundation system is simple to execute both on the experimental modeling and field construction in Indonesia.

This chapter reviews the previous researches that have a close relationship with the response of single pile in sandy soils and subjected to lateral cyclic and static loading. The literature review covers the following aspects: different type of integral abutment bridges system in practice, types of integral abutment bridge foundations, loading mechanism on pile due to environmental thermal load, methods of analysis of lateral static and cyclic loads for singe piles, shear strain of soil around the pile due to lateral displacement, and the characteristics of the common static. Some of the research activities have been presented in the literature; however, some academic issues need to be solved, which can be summarized as follows:

1. The influence of pre-bored ring and filler material on the pre-bored pile foundation system under cyclic lateral loading based on geotechnical point of view.
2. The appropriate filler properties and the dimension of this system including filler material properties, filler density, pre-bored ring diameter, and depth, that can reduce the bending moment along with the pile due to lateral displacement loading which can solve the problem on the integral abutment bridge foundation.
3. The failure mechanism of soil on the pre-bored pile foundation system under cyclic lateral loading. This failure pattern can effect on determining the effective dimension of pre-bored ring system based on the failure zone during the cyclic lateral loading.
4. Introducing the simplified model for predicting the lateral pile capacities on the pre-bored pile foundation system which consider the soil-pile interaction during the lateral loading, in order to reduce the error values between the actual measured value and estimated value.

2.8 **REFERENCES**

Abendroth, R. E., and Greimann, L. F. (2005). “Field testing of integral abutments.” Final Rep. HR-399, Iowa State Univ., Ames, Iowa,

Burdette, E., Deatherage, J. H., and Goodpasture, D. W. (2000). Behavior of laterally loaded piles supporting bridge abutments—Phase I, Univ. of Tennessee, Knoxville, Tenn.

Dicleli, M., and Albhaisi, S. M. (2004). “Estimation of length limits for integral bridges built on clay.” J. Bridge Eng., 9(6), 572–581.

EN 1991-1-5 // Eurocode 1: Actions on structures - Part 1-5: General actions – Thermalactions. - Brussels : European Committee for Standardization (CEN), 2003.

England, G. L., Tsang, N. C. M., and Bush, D. I. (2000). Integral bridges, a fundamental approach to the time-temperature loading problem, Thomas Telford, London.

Feldmann, M., Naumes, J., Pak, D., Veljkovic, M., Eriksen, J., Hechler, O., et al., 2010, Design Guide. Aachen: RWTH Aachen University, Institut für Stahlbau,

Girton, D. D., Hawkinson, T. R., and Greimann, L. F. (1989). “Validation of design recommendations for integral abutment piles.” Final Rep. HR-272, Iowa State Univ., Ames, Iowa.

Greimann, L. F., Abendroth, R. E., Johnson, D. E., and Ebner, P. B. (1987). “Pile design and tests for integral-abutment bridges.” Final Rep. HR-273 and Addendum to HR-273, Iowa State Univ., Ames, Iowa.

Pétursson H., Möller M., Collin P., 2013, Structural Engineering International, Vol. 23 , Number 3, pp. 278-284

Hassiotis, S., Lopez, J. A., and Bermudez, R. (2005). “Full-scale testing of an integral abutment bridge.” Proc., 2005 FHWA Conf. on Integral-Abutment and Jointless Bridges, Federal Highway Administration, Washington, D.C., 199–210,

Hassiotis, S., and Roman, E. K. (2005). “A survey of current issues on the use of integral abutment bridges.” Bridge Structures: Assessment, Design, and Construction, 1(2), 81–101.

Iowa Department of Transportation. (2006). Bridge design manual, Iowa Dept. of Transportation, Ames, Iowa.

Jayaraman, R., and Merz, P.B. (2001). Integral bridge concept applied to rehabilitation an existing bridge and construct a dual-use bridge. 26th Conference on Our World In Concrete & Structures. Singapore.

Kulhawy, F.H., Trautmann, C.H., Beech, J. F., O’Rourke, T. D., McGuire, W., Wood, W. A., and Capano, C. (1983): Transmission line structure foundations for uplift-compression loading. Report No. EL-2870, Electric Power Research Institute, Palo Alto, Calif.

Kulhawy, F. H. (1991): Drilled shaft foundations, Foundation engineering handbook. 2nd Ed., Chap. 14, H.-Y. Fang ed., Van Nostrand Reinhold, New York.

Jin, X., Shao, X., Peng, W. and Yan, B., (2005), A New Category of Semi-Integral Abutment in China, Structural Engineering International, 15, 3, 186-188.

Kamel, M. R., Benak, J. V., Tadros, M. K., and Jamshidi, M. (1996). “Prestressed concrete piles in jointless bridges.” PCI J., 41(2), 56–67.

Kunin, J., and Alampalli, S. (1999). Integral-abutment bridges: Current practice in the United States and Canada." Special Rep. 132, New York State Dept. of Transportation, Albany, N.Y.

Maruri, R. F., and Petro, S. H. (2005). "Integral abutments and jointless bridges (IAJB) 2004 survey summary." Proc., 2005 FHWA Conf. on Integral-Abutment and Jointless Bridges, Federal Highway Administration, Washington, D.C., pp. 12–29.

Setiati, N., (2015). "Kajian Hasil System Monitoring Jembatan Integral Sinapeul Ditinjau dari Regangan Kepala Jembatan (The Study of Sinaperul Integral Bridge Monitoring System Based on Abutment Strain)", Jurnal Jalan-Jembatan, Vol 32(1), pp. 32-43.

Tang, Q., Ma, J., Jin, X. and Shao, X. (2007). First refurbished jointless bridge in China. Conference of Highway Maintenance Technology. Guangdong, China, China Communication Press,(in Chinese).

Wasserman, E. P. (2001). "Design of integral abutments for jointless bridges." Structure (London), 8(5), 24–33.

Wasserman, E. P., and Walker, J. H. (1996). "Integral abutments for steel bridges." Highway structures design handbook, Vol. II, American Iron and Steel Institute (AISI), Washington, D.C.

Yannotti, A.P., Alampalli, S. and White, H.I., (2005), New York State Department of Transportation's Experience with Integral Abutment Bridges, Integral Abutment and Jointless Bridges (IAJB 2005), Baltimore, Maryland, 41-49.

CHAPTER III

LABORATORY SIMULATION ON SINGLE PILE UNDER STATIC AND CYCLIC LATERAL LOADING

3.1 INTRODUCTION

In this Chapter, the behavior of soil properties such as grain size and density was evaluated to reduce the pile cracking possibility. Soil material characteristic on the cyclic laterally loaded pile is also investigated. Macro-scale testing was performed to determine soil behavior due to cyclic lateral loading and to evaluate the effectiveness of the pre-bored pile foundation system. A clear description of the experimental setup, instrumentations, scale factors, ground soil material preparation, loading mechanism, and pile model used in this research are explained.

3.2 LABORATORY SIMULATION AND TEST CONDITIONS

Macro-scale testing was performed to determine soil behavior due to cyclic lateral loading and to evaluate the effectiveness of this system. The laboratory test outline is shown in Figure 3-1. An experimental study was performed using a pile model test in sandy soil that has different soil grain size and uniformity coefficient. The laboratory test consists of two aspects: (1) 1g model test, (2) soil properties test. The detailed test cases and the associated test conditions are represented in Table 3-1.

Total 31 cases of lateral loading under 1g model conditions are conducted at different soil density, soil types, pile slenderness, and different pre-bored ring diameter. Eleven test conditions are carried out in a ground soil using full circle pile with pre-bored ring and filler material. Half-circle pile conducted in 4 cases with different ring diameter. The remaining tests were constructed without the pre-bored ring conditions in the full-circle of the pile. All cases were tested under cyclic lateral loading until 50 times of the cycle.

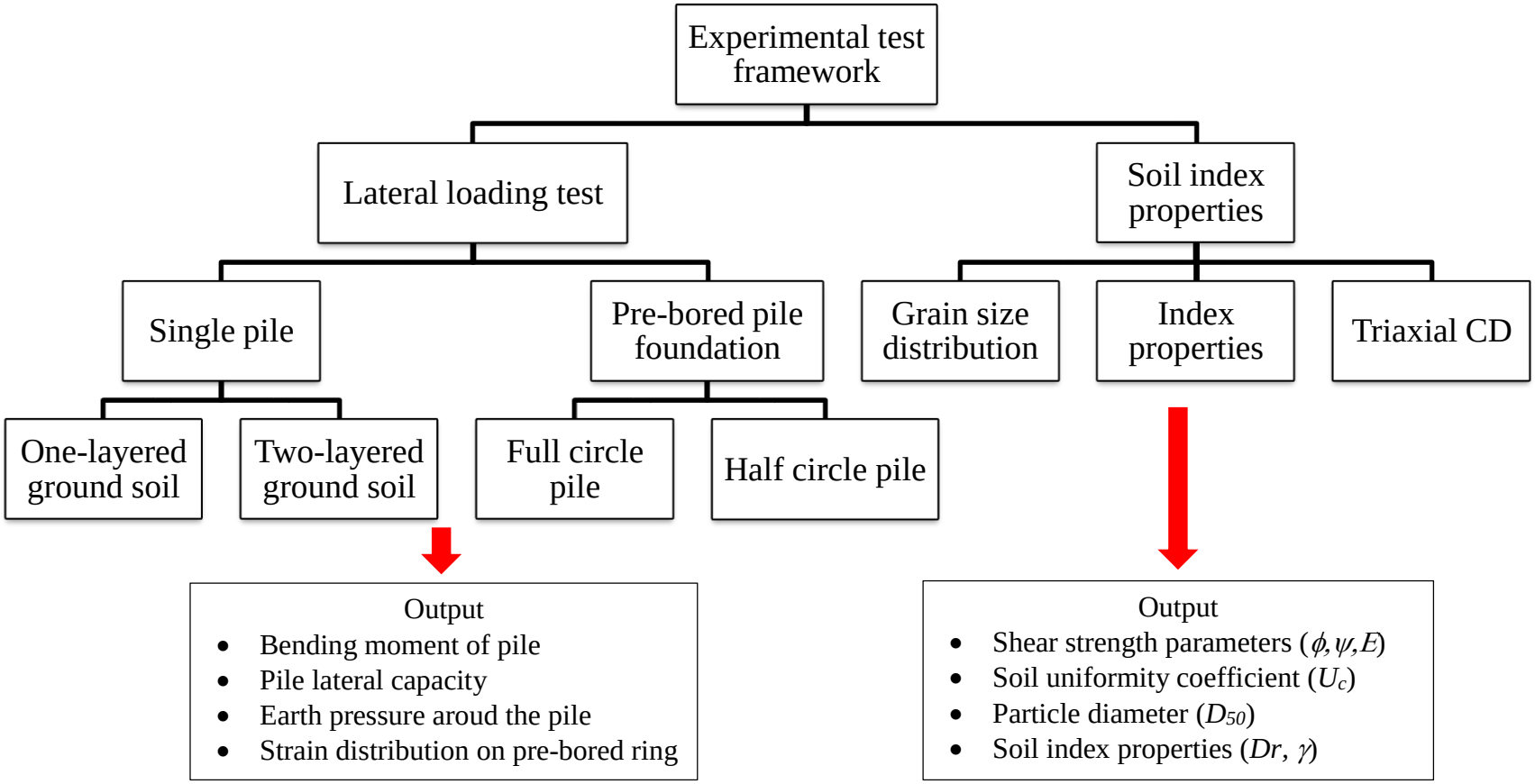

Figure 3-1 Experimental framework outlines

Table 3-1 Total number of experimental tests conditions

One-Layered Soil					
Test ID	Dr (%)	Soil type	*L/D*	Cycle time (N)	Pile head displc. (mm)
OL01	80	K7	10	50	3
OL02	80	K7	20	50	3
OL03	80	K7	30	50	3
OL04	80	K4	10	50	3
OL05	80	K4	20	50	3
OL06	80	K4	30	50	3
OL07	50	K7	10	50	3
OL08	50	K7	20	50	3
OL09	50	K7	30	50	3
OL10	50	K4	10	50	3
OL11	50	K4	20	50	3
OL12	50	K4	30	50	3
OL13	80	K7	30	50	1

Table 3.1 (continued)

Two-Layered Soil

Test ID	Dr (%)	Soil type	*x/D*	Cycle time (N)	Pile head displc. (mm)
TL01	80	K7 (bottom) K4 (upper)	3	50	3
TL02	80	K7 (bottom) K4 (upper)	10	50	3
TL03	80	K7 (bottom) K4 (upper)	17	50	3

Full circle pile of pre-bored system
(Ground Soil: K7 sand, Dr=80%)

Test ID	Dr (%)	Filler type	d/D	Load frequency (Hz)	Pile head displc. (mm)
PB01	-	Empty	-	0.020	1
PB02	40%	Toyoura	4	0.020	1
PB03	70%	Toyoura	4	0.020	1
PB04	90%	Toyoura	4	0.020	1
PB05	80%	K-7	4	0.020	1
PB06	80%	Mix soil	4	0.020	1
PB07	80%	K-4	4	0.020	1

Table 3.1 (continued)

Test ID	Dr (%)	Filler type	d/D	Load frequency (Hz)	Pile head displc. (mm)
PB08	80%	K-5	4	0.020	1
PB09	80%	Toyoura	3	0.020	1
PB10	80%	Toyoura	4	0.020	1
PB11	80%	Toyoura	5	0.020	1

Half circle pile of the pre-bored ring system
(Ground Soil: K7 sand, Dr=80%)

Test ID	Dr (%)	Filler type	d/D	Load frequency (Hz)	Pile head displc. (mm)
HOL1	80%	-	-	0.02	1
HPB1	80%	Toyoura	3	0.02	1
HPB2	80%	Toyoura	4	0.02	1
HPB3	80%	Toyoura	5	0.02	1

The objective of the one-layered soil ground laboratory testing is to investigate the effect of soil properties on single piles constructed into fully dry soil conditions, subjected to static and cyclic lateral loading. Influence of relative density of soil (*Dr*), soil properties (U_c and D_{50}), slenderness ratio of the pile (*L/D*), and the number of cycles (*N*) are parametric variables in the experimental test. The two-layered soil ground was conducted to evaluate the effect of pre-bored pile foundation system depth under cyclic lateral loading. The ratio between upper layer depth and pile diameter (*x/D*) is evaluated to determine the effective depth of this system.

The full circle pile of pre-bored ring system was carried out to investigate the effective filler material properties. Effect of filler material relative density (D_r), soil properties (U_c and D_{50}),

ring diameter ratio (*d/D*), and load frequency (*f*). Moreover, the half-circle pile of the pre-bored system was carried out to investigate the behavior of soil inside the pre-bored ring using Particle Image Velocimetry (PIV) method. The laboratory testing of soil index properties is conducted to estimate soil strength parameters, including internal friction angle φ, and Young's modulus *E*, and dilatancy angle ψ.

3.3 LABORATORY EXPERIMENTAL SETUP

In this section of the dissertation, the first aspect of experimental research, which deals with the lateral static and cyclic pile load-displacement tests, is explained in details. Macro-scale testing was performed to determine soil behavior due to cyclic lateral loading and to evaluate the effectiveness of this system. Figure 3-2 shows the experimental test setup, which is used in this study. An experimental study was performed using a pile model test in sandy soil that has different soil grain size and uniformity coefficient. Furthermore, measuring devices includes strain gauges, dial gauges, and load cell.

Testing apparatus consists of this following items:

1. Testing box

The testing box has the following dimensions: 300mm in width, 600mm in length, and 600mm in depth. The box was of wall thickness equal to 3cm made of rigid acrylic plates.

2. Servo Cylinder

The lateral static and cyclic loads are applied on the pile head with different loading frequencies by servo cylinder. The servo cylinder used in this research is RCP2-RA6C-I-56P-4 which has the maximum output force of 0.8 kN that can be applied by the servo cylinder, and the maximum stroke is 130 mm (Figure 3-3).

3. Data logger

The data logger of 9 channels was used to record data during testing.

4. Loading monitor

Loading monitor unit was used to control the number of applied cycles N, and for starting and stopping the lateral movement of the servo cylinder. This unit can supply up to 10,000 cycles per test.

5. Aluminum pile

This item was explained in details through Section 3.6.2 of this chapter.

6. Strain gauges

Strain gauges are attached on the pile model shaft to detect the bending moment created during the test. The sensor used in this research is strain gauge type FLK-2-23 for aluminum material (Figure 3-4).

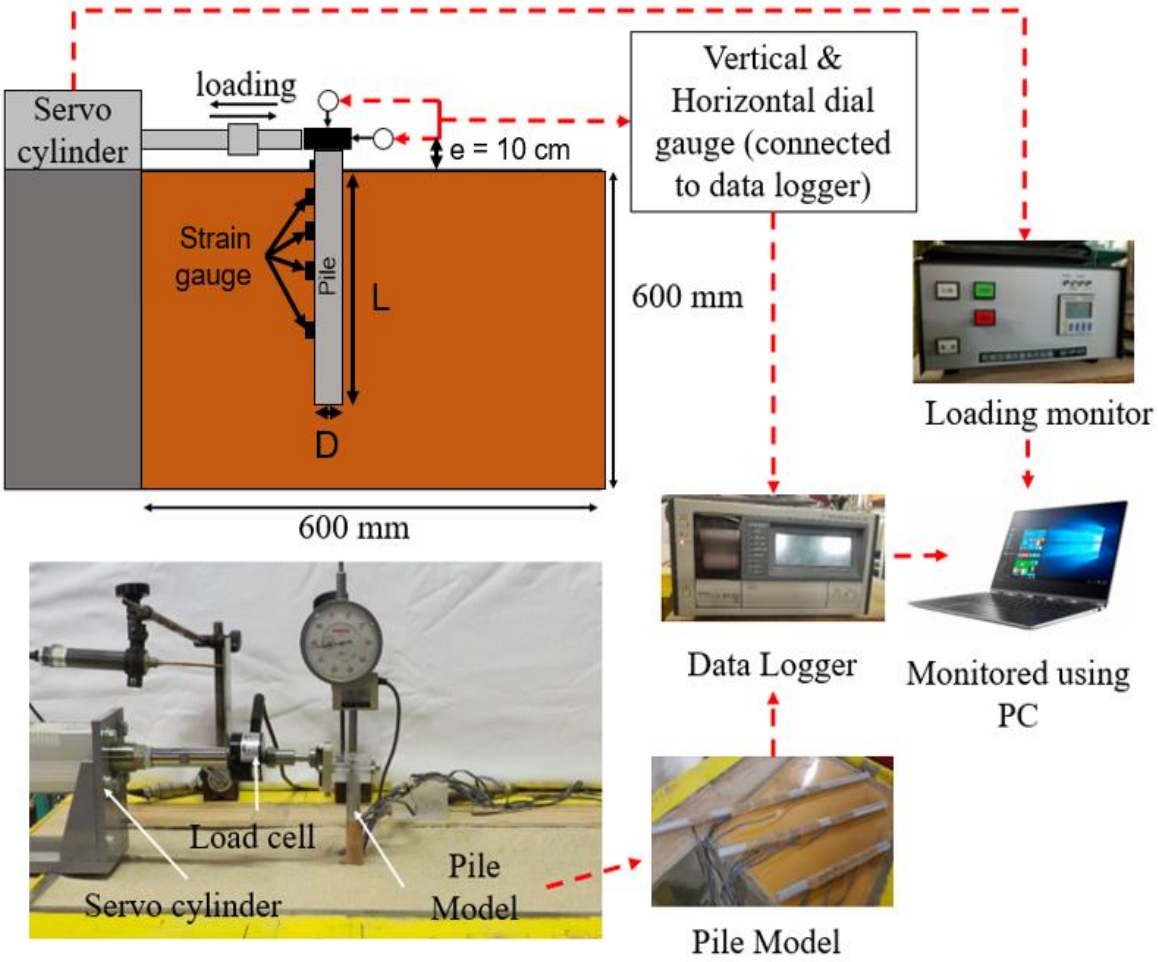

Figure 3-2 Experimental testing scheme

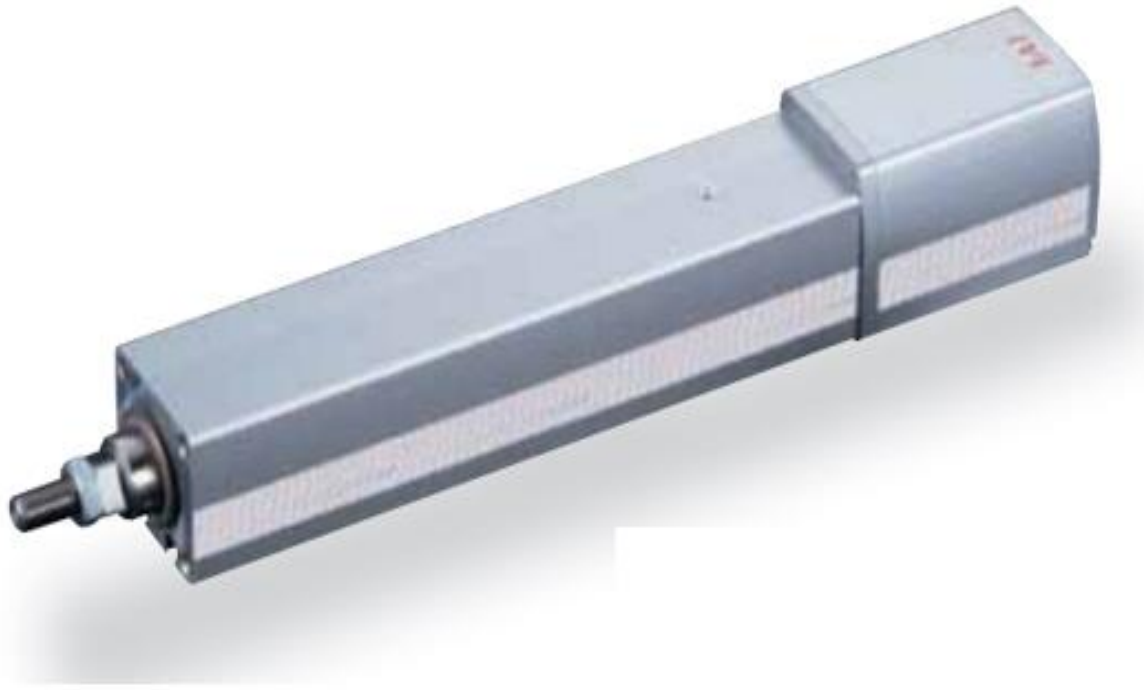

Figure 3-3 Servo cylinder of type RCP2-RA6C (https://www.iai-robot.co.jp)

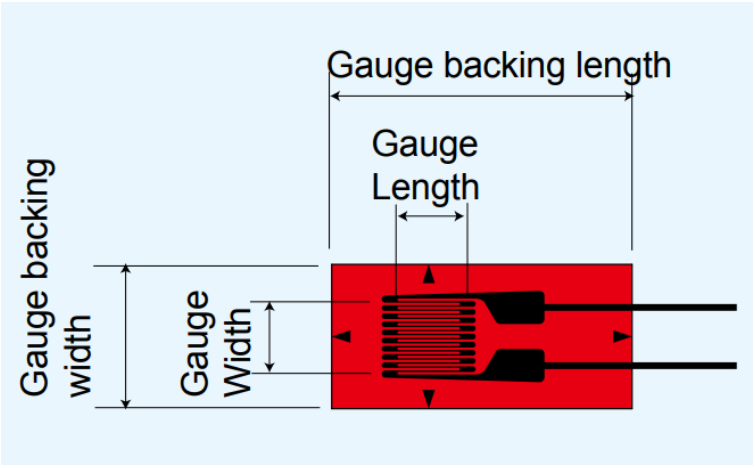

Figure 3-4 Strain gauges type FLK-2-23 attached to the pile model (https://tml.jp)

The schematic system for experimental test for one-layered ground soil system, two-layered ground soil system and pre-bored pile foundation system is shown in Figure 3-5.

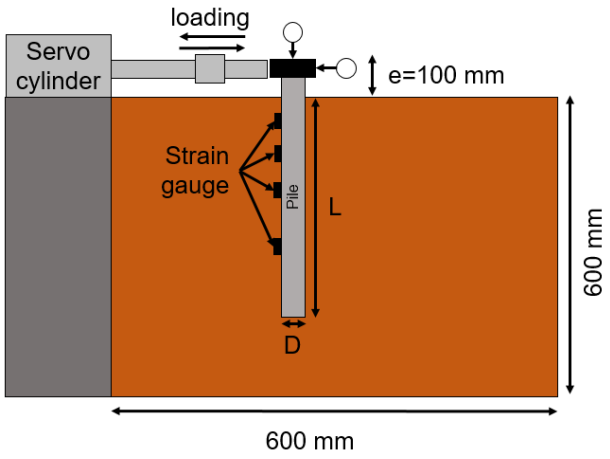

(a)

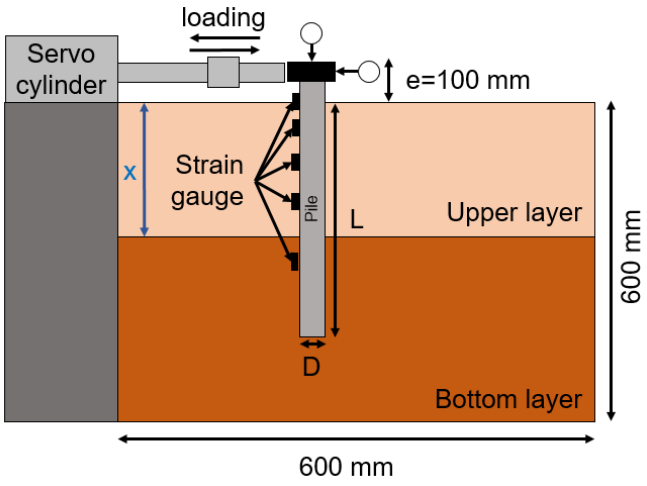

(b)

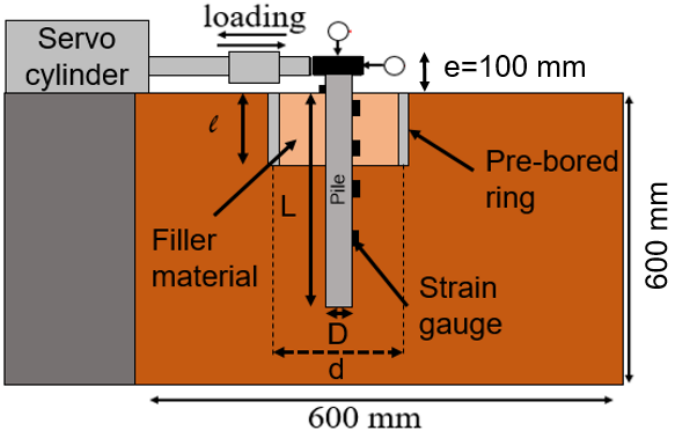

(c)

Figure 3-5 Schematic system for experimental test: (a) one-layered ground soil, (b) two-layered ground soil, (c) pre-bored pile foundation system.

3.4 **MATERIAL PROPERTIES**

3.4.1 Soil Properties

The soil, used in this experimental study, is sub-angular, Kumamoto sand type of K4 (medium sand) and K7 (fine sand) as the ground soil. The filler material uses five types of soil that are K-4, K-5, K-7, Toyoura sand, and Mix soil (mixed between K-4, K-5, K-7 to get the gap graded particle distribution). The index properties of each soil are given in Table 3-2.

The results were compared with the experimental test conducted by Awad-Allah and Yasufuku (2013), which used Toyoura sand type as a ground soil. Figure 3-6 shows the grain size distribution of the soil sample used in this study. In this study, two different states of relative densities (D_r) are considered, including medium density and dense sand of 50% and 80%.

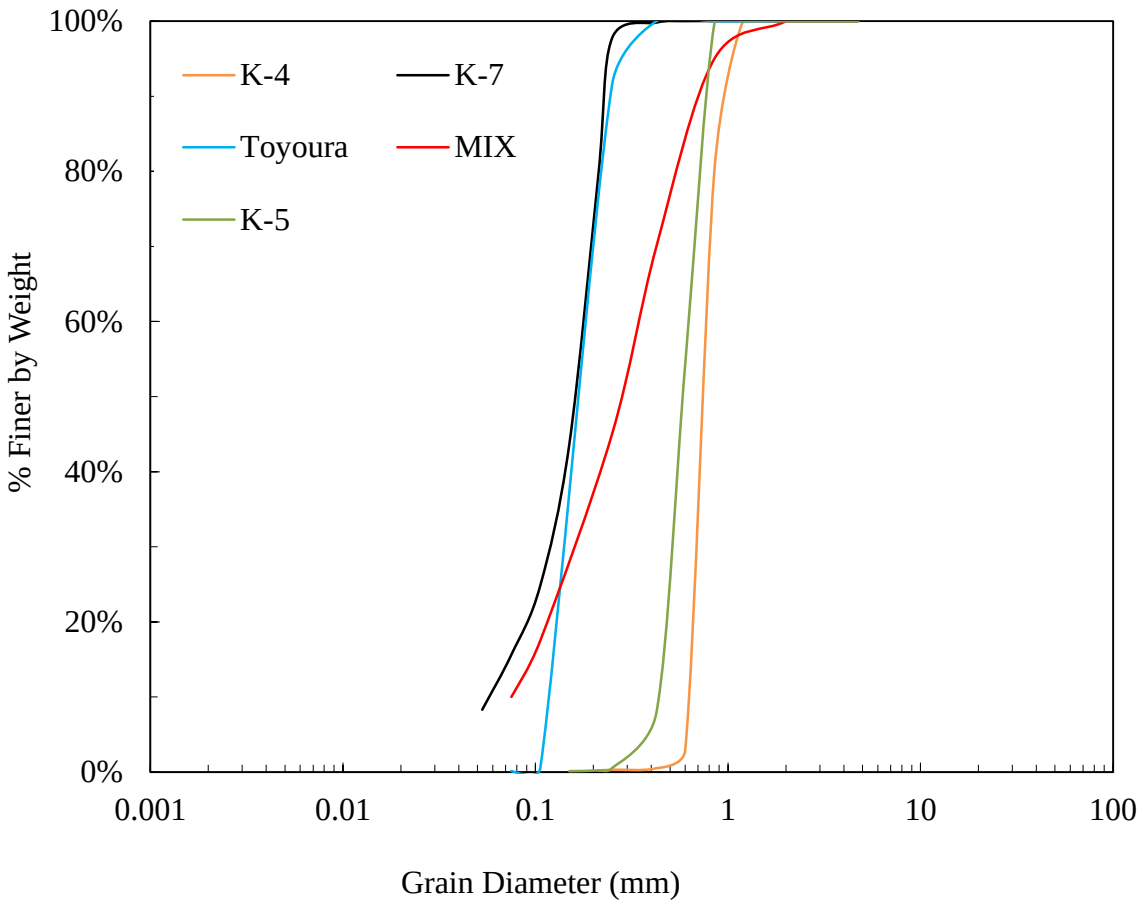

Figure 3-6 Grain size distribution of soil

Table 3-2 Index properties of ground soil

Soil properties	K-4	K-5	K-7	Mix soil	Toyoura
D_{50} (mm)	0.75	0.60	0.17	0.30	0.18
Uniformity coefficient (U_c)	1.24	1.33	2.96	4.67	1.4
Max. dry density	1.48	1.56	1.51	1.63	1.60
Min. dry density	1.24	1.27	1.18	1.30	1.31

3.4.2 Properties of Pile and Ring Model

The pile and ring models are manufactured from a closed-end aluminum alloy pipe, as shown in Figure 3-7. The outer diameter (*D*) of the pile model is 15 mm, with a thickness of 1.2 mm. Three different ring diameters (*d*) of 45 mm (3*D*), 60 mm (4*D*), and 75 mm (5*D*) with a thickness of 2 mm and 150 mm (10*D*) of ring length is used. The Young's Modulus of the used aluminum alloy pile model is $7x10^{10}$ KN/m^2. The detail properties of the pile and ring material are shown in Table 3-3.

Table 3-3 Properties of pile model using aluminum alloy 6061

Parameter	Value	Unit
Density	2.70	gr/cm^3
Ultimate tensile strength	89.60	MPa
Yield tensile strength	48.30	MPa
Elastic modulus	70000	MPa
Poisson's ratio	0.33	-
Fatigue strength	55.20	MPa
Shear strength	68.90	MPa

(a) (b)

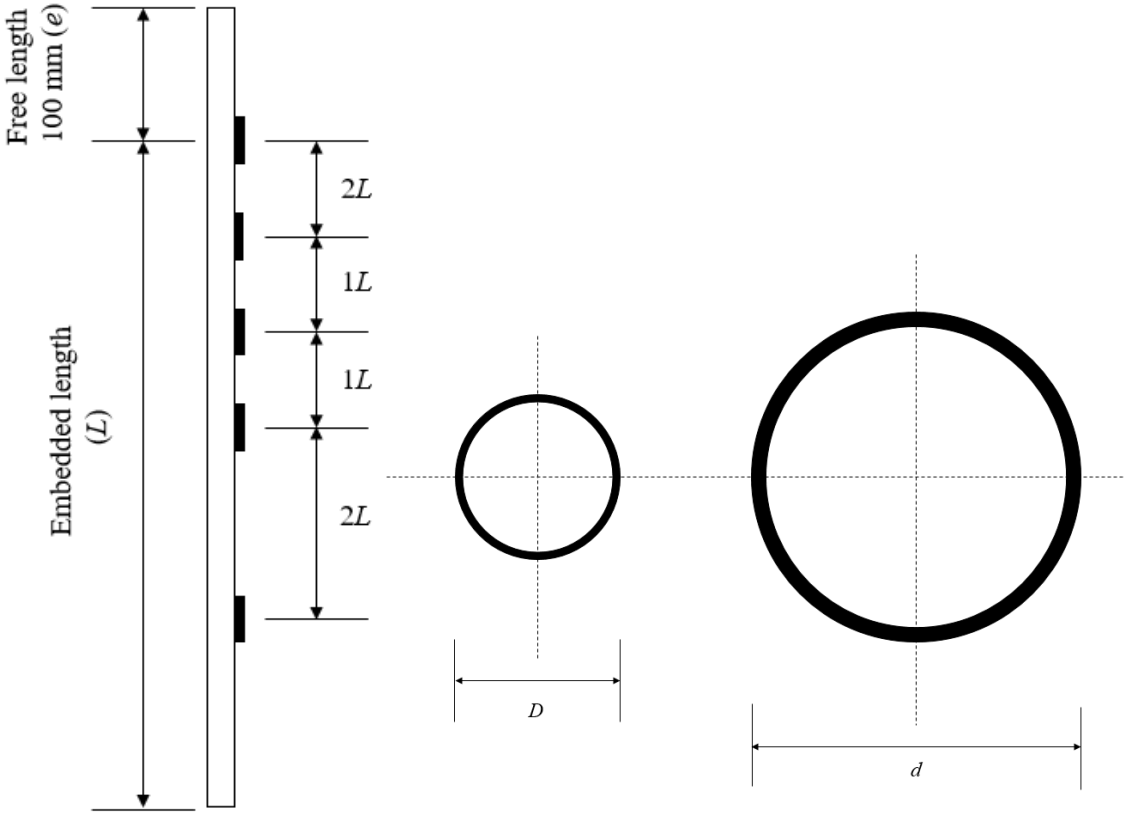

(c) (d) (e)

Figure 3-7 Pile and ring model used in this research: (a) pile model, (b) aluminum ring, (c) schematic figure of embedded pile attached with strain gauges, (d) cross-section of pile model, (e) cross-section of ring model

3.5 **SCALE FACTOR**

The experimental model is conducted at much smaller scales than the full-scale testing conditions. Full-scale testing is experimental testing where the parametric features are constructed based on a real scale. If the model is not conducted in the full-scale conditions, it needs consideration about the scale factor which can represent the model scale to the full-scale condition. Equivalence law is used for designing the model pile material, dimensions, the applied speed, and displacement. The scaling formula for the 1g model proposed by Wood et al. (2002) for pile flexural rigidity (*EI*) and length (*L*) are shown in Equation 3-1 and Equation 3-2, respectively.

$$\frac{E_m I_m}{E_p I_p} = \frac{1}{n^{4+\alpha}} \tag{3-1}$$

$$\frac{L_m}{L_p} = \frac{1}{n} \tag{3-2}$$

where:

E_m = modulus of elasticity of pile model,
E_p = modulus of elasticity of prototype pile,
I_m = moment of inertia of model pile,
I_p = moment of inertia of prototype pile,
L_m = length of model pile,
L_p = length of prototype pile,
n = scale factor
α = 0.5 for sands and 1.0 for clays (Woods et al., 2002)

In the experimental testing, the scaling factor for stiffness and length is adopted as n=15. Hence, if an aluminum tube pile model of outer diameter 15 mm and wall thickness 1.2 mm is used, it will be equivalent to a prototype of steel hollow pile of outer diameter 0.4 m with a wall thickness of 5 mm in terms of the flexural stiffness. Table 3-4 shows the parameters for prototype and model scale. Therefore, the model is valid for the interaction of soil and pile.

Table 3-4 Properties of pile model compared to pile prototype

Parameter	Prototype	Model	Unit
Material	Steel	Aluminum	-
Elastic modulus of the pile, E_p	200000	70000	MPa
Pile embedded length, L	4, 8, 12	0.15, 0.30, 0.45	m
Pile diameter, D	400	15	mm
Eccentricity, e	4.00	0.10	m
Ring diameter	1.2, 1.6, 2.0	0.045, 0.060, 0.075	m
Ring embedded length	4.00	0.15	m

3.6 CLASSIFICATION OF PILES RIGIDITY

Classification of pile rigidity in this research can be evaluated using the relative stiffness factor (K_{rs}). If the relative stiffness factor value is greater than 0.01, the pile is classified as rigid pile, and for relative stiffness factor value less than 0.01 the pile classified as a flexible pile. The relative stiffness factor is calculated using the equation proposed by Poulos and Davis (1980), as mention in Equation 4.1.

$$K_{rs} = \frac{E_m I_m}{E_p L^4} \tag{3-3}$$

where:

E_m = Elastic modulus of the pile model

I_m = moment of inertia of the model pile

E_s = Elastic modulus of soil

L = Embedded length of pile model

Table 3-5 shows the calculated values of (K_{rs}) for each pile used in this research. Based on the K_{rs} value, the pile models are classified as rigid piles for pile with slenderness ratio (L/B) of 10 (K_{rs} > 0.01), and flexible piles for pile with slenderness ratio (L/B) of 20 and 30 (K_{rs} < 0.01).

Table 3-5 Summarize of relative stiffness of pile

Relative density, D_r	E_s (N/mm^2)	L (mm)	L/B	E_mI_m (N.mm^2)	K_{rs}	Pile classification
Dense sand (D_r=80%)	7.59	150	10	5.98E+07	0.01557	Rigid
		300	20		0.00097	Flexible
		450	30		0.00019	Flexible
Medium sand (D_r=50%)	5.98	150	10		0.01977	Rigid
		300	20		0.00123	Flexible
		450	30		0.00024	Flexible

3.7 **LOADING MECHANISM**

The single piles were subjected to either static or cyclic lateral loading through a loading jack and applied on the pile head. During the laboratory test, two loading scheme under deformation control conditions is performed: monotonic test (static loading, N=0), and cyclic test (loading up to N=50 cycles). The objectives of conducting deformation control test rather than stress control test are: to obtain the real simulation of thermal displacement on a girder bridge induced in pile foundation, and to achieve ultimate lateral pile capacity at head displacement of 5% and 20% pile diameter; this mechanism will help to evaluate the ultimate lateral pile capacity. The load applied on the pile head assume as a pinned connection on the superstructure.

3.7.1 Actual Field Loading Conditions

Two-way symmetric cyclic lateral loading is horizontally imposed on two opposite sides of a pile head model to provide horizontal deflection on the pile head. Pile head displacement of 3 mm (20% of pile diameter) was applied for each side to evaluate the soil-pile behavior in one-layered soil and two-layered soil cases. In case of pre-bored pile foundation model test, pile head displacement of 1 mm (about 6% of pile diameter) was applied to evaluate the behavior of soil and pre-bored pile structure impacted by girder displacement due to thermal force. Khodair and Hassiotis (2005) show the thermal loading, equivalent to a change in temperature up to 42 °C, is corresponded to a change in displacement up to 0.023 m (about 6-7% of pile dimension) with pile dimension design of 0.376 m x 0.356 m. The cyclic lateral load is applied to 0.008 Hz (y=3mm) and 0.020 Hz (y=1mm), and it is applied to 50 cycles in all experiments, so it generally can simulate the impact of the slow cyclic lateral displacement loading of a girder bridge. The bending moment, lateral load capacity, horizontal displacement, and vertical settlement were measured and monitored during the experimental tests. Lateral cyclic displacement was applied to the pile head. Figure 3-8 illustrates the cyclic loading pattern of lateral load applied to the pile head model during experimental testing.

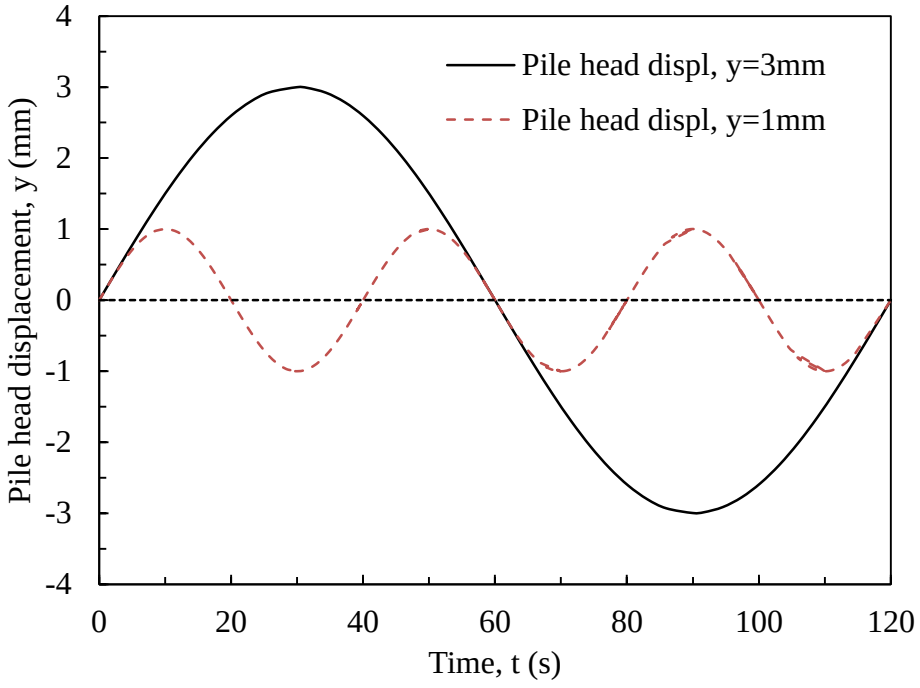

Figure 3-8 Typical sinusoidal harmonic lateral loading

3.7.2 Monotonic test loading

In monotonic loading, the pile head moves horizontally by displacement of 3 mm (20% of pile diameter). The lateral load and pile head displacement are measured, as shown in Figure 3-9. A monotonic load has been applied at the pile head for single piles in one-layered ground soil, which were installed into medium dense and dense sand of *Dr*= 50% and 80% with a loading rate of 0.1mm/s. During the experimental test, lateral pile head displacement (*y*), lateral load (*H*), and pile bending strain (ε) were continuously recorded.

3.7.3 Cyclic test loading

In cyclic loading, a symmetrical cyclic lateral load is applied horizontally on two opposite sides of pile head that simulate the impact of girder bridge expansion on pile foundations. The input displacement cycle at pile head is as follows: pile head is pushed laterally by 3 mm, and it is pulled back in the opposite direction laterally by 6 mm, then it pushed back by 3 mm (i. e., set back to initial position), as shown in Figure 3-10. The same condition also applied in 1 mm of pile head displacement case. Cyclic lateral displacement is applied for 50 cycles in all experiments. The pile is loaded horizontally only, the vertical load being.

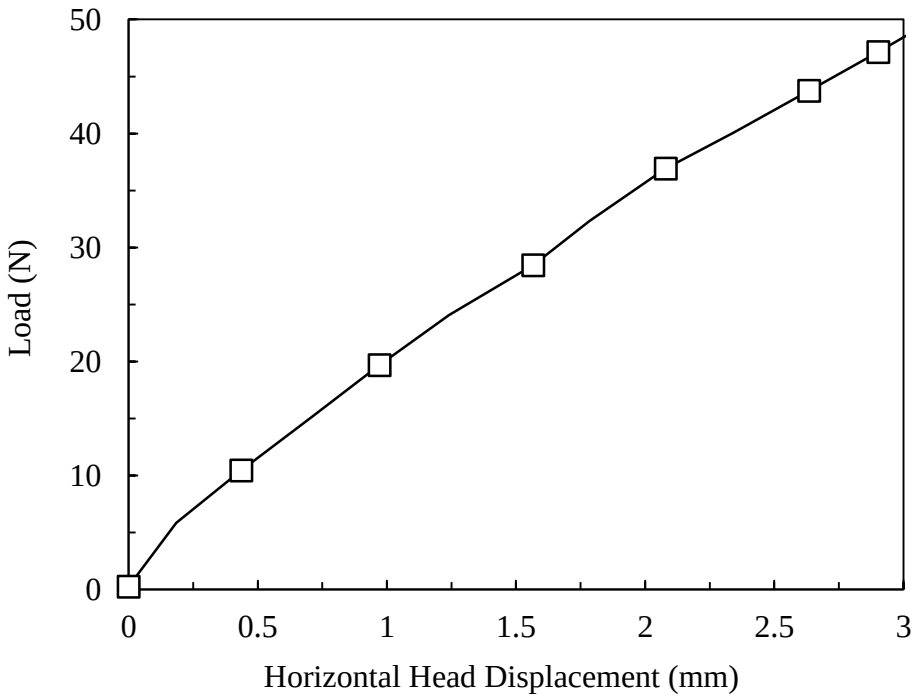

Figure 3-9 Typical result of a monotonic test for single pile

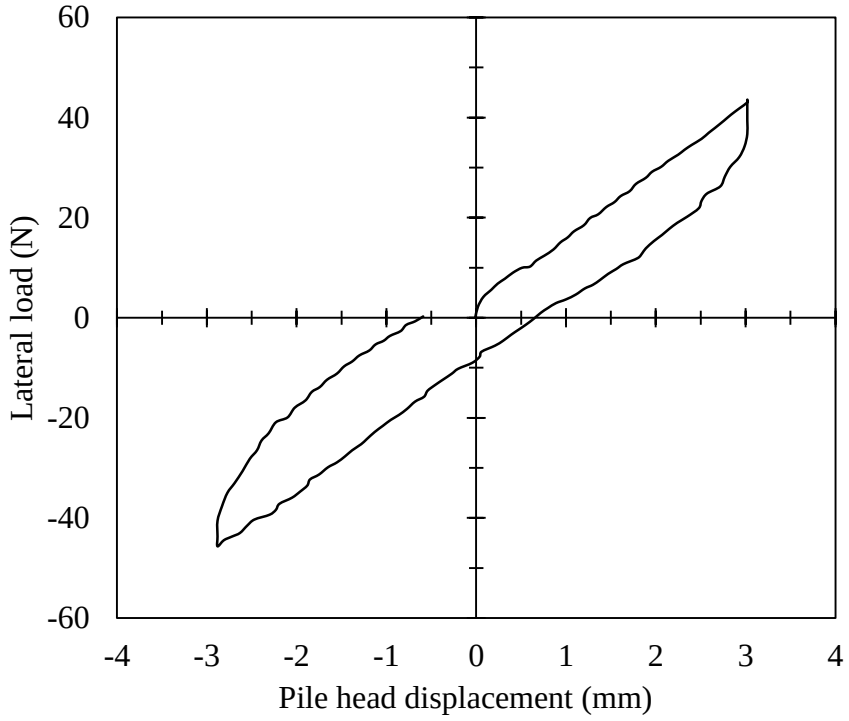

Figure 3-10 Symmetrical cyclic lateral displacement corresponding to lateral load

3.8 **PROCEDURES OF EXPERIMENTAL TESTING**

3.8.1 Preparation of ground soil

The relative density of soil was achieved using Multiple Sieving Pluviation (MSP) method (Miura and Toki, 1982) as shown in Figure 3-11. They introduced a method for preparation of sand samples using MSP apparatus by controlling the rate of sand discharge. The medium density and dense sand of relative densities of 50% and 80% have been achieved by using this method. The height of the falling and nozzle diameter can control the rate of sand discharge. The calibration of the height and nozzle diameter was conducted to obtain the targeted density. The advantages of using this method are protecting sensors attached to the pile from damage, and producing homogenous testing ground around the pile without applying vibration or impact load.

However, for the soil contained fines aggregate or non-uniform soil such as K-7 sand, this method cannot significantly have used for soil preparation in a massive amount of soil. Based on the calibration results of the apparatus, as shown in Figure 3-12, for K-7 sand, it needs a

very high height of falling to reach the high density. This conditions occurred because the K-7 sand contained a fines particle that becomes dust and flies away when the sieving process carried out, so the particle distribution of ground soil might be changed. For the high density of K-7 ground soil, compaction process was conducted to achieve the high density of ground soil.

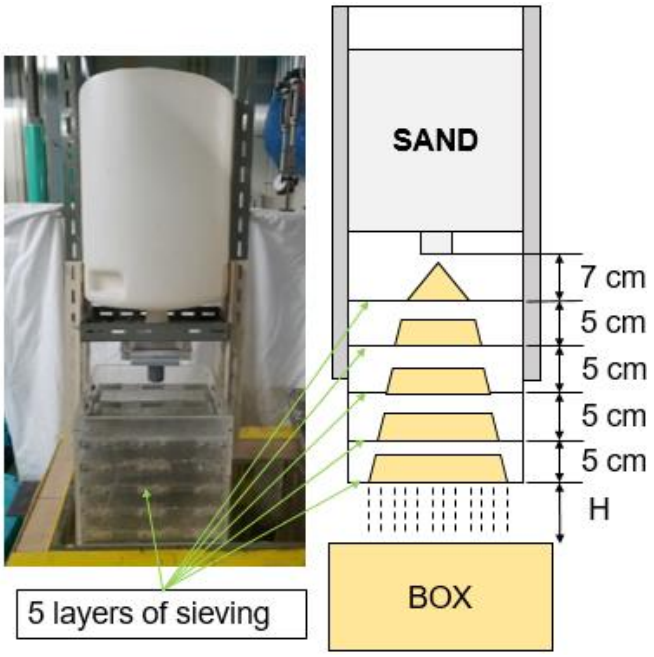

Figure 3-11 Multiple sieving pluviation (MSP) method by Miura and Toki (1982)

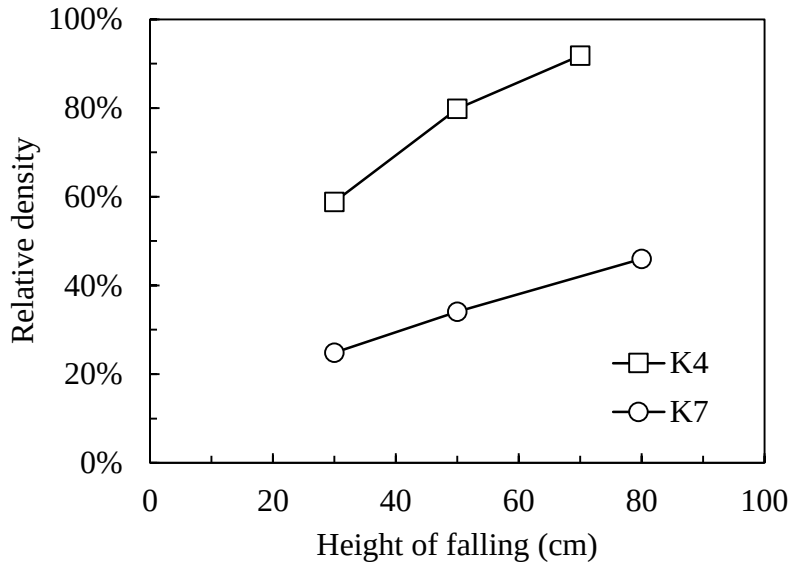

Figure 3-12 Calibration graph of Multiple sieving pluviation (MSP) apparatus

Figure 3-13 Pile model clamping on a guide bar during soil setup

3.8.2 Test procedures

The following steps are performed for experimental testing of the single pile under monotonic and cyclic lateral loading:

1. The testing box is cleaned up to make sure that there are no other materials inside the box.
2. Pile model is placed at the center of the testing box by clamping it on a guide bar to make sure the position of the pile in the horizontal and vertical axis, as shown in Figure 3-13.
3. Then, sand is poured in carefully, slowly, and evenly layers of 10 cm of thickness using the previously described method Miura and Toki (1982).
4. For the soil that cannot set up by MSP, the compaction method was used to set up the ground soil every 10 cm of layer thickness according to the ground density, volume of box and weight of soil.
5. After reaching the target surface layer of sand, the guide bar is removed and the top surface is flattened.
6. Lateral cyclic cylinder jack and other devices are assembled to the pile head.
7. The loading frequency (f) and the number of cycles (N) are adjusted through the external control unit, which is connected by computer and data logger.

3.9 SUMMARY

This chapter focus on the development of a small-scale (1g) lateral pile test condition which is capable of simulating the soil-pile behavior and failure mechanism on a pre-bored pile foundation system in integral abutment bridges due to cyclic lateral displacement. The experimental laboratory testing conducted in this research included: determining the properties of ground soil and filler material, experimental test setup, loading mechanism applied on pile model, and experimental test procedures. Static and cyclic lateral loading tests were performed from the aspects of instrumentation, features, and scaling factors compared to actual field scale. The summary of this chapter can be described generally as follows:

1. A small-scale lateral static and cyclic test setup (1g laboratory model) has been developed to evaluate the behavior of pre-bored pile foundation system which consists of testing box, LDVT, lateral loading servo cylinder, strain gauges, earth pressure sensors, and data acquisition system.
2. The features of this apparatus are the ability: to simulate the effect of lateral cyclic loading created due to girder displacement on pre-bored pile foundation, that can control the loading frequency, loading amplitude and the number of cycles. The behavior of pre-bored ring and filler material also can be controlled to determine the optimum design. The attachment of strain gauge, especially on the top area of the pile, can measure the pile bending moment along the pile body and pile displacement.
3. In the 1g laboratory model, the lateral loading is applied on the top of the pile head which embedded in sandy ground soil. Evaluation of pre-bored pile foundation system was obtaining in dry condition of ground soil and filler material. Filler material of the pre-bored system is evaluated using sandy soil properties such as soil uniformity coefficient, particle diameter and density.

3.10 REFERENCES

Awad-Allah, M.F., and Yasufuku, N. Comparative Study between the Methods Used for Estimating Ultimate Lateral Load of Piles in Sandy Soil. Proceedings of the 5th International Young Geotechnical Engineers' Conference, Paris, France., 2013, pp. 165-168.

Awad-Allah, M.F. and Yasufuku, N. Performance of Pile Foundations in Sandy Soil Under Slow Cyclic Lateral Loading. The 5th International Geotechnical Symposium on Geot. Eng. For Disaster Prevention & Reduction, Incheon, 2013, pp. 291-300.

Awad-Allah, M.F., Yasufuku, N. and Mandandhar, S. Three dimensional (3D) failure pattern of flexible pile due to lateral cyclic loading in sand. Lowland Technology International. 19 (1). 2017, pp. 1-12.

Dunker, Kenneth F, and Liu, Dajin. Foundations for Integral Abutments. Pract. Period. Struct. Des. Constr., 12(1), 2007, pp. 22-30.

Japanese Geotechnical Society Standard, JGS 0524. Method for Consolidated-Drained Triaxial Compression Test on Soils.

Japanese Industrial Standard, JIS A1202 Test Method for Density Of Soil Particles

Japanese Industrial Standard, JIS A1204. Test method for particle size distribution of soils. Methods and Explanation for Soil Test.

Japanese Industrial Standard, JIS A1224. Test Method for Maximum and Minimum Densities of Sands.

Japanese Industrial Standard, JIS A 1203. Test Method for Water Content of Soils. Methods and Explanation for Soil Test.

Khodair, Yasser A and Hassiotis, Sophia. Analysis of Soil–pile Interaction in Integral Abutment, Computers and Geotechnics 32, 2005, pp. 201–209.

Miura, S. Toki, S. A simple preparation method and its effect on static and dynamic deformation-strength properties of sand, Soils and Foundations, 22 (1), 1982, pp. 61-77.

Poulos HG and Davis EH (1980). Pile Foundation Analysis and Design. John Wiley & Sons New York.

Wood, M. D., Crewe, A. and Taylor, C. Shaking table testing of geotechnical models, International Journal of PhysModell Geotech 1, 2002, pp.1–13.

CHAPTER IV

EVALUATION OF FILLER PROPERTIES ON PRE-BORED RING FOUNDATION SYSTEM

4.1 INTRODUCTION

In this chapter, the effectiveness of filler material properties such as soil uniformity and density are evaluated to reduce the pile bending moment. The effective dimension of the pre-bored hole that can maintain the bending moment of the pile foundation also evaluated in this chapter. The holes in empty condition may cause long-term maintenance problems, so the holes should be filled with an elastic material, such as bentonite, loose sand, or pea gravel. The previous researchers only focus on the structural system, but the behavior of soil and soil response due to the flexible piling design is still rarely explained. The characteristic of filler material and standard design of this foundation system is still in development. The appropriate filler properties and the dimension of this system are expected to reduce the bending moment along with the pile due to lateral displacement loading, which can solve the problem on the integral abutment bridge foundation. The effective system is evaluated by considering the soil behavior due to cyclic lateral loading on the pile foundation.

4.2 LATERALLY LOADED PILE IN ONE-LAYERED SOIL GROUND

In this section, the behavior of laterally loaded pile constructed in one-layered ground soil is evaluated with different pile slenderness ratio and different ground soil properties such as (D_{50} *and* U_c). Influence of ground soil density also evaluated.

4.2.1 Lateral Capacity

Monitoring of lateral loading (H) and lateral displacement (y_H) was also measured by using load cell and dial gauge that was recorded using data logger and PC. The incremental ratio gives the tangent stiffness modulus of the system.

1. Monotonic loading

Results of lateral pile capacity with different soil ground density and pile slenderness ratio are shown in Figure 4-1. It was observed that the maximum lateral pile capacity under the

monotonic load influenced by pile slenderness ratio and ground soil density. The longer pile embedded length and the higher density of ground soil provide the higher pile lateral capacity. In this case, the K-7 with high density provide the highest value of the lateral load. However, in the case of medium density, the K-7 sand provides the lowest lateral load than the other soil.

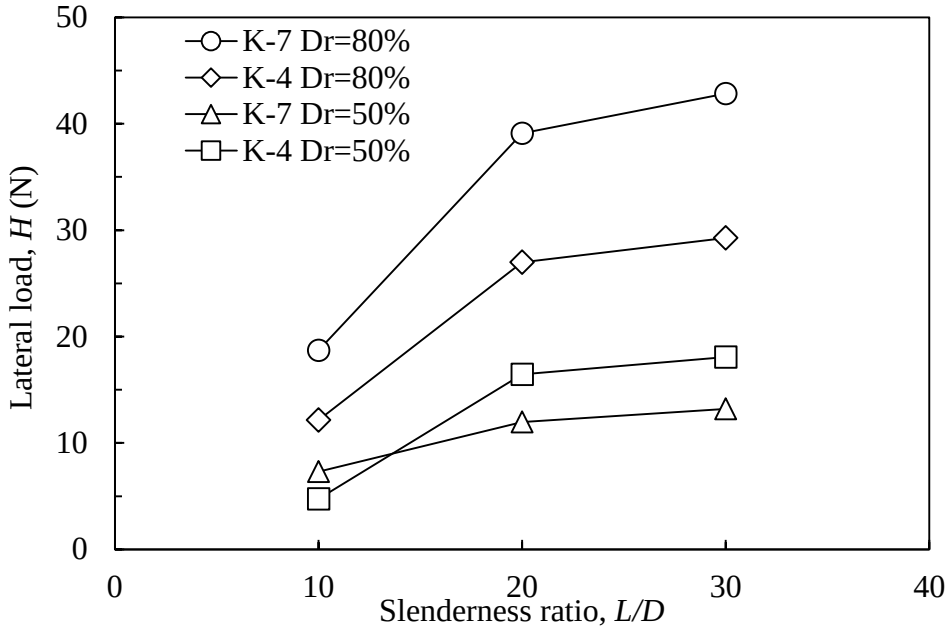

Figure 4-1 Effect of pile slenderness ratio due to the static lateral loading

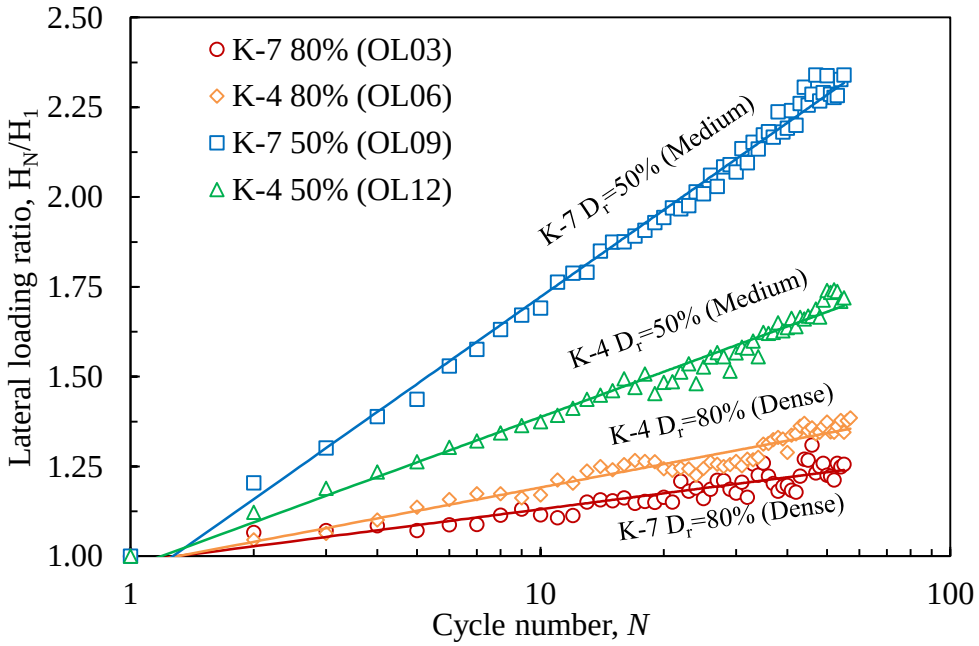

Figure 4-2 Effect of cyclic lateral loading on pile lateral capacity

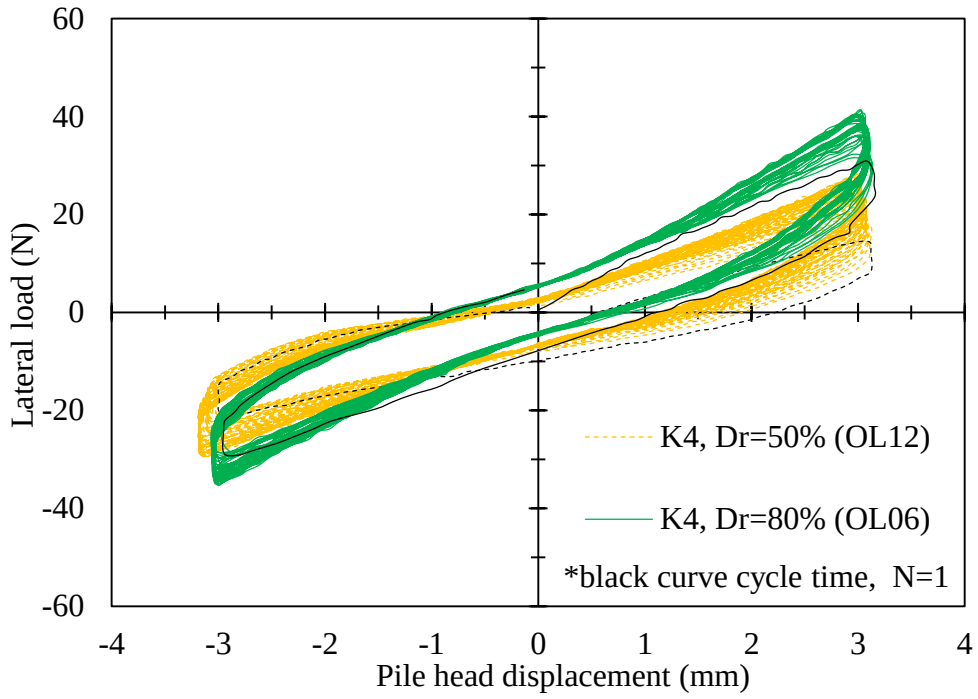

(a)

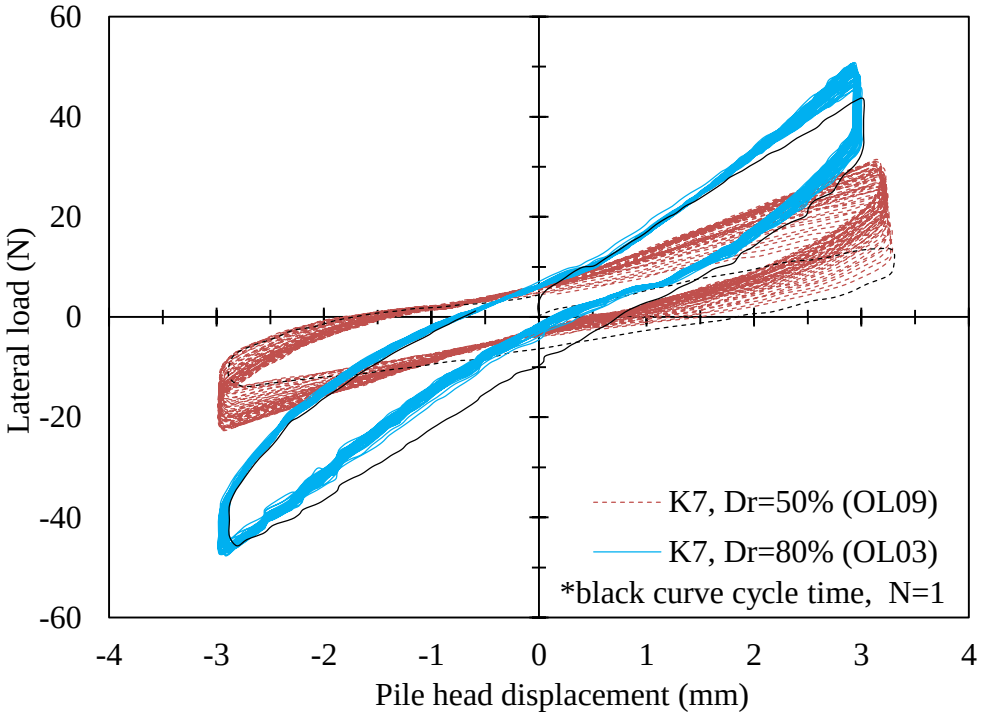

(b)

Figure 4-3 Cyclic load-lateral displacement curves for single piles in dense and medium-density soils: (a) K-4 sand ground soil, (b) K-7 sand ground soil

2. Cyclic loading

Figure 4-2 shows the cyclic effect on pile lateral capacity on the top of the pile foundation. The effect of cyclic loading on the lateral capacity of the pile is evaluated using the parameter of (H_N/H_1). H_N is the lateral load on N cycles, and H_1 is the lateral load in the initial condition at the first cycle. In the case of ground soil with medium density, the increase of lateral loading is higher than the dense ground soil. The increasing of lateral pile capacity on K-7 with medium density provide the highest value of 2.3 times under 50 times of cyclic loading. Typical results of cyclic lateral loading tests are shown in Figure 4-3 for each K4, and K7 sand with high and medium density and the cyclic loading is performed to 50 cycles. Based on Figure 4-3, it can be noticed that the first loading cycle generates a lower lateral load then increase during the cyclic loading until it reaches 50 times of cyclic load. The tangent stiffens related to the first cycle is lower than those related to the cyclic phase. The stiffness increases with the number of cycles, *N*, tending then towards a maximum value. This happened due to cyclic loading leads to hardening of sandy soil and reduction of void ratio. Consequently, enhancement of soil properties occurs for loose sand, and confining pressure increases during cyclic loading.

4.2.2 Bending Moment

In most cases, the maximum bending moment of the pile is considered as the key parameter in laterally loaded piles design. The main focus of this experiment is pile bending moment measurement, which is periodically monitored by using attached strain gauges along with the pile. Then, those measured values were analyzed, and the maximum measured value (M_m) was normalized against the yielding moment (M_y). The normalized bending moment, which is the ratio of the measured bending moment to the yielding moment of pile material (M_m/M_y), were estimated. The bending moment is calculated from the bending strain measured at various points along the length of the instrumented model piles using the following equation.

$$M_m = \frac{E_m I_m \varepsilon}{r} \qquad (4\text{-}1)$$

Yielding moment (M_y) of the pile model is calculated by using Equation 4-2, with σ_y is yield stress of model pile material.

$$M_y = \frac{\sigma_y I_m}{r} \tag{4-2}$$

where,

E_m = Young's modulus of the model pile model material,

I_m = moment of inertia of the model pile,

ε = measured bending strain and

r = horizontal distance between strain gauge position (outer surface of the pile) and neutral axis.

1. Monotonic loading

Figure 4-4 shows the results of the normalized bending moment along the pile body under lateral loading for three different pile embedded length. Based on the results, longer embedded pile length provides a higher maximum bending moment, especially on the flexible pile, because on the flexible pile the bottom layer of the pile is restrained by high soil pressure and the bending occurred on the upper area of the pile which has smaller soil pressure. The rigid pile results in a small bending moment because the restrained soil pressure is very small that can inflict the rotation on the pile. This conditions occurred on both medium and dense ground soil.

Figure 4-5 illustrates the relationships between normalized bending moment and pile depth for single piles constructed into medium dense sand (D_r=50%) and dense sand (D_r=80%) in K-4 sand and K-7 sand under static lateral loading. It is noticed that the higher density provides a higher bending moment. K-7 sand with high density provides three times higher bending moment value than the medium density. While the high density of K-4 sand provides 1.5 times higher bending moment value than the medium density, it indicates the potential of increasing bending moment on the K-4 sand that has lower uniformity coefficient, is smaller than the K-7 sand. The maximum bending moment location and point of rotation (bending moment ≈ 0) also changed on the different soil density. This phenomenon occurred due to the different stiffness of dense and medium density of soil. Dense sand provides a lower point of rotation due to the soil stiffness is higher to hold the pile movement.

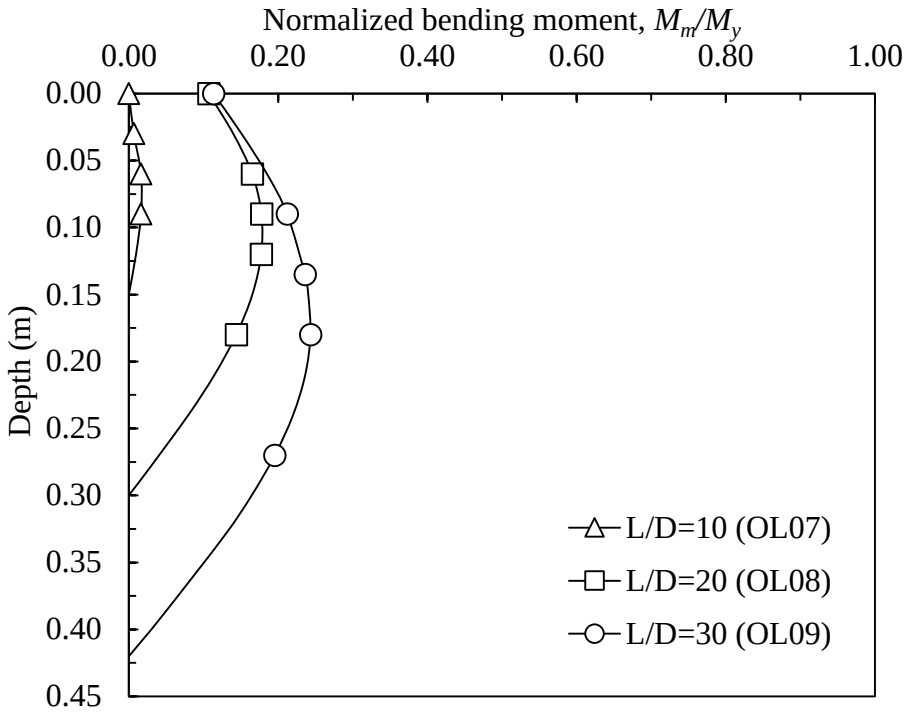

(a)

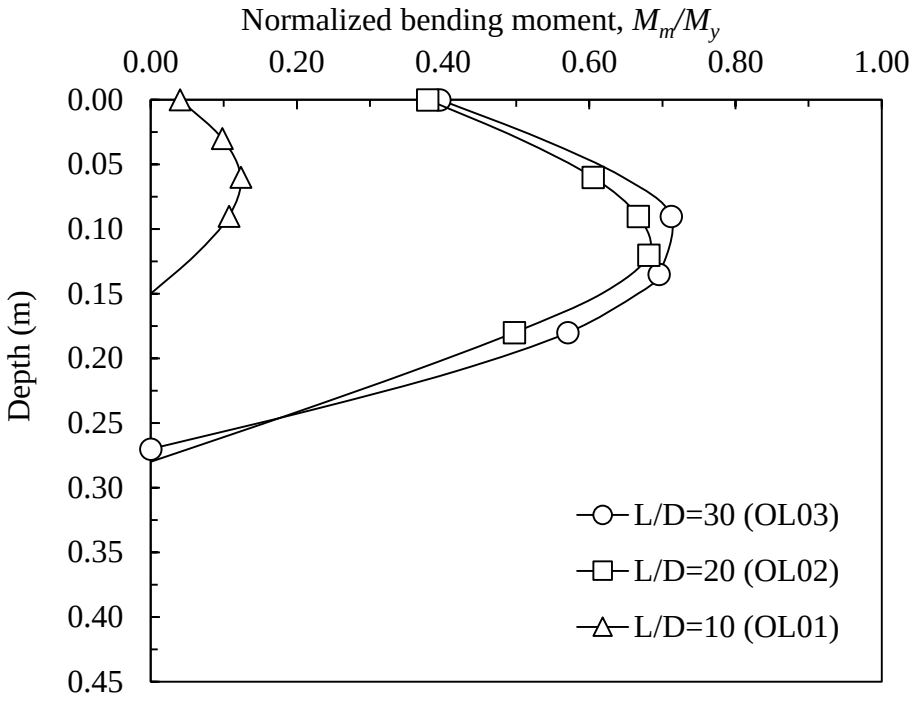

(b)

Figure 4-4 Effect of pile slenderness on bending moment: (a) medium sand ground soil and (b) dense sand ground soil

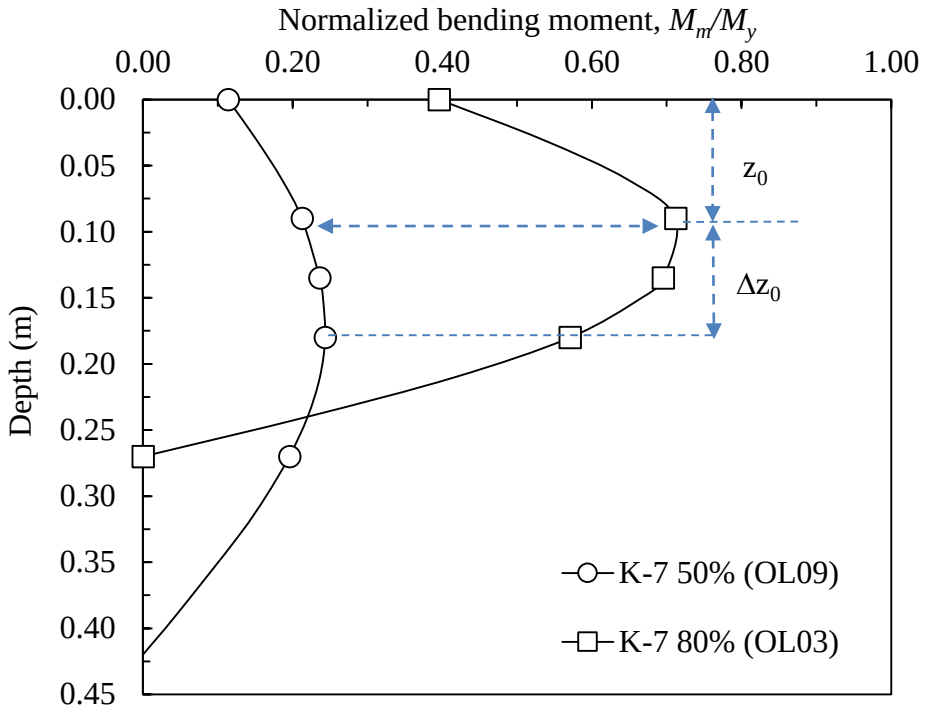

(a)

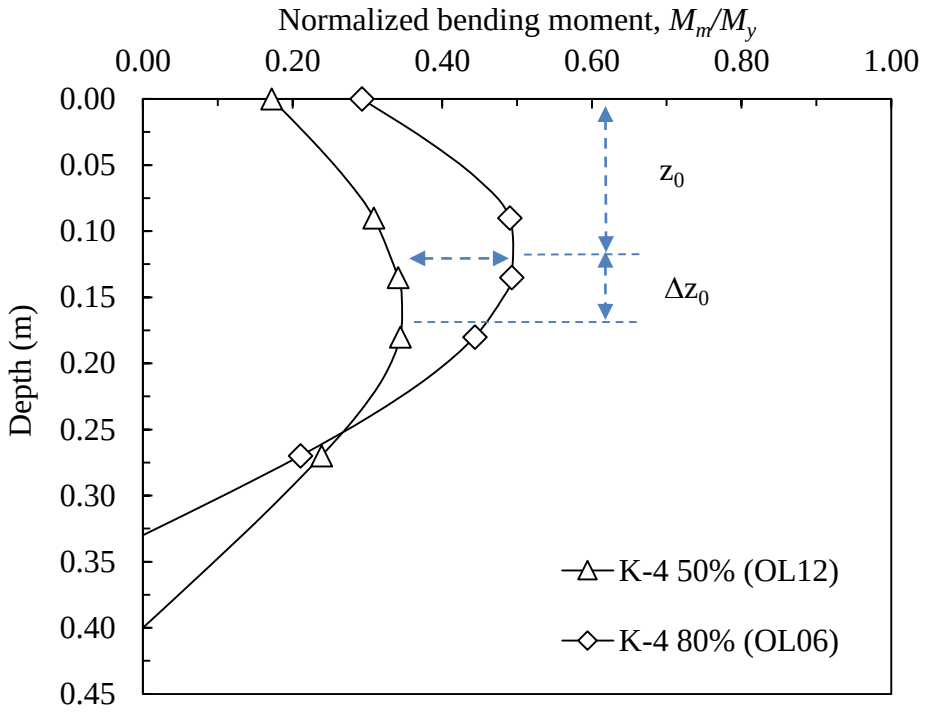

(b)

Figure 4-5 Effect of soil density on bending moment: (a) K-7 sand ground soil, (a) K-4 sand ground soil

2. Cyclic loading.

The effect of cyclic lateral loading is evaluated in this section based on the value of bending moment ratio (M_N/M_1). M_N is the bending moment of the pile in N cycles, and M_1 is the initial bending moment at the first cycle. The cyclic lateral loading effect is shown in Figure 4-6. Based on Figure 4-6, the bending moment of pile foundation on K-7 sand ground soil with medium density increase significantly until 2.5 times under 50 times of cyclic loading. The bending moment ratio for the K-4 medium, K-4 dense, and K-7 dense until 50 times of cyclic loading are 1.7, 1.4, and 1.3 respectively. The value of bending moment ratio under cyclic loading in the K-7 sand with medium density is the highest increasing ratio than the others. The range of bending moment ration between medium and dense ground soil for K-7 sand provide a different high range of bending moment ratio from 1.3 and 2.5. Whereas, the K-4 sand ground provide the lower range of bending moment ratio between medium and dense sand from 1.4 to 1.7. It indicates that the K-4 sand which has lower uniformity (U_c = 1.24) provide more stable bending moment during cyclic loading than the K-7 sand (U_c = 2.96), so the densification potential on the uniform soil is very low.

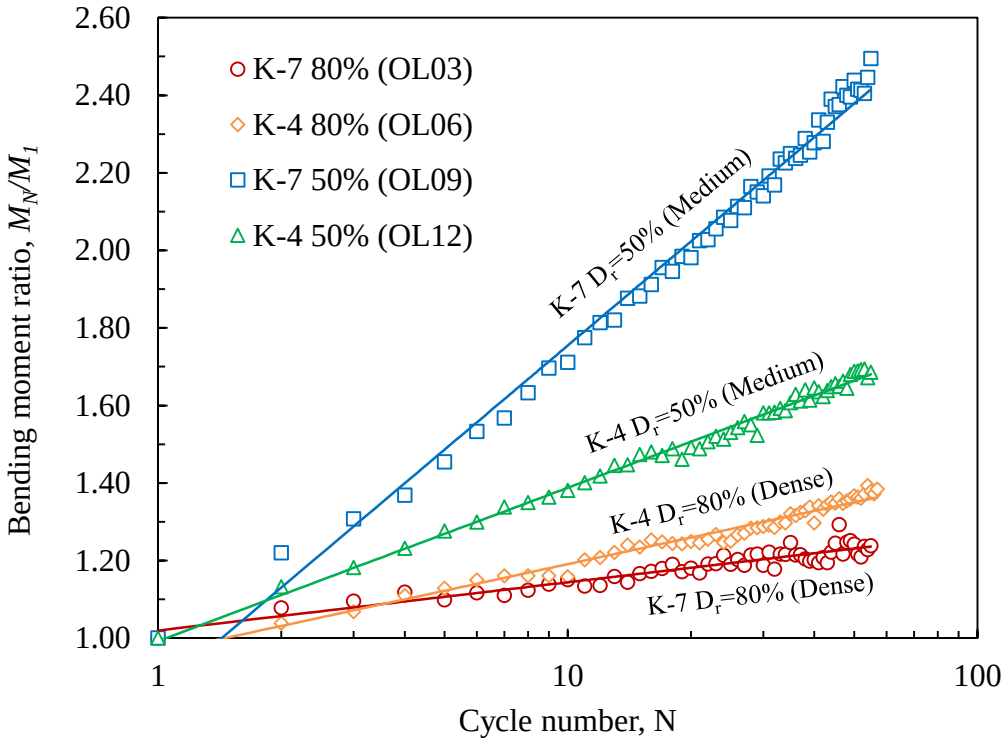

Figure 4-6 Effect of cyclic lateral loading on medium and dense soil

Due to cyclic lateral loading, degradation or amplification of "*p-y*" curves may occur depending on soil properties and depth from the ground surface. Table 4-1 shows the values of degradation factors (*r*) for p-y curves at certain soil layer depth below the ground surface. These factors are calculated using Equation (4-3):

$$r = \frac{p_N}{p_1} \tag{4-3}$$

where:

p_N = soil reaction on Nth loading cycle and;

p_1 = soil reaction during the monotonic test (N=0)

Figure 4-7 shows the variation of *r*-factor with the layer depth below the ground surface and the number of cycles. It indicates that the most affected area due to cyclic lateral loading is on the top area of the pile. Based on the test results, the area that potentially affected by lateral cyclic loading is about nine times of pile diameter (135mm in this case). It is also following Awad-Allah et al. (2017) that explained the failure pattern of the laterally loaded pile is about 9D from the surface in the case of 3 mm lateral pile head displacement.

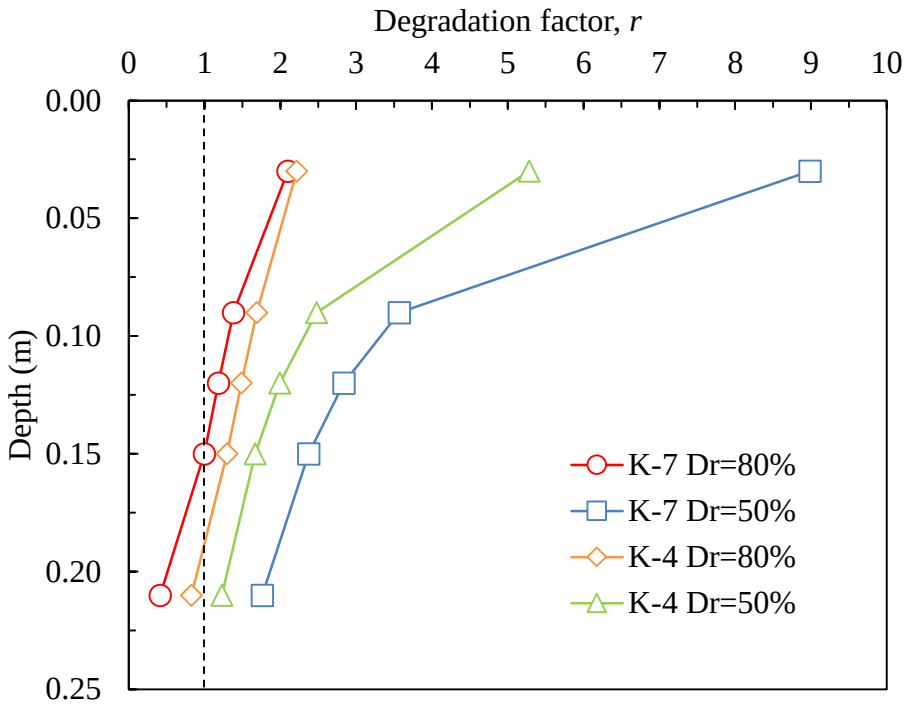

Figure 4-7 Degradation factor after 50 times of cycle for every depth

Table 4-1 Summary of degradation factor in one-layered ground soil

Soil ground	Degradation ratio, r				
	z=0.03 m	z=0.09 m	z=0.12 m	z=0.15 m	z=0.21 m
K-4 Dr=50%	5.28	2.47	1.99	1.66	1.22
K-4 Dr=80%	2.21	1.69	1.48	1.29	0.82
K-7 Dr=50%	8.98	3.56	2.83	2.37	1.76
K-7 Dr=80%	2.09	1.38	1.18	0.99	0.41

4.2.3 Comparison with previous researcher results

Figure 4-8 shows the effect of the ground soil type for each pile slenderness ratio compared with the results from Awad-Allah and Yasufuku (2013). Pile with higher slenderness ratio provides the higher bending moment for all soil cases. It shows that soil with the higher grain size (D_{50}) and lower uniformity coefficient (U_c) such as K4 sand provides a lower bending moment with similar soil relative density. The cyclic lateral loading effect is shown in Figure 4-9 compared with the results from Awad-Allah et al. (2012) that used Toyoura sand as a ground soil. While the cyclic loading was conducted 50 times, there is no significant increase in the bending moment of piles in the sand with a lower uniformity coefficient compared with the higher uniformity coefficient soil ground. It indicates that small densification effect occurred due to the cyclic loading.

Figure 4-10 shows the summary of the bending moment due to static and cyclic loading on each soil type and density. Sand with high uniformity coefficient and high density provides stable bending moment during the cyclic loading, but the values of bending moment are so high. If the density is reduced to be medium, the bending moment will be smaller, and it will increase significantly of 54.71% (OL12) after 50 times of cyclic loading was applied. However, the sand with lower uniformity coefficient, such as K4 sand and Toyoura sand (Awad-Allah and Yasufuku, 2013), provides a stable bending moment during the cyclic loading.

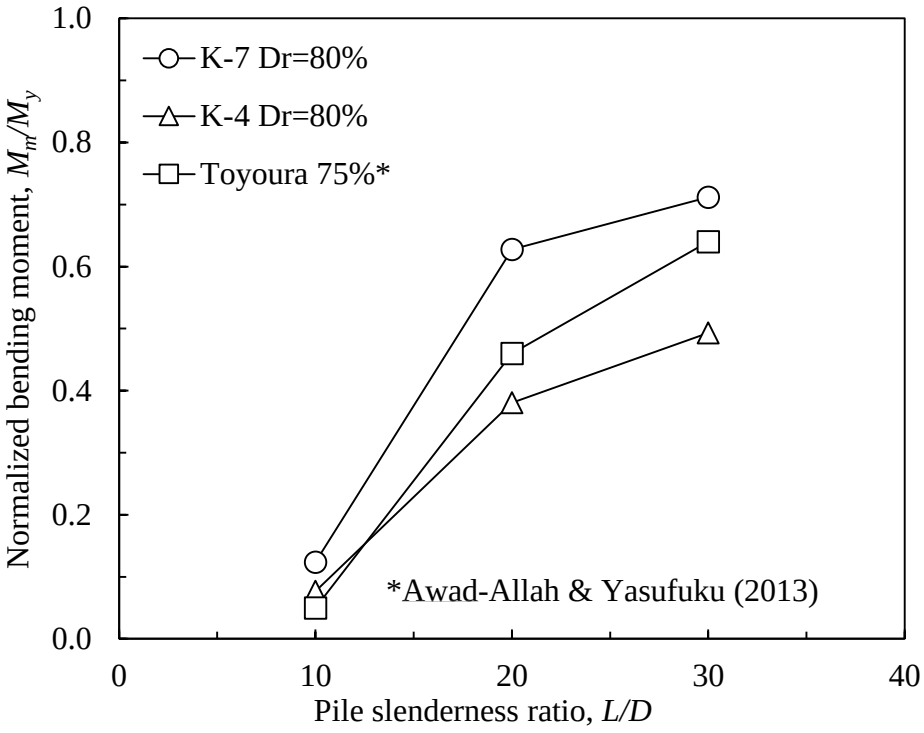

Figure 4-8 Effect of pile slenderness ratio due to the static lateral loading

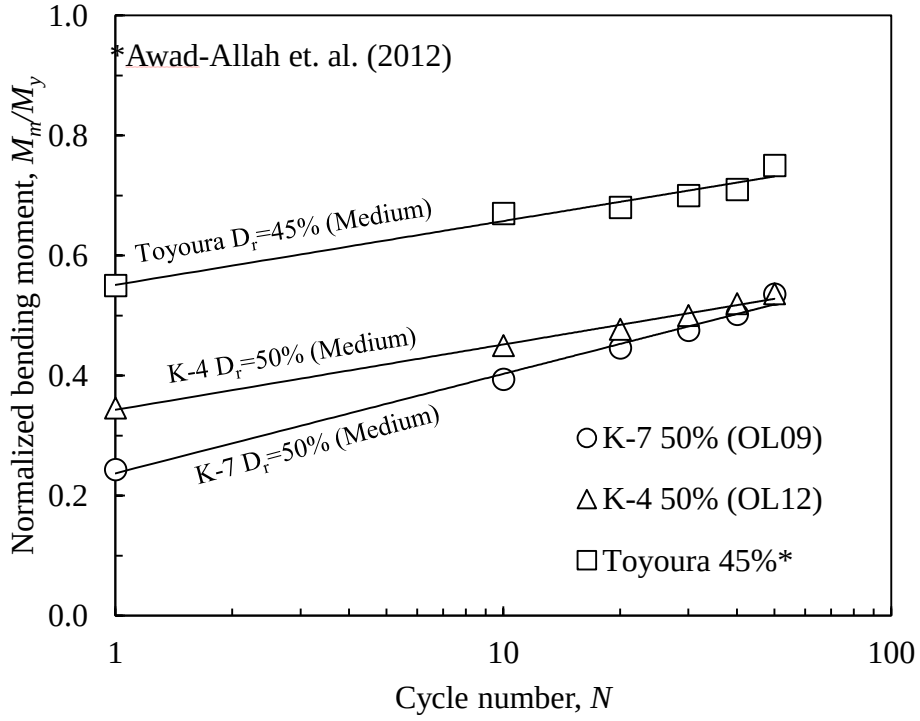

Figure 4-9 Effect of cyclic lateral loading on medium soil density

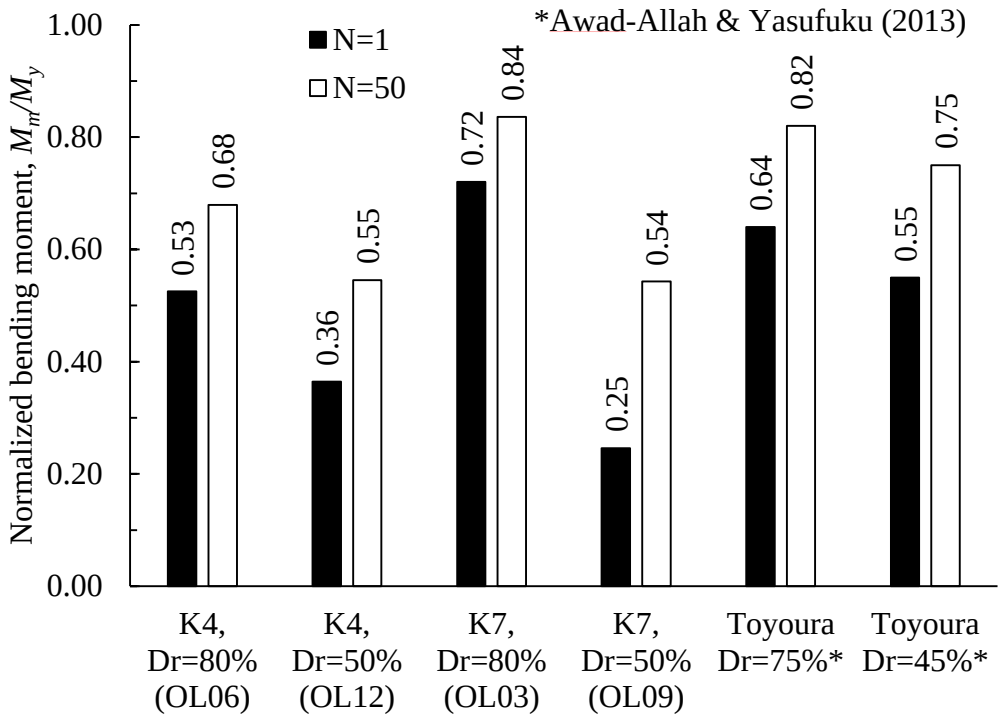

Figure 4-10 Summary of bending moment on each soil type

4.3 **LATERALLY LOADED PILE IN TWO-LAYERED SOIL GROUND**

Based on the results of one-layered ground soil tests, the most affected area due to cyclic lateral loading is on the top area of the pile. So to determine the effective system of pre-bored pile foundation, the upper area of the embedded pile is change with the uniform soil and evaluated with different thickness of the layer. Three different layer thickness was evaluated to determine the effective depth of the system. The effective pre-bored system depth determined by the depth of the top layer resulting in the most stable decrement of the bending moment. Figure 4-12 illustrates the effect of the laterally loaded pile in the two-layered soil to the maximum normalized bending moment of the pile with the variation of top layer depth. Based on the result, it shows the maximum bending moment of the pile can be reduced by changing the topsoil layer using the uniform sandy soil. There is no significant further reduction of bending moment is observed by changing the top layer depth beyond the layer depth ratio (x/D) of 3 for static lateral displacement loading. The result is following Yang and Robert (2006), that explained the lateral performance of a pile was highly affected by the stiffness of the surface with the layer depth ratio (x/D) of 2.

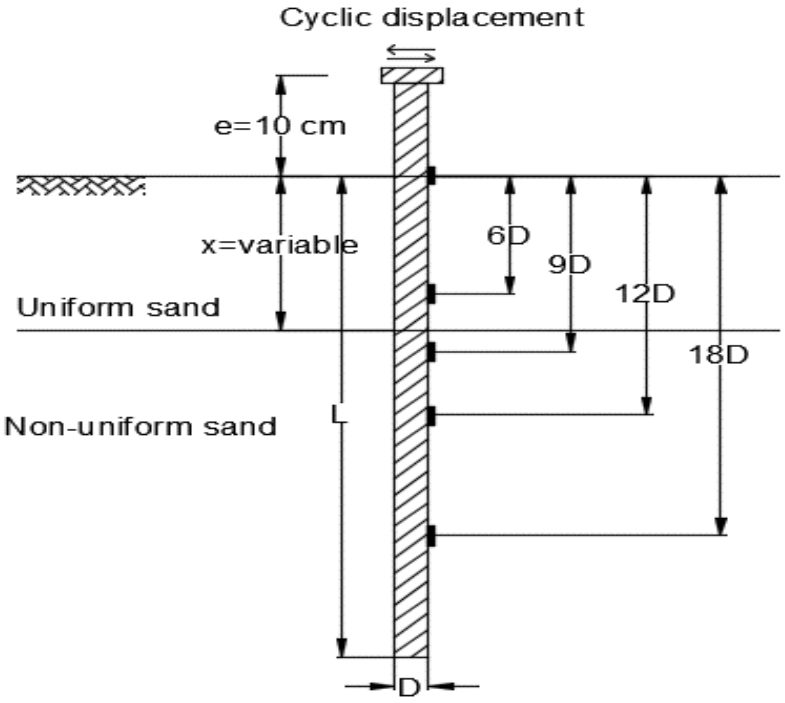

Figure 4-11 Schematic figure of two-layered ground soil tests

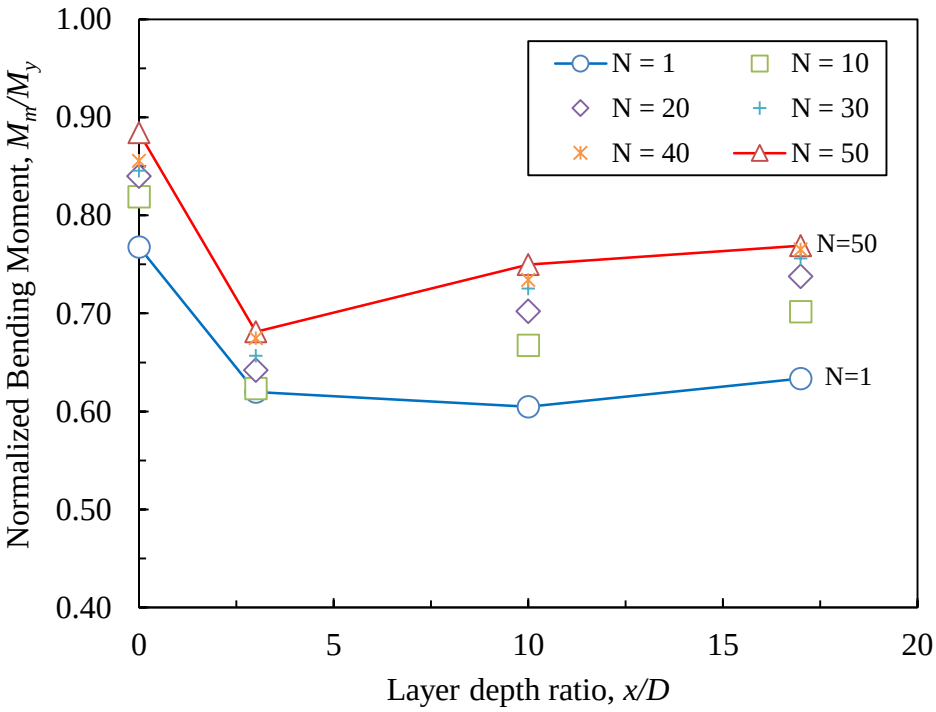

Figure 4-12 Normalized bending moment with various depth ratio of the upper layer

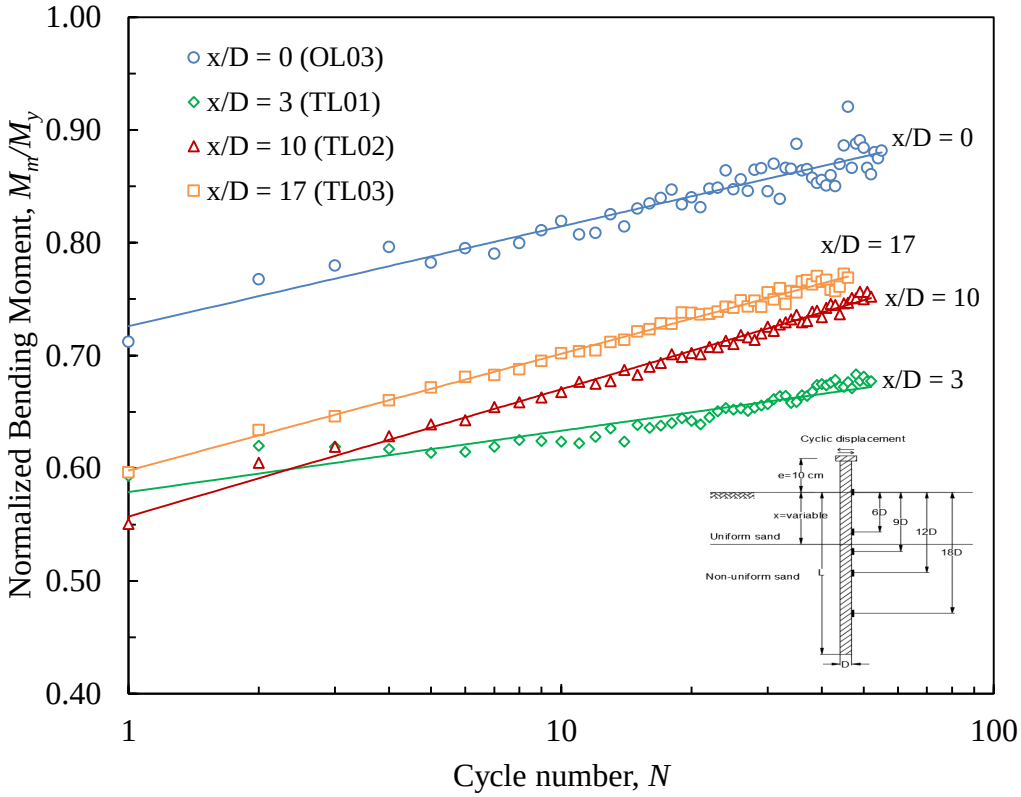

Figure 4-13 Effect cycle time to the bending moment of the pile with the variation of first layer depth

During the cyclic loading, there is no significant increase in the bending moment, and lateral loading occurred on the layer depth ratio (x/D) of 3, as shown in Figure 4-13. However, this condition only occurred in the layer depth ratio (x/D) of 3, for the other layer thickness, the bending moment and lateral loading increase during the cyclic displacement loading. This conditions occurred due to the plastic deformation of the soil on the surface layer during the cyclic lateral loading. Plastic deformation that occurred in the surface area (Figure 4-14a) cause the soil-pile interaction reduced, and it makes the bending moment, and lateral capacity insignificantly increases during the cyclic loading. Moreover, on the layer depth ratio (x/D) equal to 3, the upper soil layer was moving down into the bottom layer (Figure 4-14b) due to the high lateral deflection of the pile in this area. This condition also can increase the plastic deformation of the upper soil layer. This condition is not occurred on the layer depth ratio (x/D) of 10 and 17 because of the lateral pile displacement is very small in this area, so the upper soil layer cannot enter the bottom layer.

(a) (b)

Figure 4-14 Soil condition after 50-time of cyclic loading for the layer depth ratio (*x/D*) of 3, (a) condition on surface layer (b) condition on the border layer

Based on the experimental results, the changing of the topsoil layer using uniform sandy soil can reduce the bending moment of the pile on cyclic lateral displacement loading. There is no significant reduction of pile bending moment observed by changing the topsoil layer beyond the layer depth ratio (*x/D*) of 3 for static lateral displacement loading. During the cyclic loading, the bending moment of the pile on the layer depth ratio (*x/D*) of 3 did not significantly increase until cycle time of 50 due to the plastic deformation occurred on the surface layer and reduced the soil-pile interaction. The effective depth of the pre-bored system (*x*) selected on the layer depth ratio (*x/D*) of 10 that provide more stable results of pile bending moment.

4.4 FAILURE PATTERN OF PILE FOUNDATION DUE TO CYCLIC LATERAL LOADING

4.4.1 Plastic Deformation on Surface Layer

In order to optimize the utilization of filler material, the effective diameter of the pre-bored ring needs to be determined. It is expected to maintain the bending moment with the optimum utilization of filler material. The pre-bored ring diameter is determined based on the failure zone during the cyclic lateral loading. Awad-Allah et al. (2017) as shown in Figure 4-15 illustrated the plastic deformations which was created on the topsoil surface were extended

laterally as a shape of an ellipse with major and minor axes of 6D and 4D after applying 50 times of lateral cyclic loadings. The plastic deformation width on the surface area, in the loading direction, occurred about 50-70mm or 3 to 5 times of pile diameter and 30-40mm or 2 to 3 times of pile diameter for 3mm and 1mm pile head displacement respectively as shown in Figure 4-16.

4.4.2 Effective Diameter of Pre-Bored Ring

Experimental tests on the pile with a pre-bored ring system using ring diameter of 4D (60mm) and ring depth of 10D (150mm) were conducted with pile head displacement load 3mm and 1mm. Based on the results of cyclic lateral loading in pre-bored system foundation, the ring was moved up about 10 mm after 50 times of cyclic loading due to 3mm pile head displacement (Figure 4-17a), but for 1mm pile head displacement the ring was not significantly moved as shown in Figure 4-17b. It occurred because the ring was placed in the area of the failure zone. In this area, the plastic deformation of the soil occurred during the cyclic lateral displacement, so the friction between soil and ring inflict the movement of the ring. The different properties of soil inside and outside the ring also could affect the ring movement.

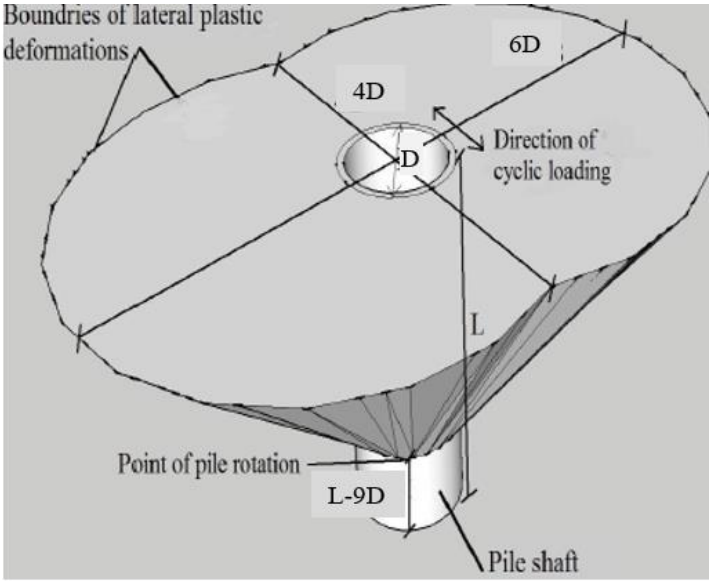

Figure 4-15 Three dimensional (3D) conical failure zone around the pile shaft due to lateral cyclic loading in medium dense sand (Awad-Allah et al.,2017)

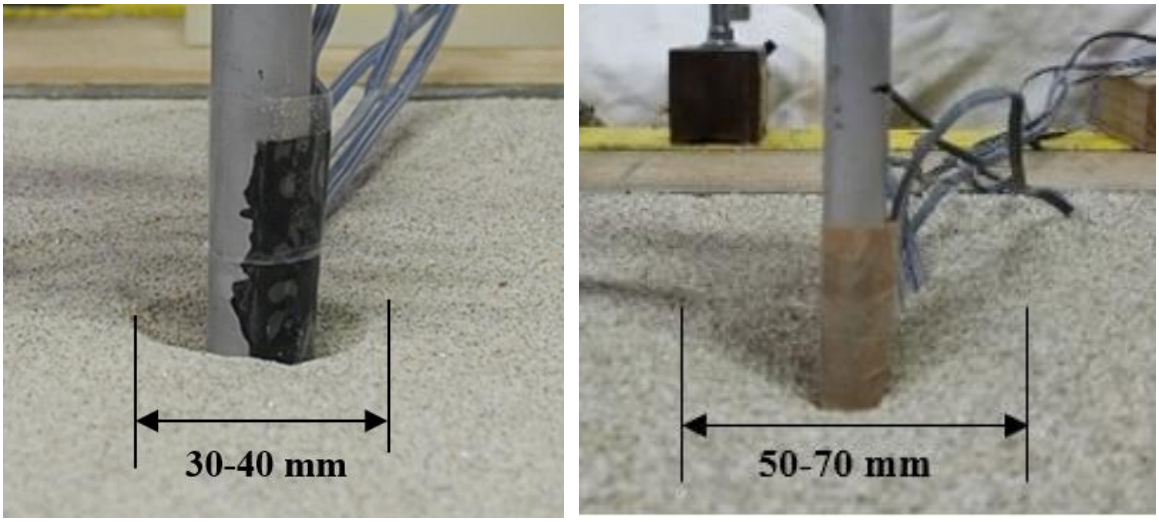

(a) (b)

Figure 4-16 Conditions after 50 times of loading with (a) 1 mm pile head displacement (b) 3 mm pile head displacement.

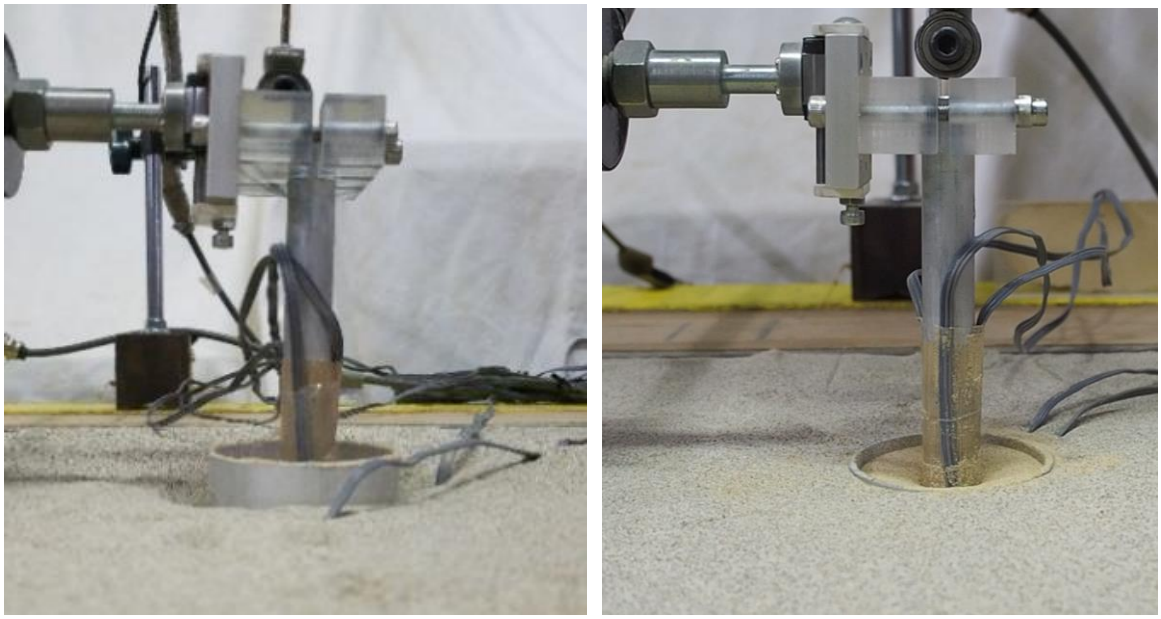

(a) (b)

Figure 4-17 Conditions after 50 times of cyclic displacement with ring diameter 4*D* (a) 3mm pile head displacement (b) 1mm pile head displacement

4.5 EFFECT OF FILLER MATERIAL ON PRE-BORED PILE FOUNDATION SYSTEM

4.5.1 Effect of Ring Diameter

Based on the failure pattern of the laterally loaded pile in one-layered ground soil, the placement of the ring inside the failure zone (about 2*D* in case of 1mm pile head displacement) influenced the ring behavior. So, in this experiment, three types of ring diameter were used to evaluate the effective diameter of the pre-bored ring system. The ring diameter with the ratio between ring diameter (*d*) and pile diameter (*D*), of 3*D*, 4*D*, and 5*D* was used to determine the effect of ring diameter on filler material behavior due to cyclic lateral loading with the same filler material of Toyoura sand with 80% of relative density. All the ring diameter is placed outside the predicted plastic deformation to avoid the potential displacement of the ring. Figure 4-18 shows the effect of pre-bored ring system on pile bending moment. Placement of pre-bored ring with a ring diameter of 3*D* and 4*D* provide a little higher value of bending moment compared to the one-layered condition at the first cycle. The pre-bored ring with a diameter of 3*D* and 4*D* results in similar values of bending moment and the ring diameter of 5*D* provides the smallest pile bending moment at the first cycle.

However, under the cyclic lateral loading, the pile bending moment on the one-layered condition and ring diameter of 5*D* is increasing significantly. Whereas, the 3*D* and 4*D* of ring diameter results in a more stable bending moment until 50 times of cyclic loading. Figure 4-19 shows the effect of ring diameter on pile bending moment under cyclic lateral loading. The increasing of bending moment explained by using bending moment ratio (M_N/M_1). In one-layered condition, the bending moment is increasing by about 9.4% under 50 times of cyclic loading. The pre-bored ring with wider diameter also results in an increasing pile bending moment about 10.3% during the cyclic loading. On the other hand, the pre-bored ring with a ring diameter of 3D and 4D provide similar results and more stable pile bending moment under cyclic loading. Based on the results, it indicates that there is an influence of pre-bored ring that can maintain the pile bending moment during cyclic loading. However, the wider ring diameter provides the increasing of pile bending moment during cyclic lateral loading, the similar conditions with the one-layered ground soil test results.

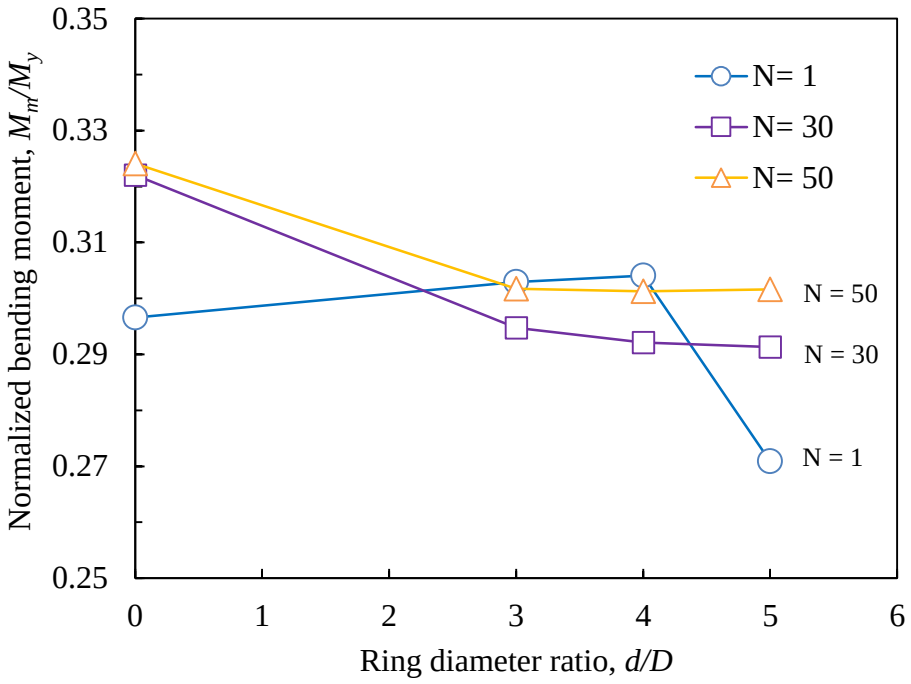

Figure 4-18 Effect of ring diameter on bending moment of pre-bored pile system under cyclic lateral loading

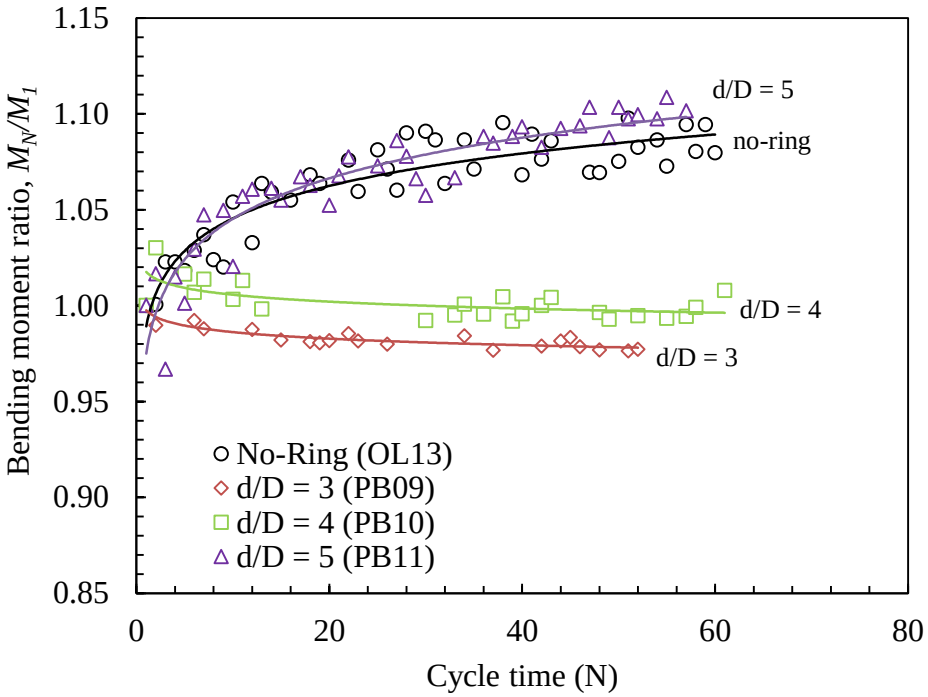

Figure 4-19 Effect of ring diameter on bending moment of pre-bored pile system under cyclic lateral loading

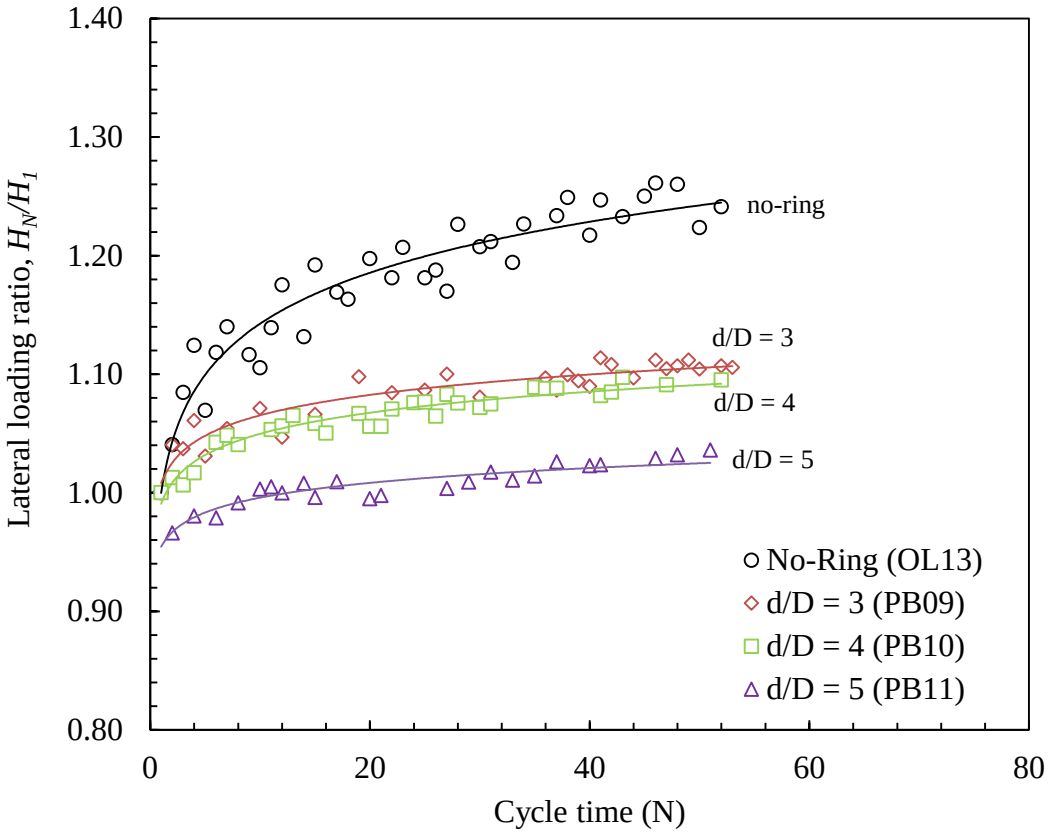

Figure 4-20 Effect of ring diameter on lateral pile capacity of the pre-bored pile system

The placement of pre-bored ring also effected on the lateral capacity of the pile. Due to the changing of soil material on the top area of the pile, the potential increase of lateral capacity also reduced. In the one-layered experimental test condition, the lateral capacity increase to 26% due to 50 times of cyclic lateral loading. The placement of pre-bored ring can reduce the potential increase of lateral capacity to 11.2%, 9.5% and 3.6% for ring diameter of 3*D*, 4*D*, and 5*D*, respectively as shown in Figure 4-20. It indicates the placement of pre-bored ring can maintain the lateral soil reaction of pile foundation during the lateral cyclic loading. The stable results of lateral capacity during the cyclic loading can maintain the behavior of soil during cyclic loading condition due to girder expansion in this system. So the elimination of elastomeric bearing on integral abutment bridge can be replaced by a pre-bored pile foundation system. However, the reduction of the potential increase of lateral capacity is small in comparison with the reduction of the potential increase of pile bending moment under cyclic loading.

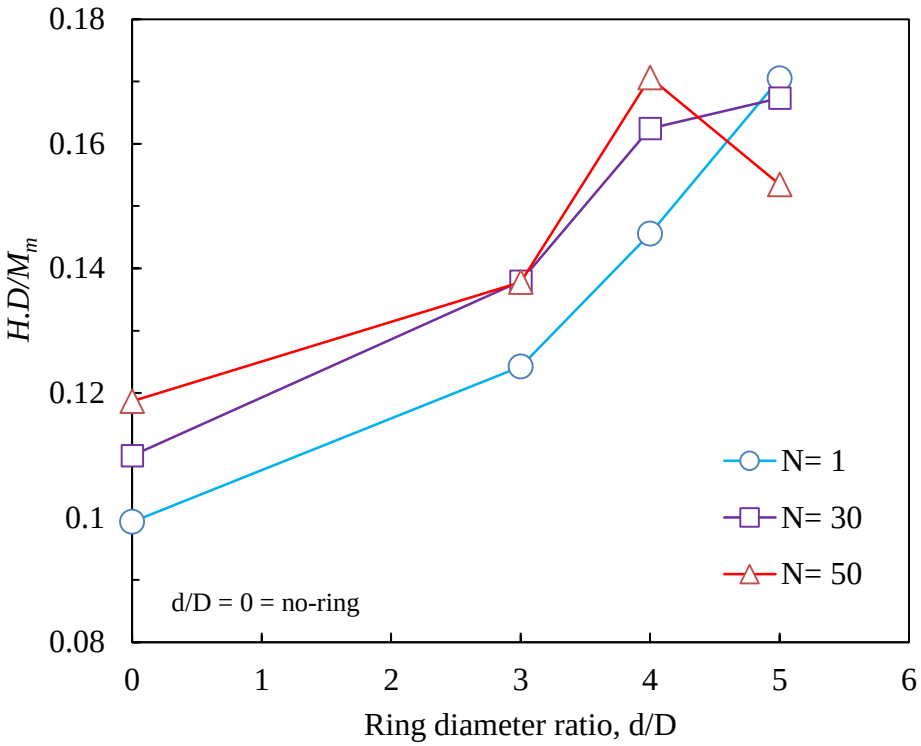

Figure 4-21 Effect of ring diameter on the reduction of lateral pile capacity of the pre-bored pile system

In order to evaluate the effect of lateral pile capacity reduction in comparison with bending moment reduction, the ratio between maximum lateral capacity and maximum bending moment ($H.D/M_m$), with H is lateral loading, D is pile diameter and M_m is measured bending moment, is determined for every ring diameter variation as shown in Figure 4-21. Based on the value of ($H.D/M_m$), the placement of pre-bored ring with filler material provides a higher ratio than the one-layered condition. It means the pre-bored ring system can effectively reduce the potential increase of pile bending moment with a small reduction of lateral capacity. During cyclic loading, the value of ($H.D/M_m$) is increasing for all cases except the pre-bored ring with a diameter of 5D. This condition happened due to there is no effect of the ring to hold the displacement of filler material that can reduce the lateral capacity due to cyclic lateral loading.

4.5.2 The Density of Filler Material

Results of lateral capacity for the pre-bored system with different filler material density of 40%, 70%, and 90% are shown in Figure 4-22, and the change of maximum lateral pile capacity during the cyclic loading is shown in Figure 4-23. It was observed that the

maximum lateral pile capacity at the first time of cyclic loading reached to 19.68 N, 20.90 N, and 24.78 N for each density of 40%, 70%, and 90%, respectively. Based on Figure 4-22, it can be noticed that the filler material with 40% of density generates the lowest lateral capacity at the first cycle.

However, these values significantly increase with increasing of loading cycles number (*N*) as shown in Figure 4-23. The results of another filler material density, the lateral capacity were increased, but it is not in a significant difference from the first cycle until 50 times of the cycle. It indicates that the cyclic loading leads to improve the properties and reduction of the void ratio of filler material inside the ring. The soil particle was moving and causing the hardening of soil. Consequently, enhancement of soil properties occurs for loose sand, and confining pressure increases during cyclic loading. On the other hand, filler density of 70% and 90% provide a stable lateral capacity until 50 times of cyclic loading.

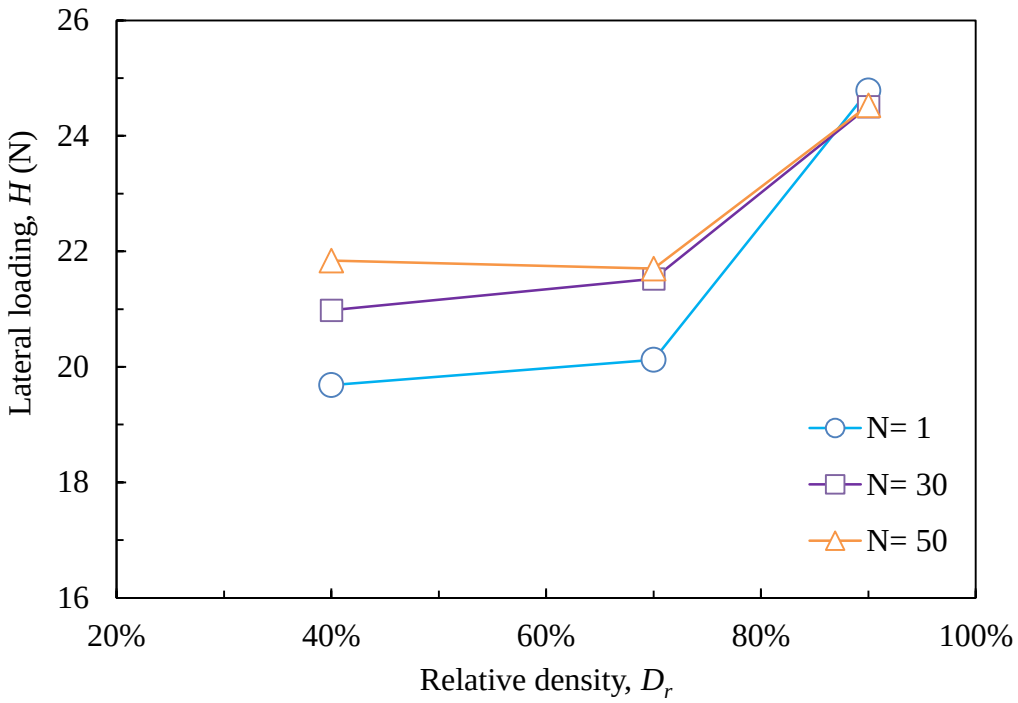

Figure 4-22 Lateral capacity of pre-bored pile foundation with different filler material density

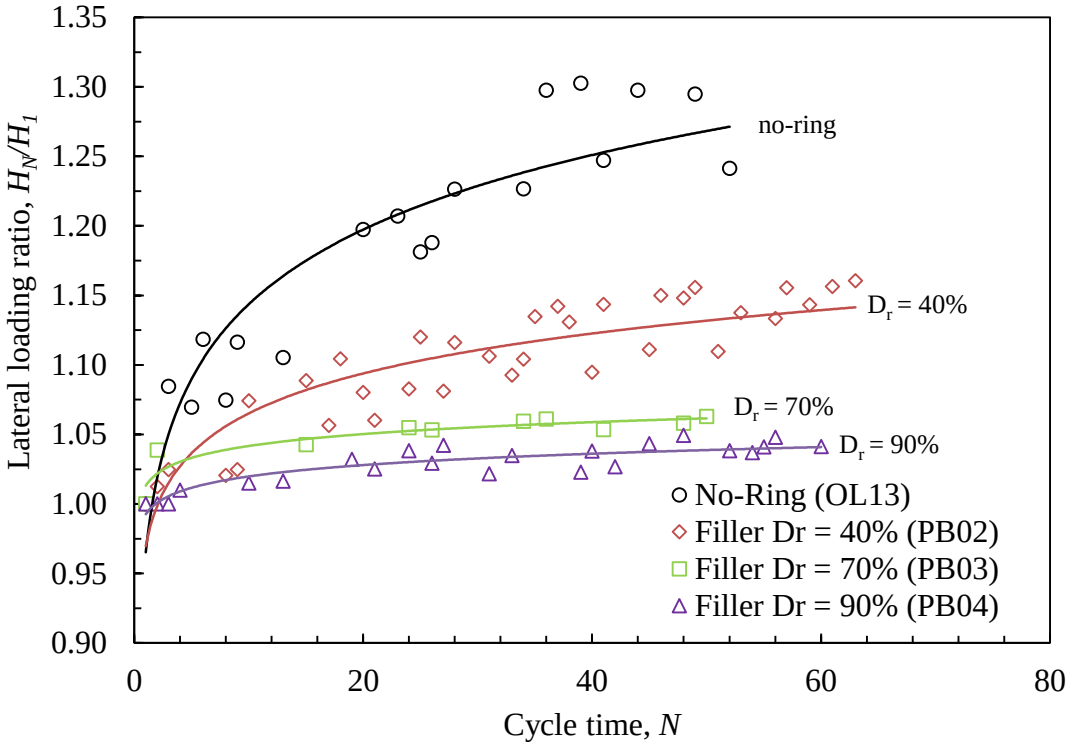

Figure 4-23 Potential increasing of pile lateral capacity under cyclic lateral loading

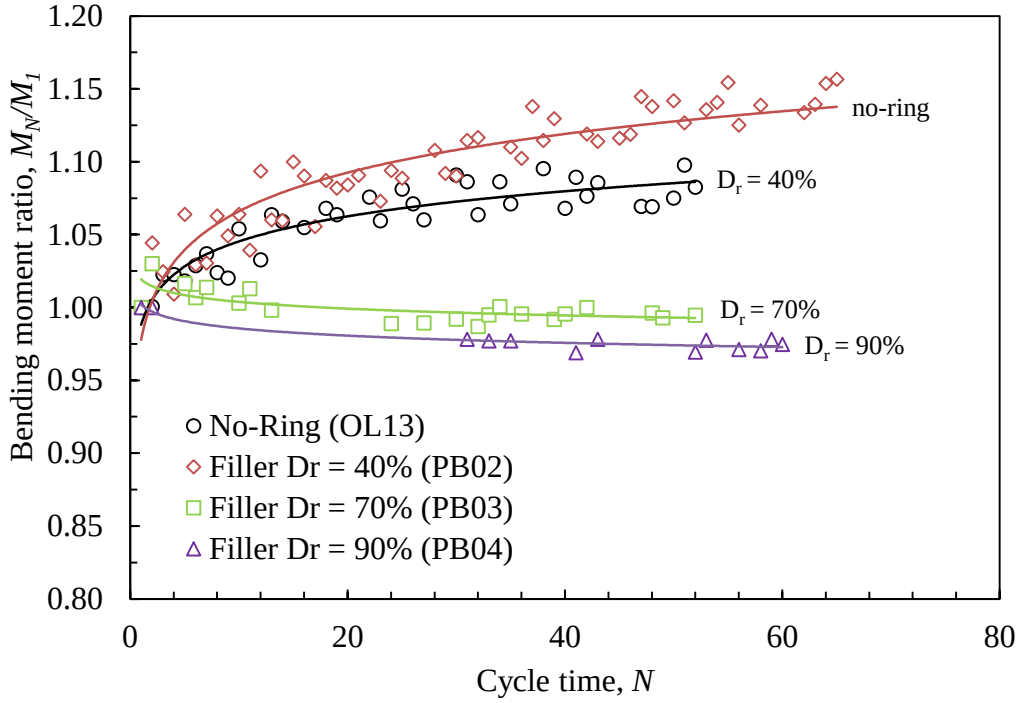

Figure 4-24 Effect of density on bending moment of pre-bored pile system under cyclic lateral loading

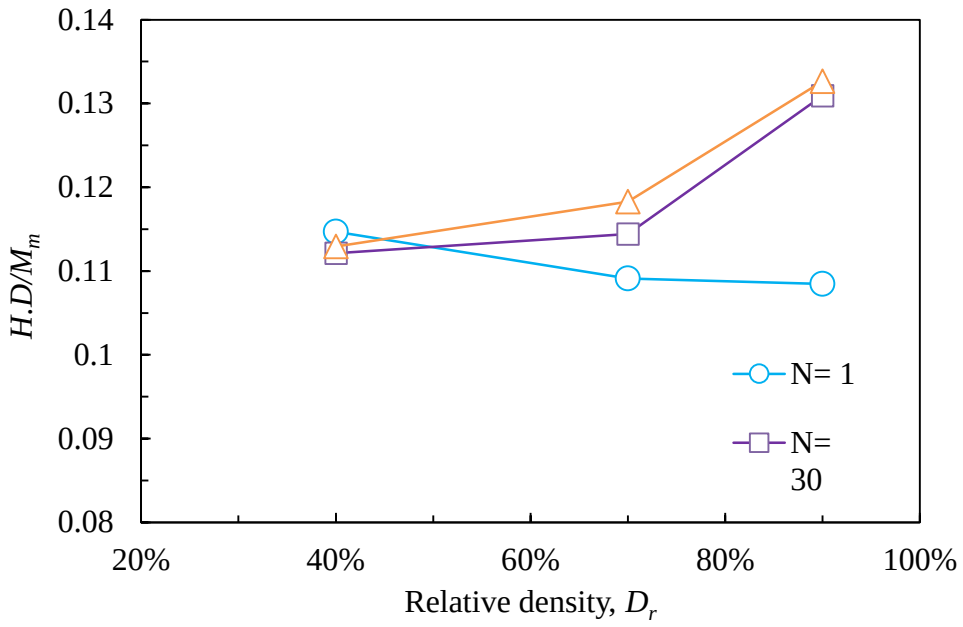

Figure 4-25 Effect of ring diameter on the reduction of lateral pile capacity of the pre-bored pile system

The density of filler material also evaluated to determine the effective density of pre-bored pile foundation system that can maintain the potential increase of pile bending moment due to cyclic lateral loading. The bending moment ratio (M_N/M_1) during cyclic loading is evaluated in this section for three different filler material density as shown in Figure 4-24. Similar with the lateral capacity, the lower density of filler material provides the higher possibility increasing of pile bending moment during the cyclic loading. The potential increase of the pile is 15.7% for the 40% of filler material density. The other density provides a more stable value of bending moment. The value of ($H.D/M_m$) also determined for every filler material density variation, as shown in Figure 4-25. During cyclic loading, the value of ($H.D/M_m$) is increasing for all cases except the pre-bored ring with low filler material density. This condition happened due to high potential increasing of both bending moment and lateral capacity under cyclic lateral loading. The value of ($H.D/M_m$) is increased with the increasing of filler material density at the 50 times of cyclic loading. This condition occurred because of in the loose density of filler material; densification highly occurs on the surface area. The soil surface of filler material moves down for each density 40% and 70% for 0.7mm and 0.4mm, and there is no densification on the 90% of filler density for pile head displacement of 1mm as shown in Figure 4-26.

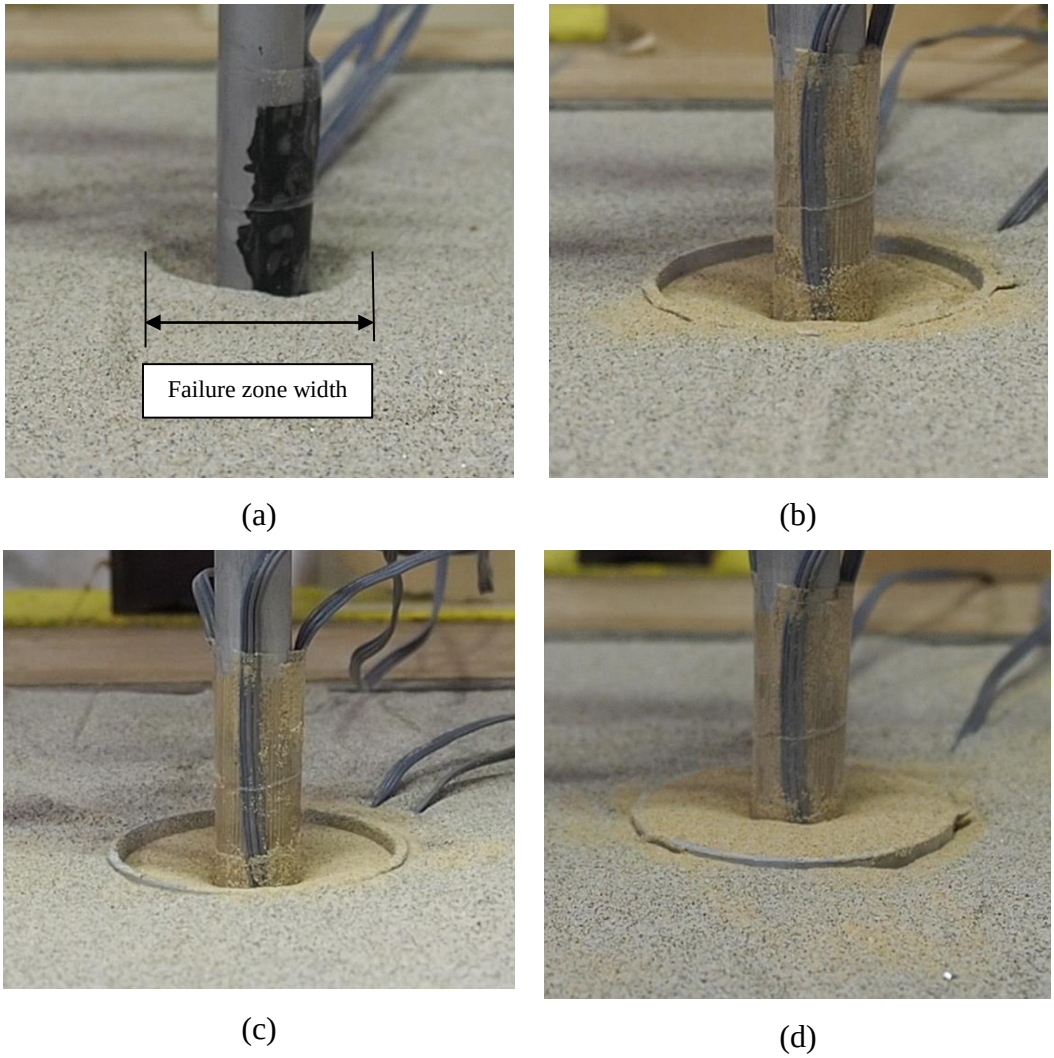

Figure 4-26 Conditions after 50 times of cyclic lateral displacement with lateral displacement in pile head of 1mm (a) K7 80% without the ring (b) Filler density 40% (c) Filler density 70% (d) Filler density 90%

The experimental test of the empty ring also conducted. The Canadian researcher proposed to use the pre-bored ring without filler material (empty ring) to reduce the potential increase of pile bending moment due to lateral cyclic loading. In this research, the empty ring case also evaluated under static and cyclic loading. Figure 4-27 shows the results of the bending moment along with the pile depth with the various density of filler material on static loading condition. Based on Figure 4-27, the smallest bending moment provided in the empty ring case for static loading condition. The maximum pile bending moment point also changed to a deeper location. However, the concentrated moment occurred in the maximum value, so it is possible to inflict a pile buckling.

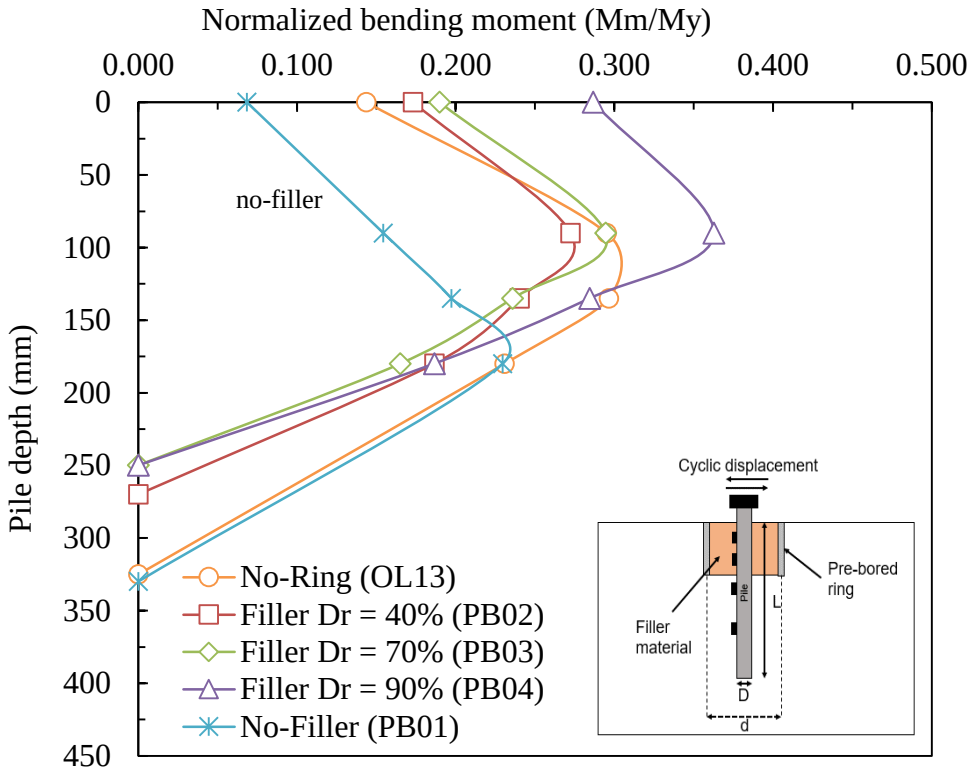

Figure 4-27 Effect of filler material properties on static lateral loading with 1 mm pile head displacement

Table 4-2 Mechanical and physical properties of soil

Soil properties	Toyoura			Mix soil	K-7
Relative density (%)	50	70	90	80	80
Dry density (kN/m^3)	13.93	14.72	15.21	15.01	14.13
Cohesion (kN/m^2)	0.91	0.91	0.45	0.26	0.89
Friction angle, ϕ (°)	35.20	36.67	39.59	36.18	38.03
Elastic modulus, E_{50} (kN/m^2)	9811.38	12685.98	17251.07	5152.86	7590.42
Poisson's ratio, ν	0.29	0.24	0.29	0.22	0.26
Dilatancy angle, ψ (°)	8.14	18.06	23.94	7.01	15.78

4.5.3 Effect of Filler Material

Three types of soil with the uniformity coefficient in a range of 1.40 to 4.67 were used as filler material. Table 4-2 shows the mechanical and physical properties of filler material with different uniformity coefficient. Based on Figure 4-28, the filler material with a lower uniformity coefficient provides a more stable increasing potential of pile bending moment. The higher uniformity coefficient of filler material has experienced an increase in bending moment during the cyclic loading. The filler material with higher uniformity coefficient, which has a well-graded particle distribution, provide the increasing of pile bending moment with the increasing of cycle number. However, after 20 times of cyclic loading, the values of bending moment are reduced until the end of loading. It happened due to the plastic deformation occurred on the soil, as shown in Figure 4-29. It shows that the plastic deformation occurred after cyclic loading number (N) of 20, and it increases until 50 times of cyclic loading. This plastic deformation effect on the soil-pile interaction that reduces the soil resistance on the pile during the lateral cyclic loading. It occurred due to the higher uniformity of filler material consists of some fine particles that are filled the particle void during the cyclic loading and increase the stiffness of soil, that reduced the soil-pile interaction.

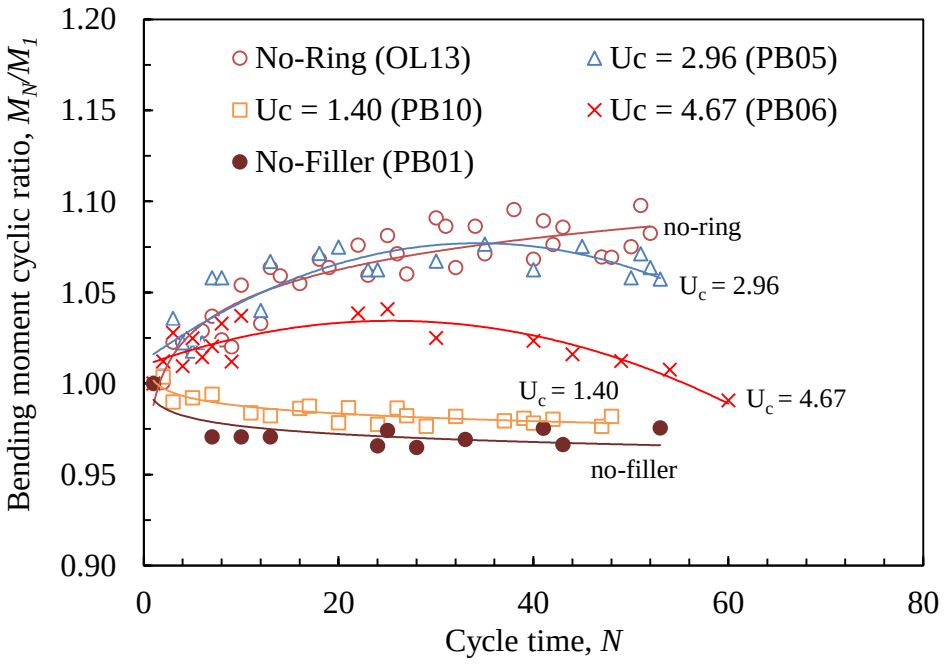

Figure 4-28 Effect of soil uniformity on the bending moment of pre-bored pile system under cyclic lateral loading

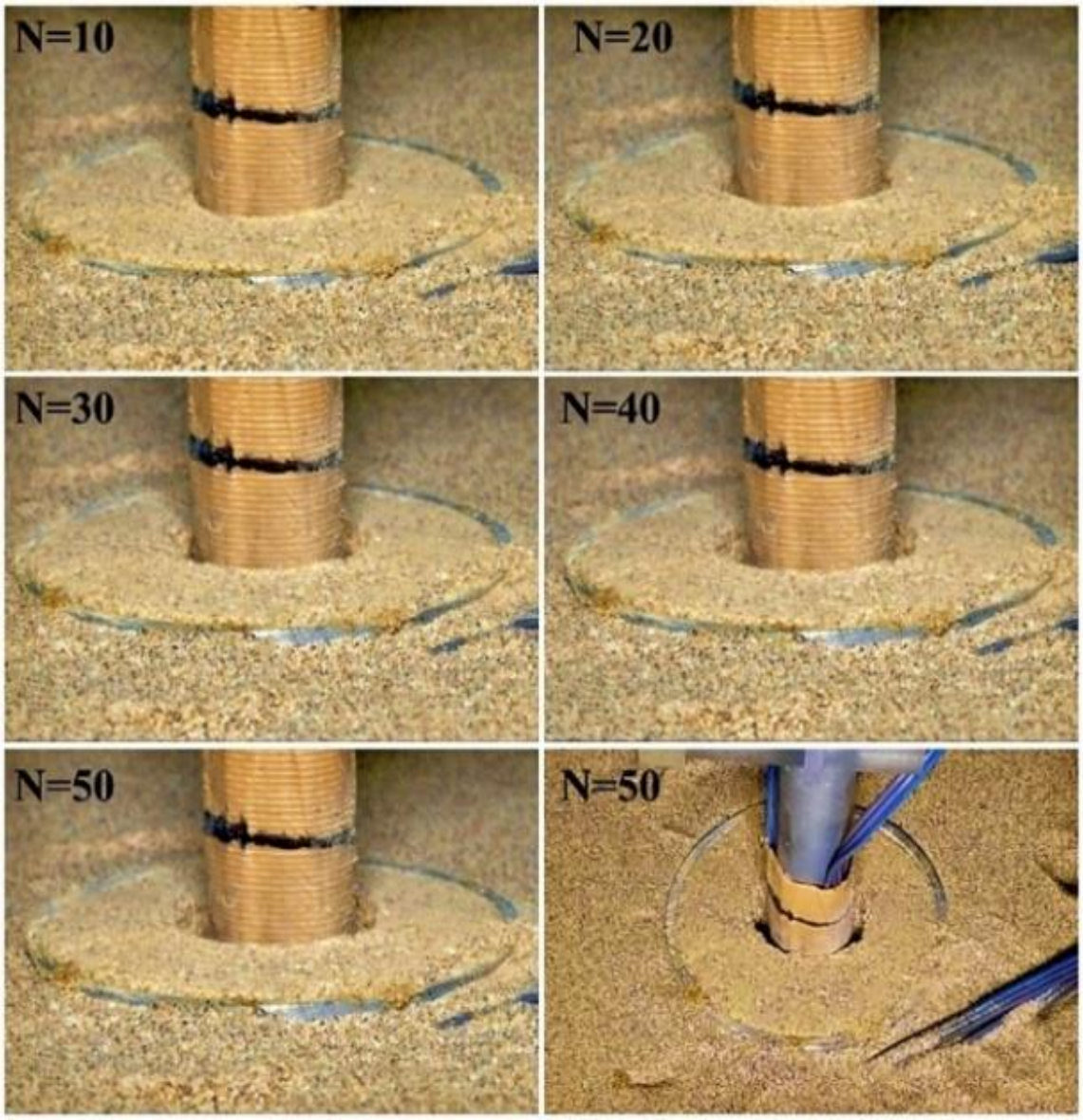

Figure 4-29 Plastic deformations after cyclic loading applied.

The reduction of potential bending moment due to the pre-bored ring system under cyclic loading also affected on the pile lateral capacity. In case of single pile in one-layered soil, there is a potential increasing of lateral capacity of 1.3 times for 50 loading cycles. Utilization of pre-bored ring system with uniform filler material result a reduction of pile lateral capacity as shown in Figure 4-30. It was occurred due to the reduction of soil confining pressure as a results of uniform sand used as a pre-bored filler material. However, the reduction of pile capacity was accompanied with the high reduction of potential bending moment of pile which provide more stable performance of pile foundation under cyclic loading.

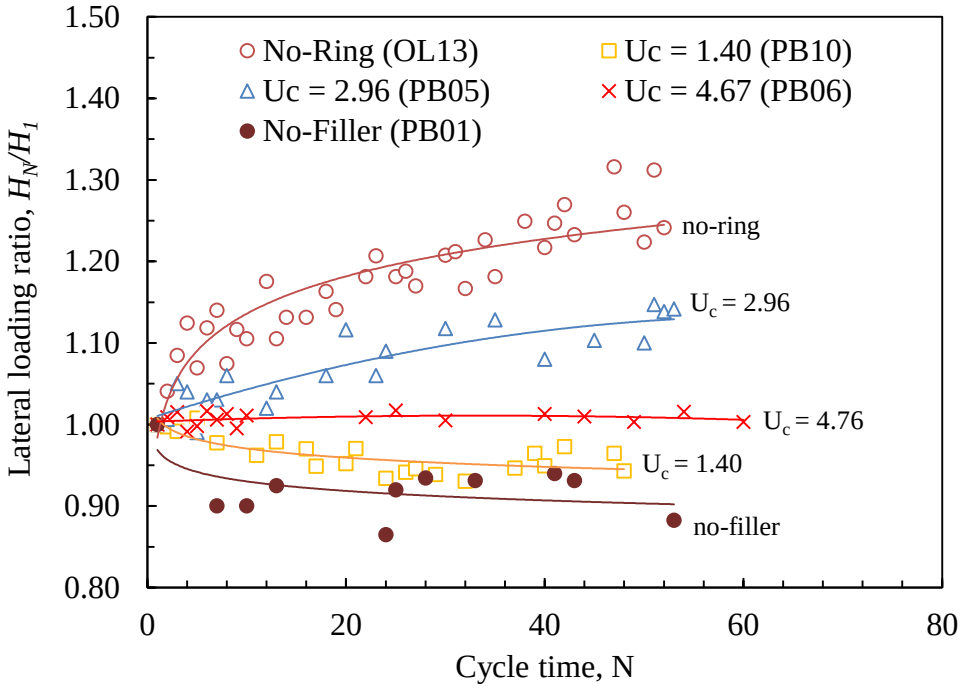

Figure 4-30 Effect of soil uniformity on the lateral capacity of pre-bored pile system under cyclic lateral loading

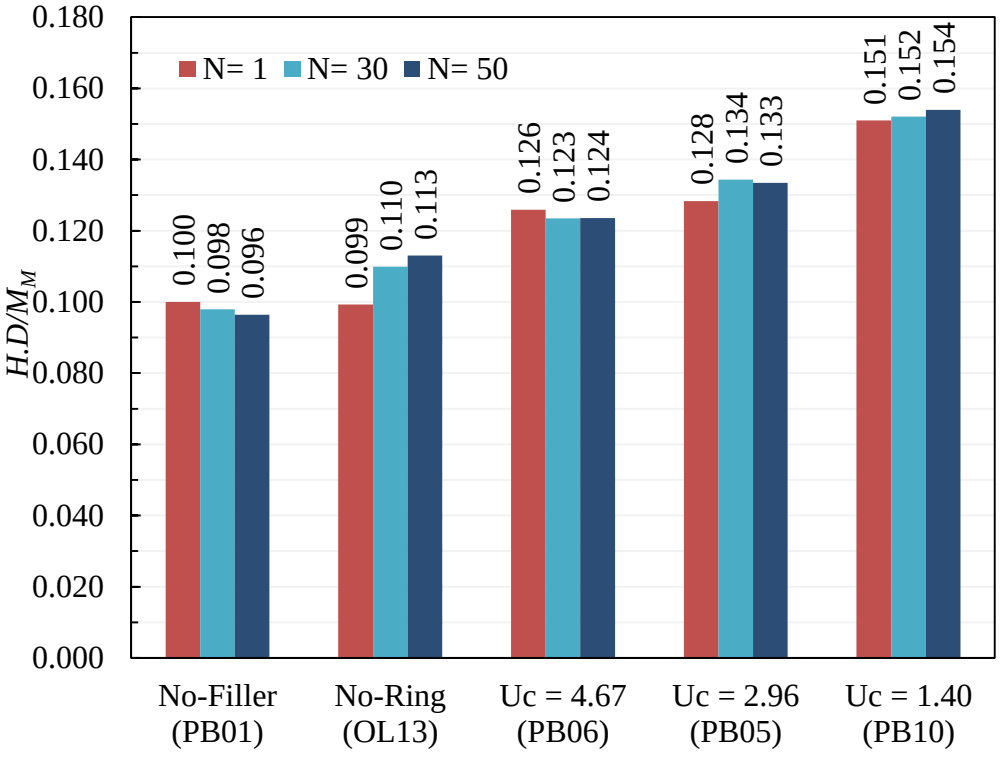

Figure 4-31 Effect of soil uniformity on the reduction of lateral pile capacity of the pre-bored pile system

Figure 4-31 shows the influence of soil uniformity on the reduction of lateral pile capacity of pre-bored pile system. It shows that the filler material with a low uniformity coefficient provides the highest ratio of ($H.D/M_m$) than the other cases. The value of ($H.D/M_m$) is the ratio between the lateral capacity of the pile and maximum bending moment occurred on the pile body. It means the reduction of potential lateral capacity due to cyclic lateral loading is still can be accepted because the potential increase of bending moment also highly reduced. So, it can maintain the lateral movement of the bridge superstructure in the integral abutment bridge system.

Furthermore, the effect of soil particle diameter also evaluated to determine the effect of filler material properties that can maintain the pile bending moment during the lateral cyclic loading. Figure 4-32 shows the potential increase of pile bending moment due to lateral cyclic loading on pre-bored pile foundation system with different filler particle diameter. Three different particle size diameter with similar uniformity were evaluated as filler material inside the pre-bored ring system. Range of particle diameter ratio (D/D_{50}) used in this research are from 12 to 50 with D is pile diameter, and D_{50} is the mean diameter of filler material particle.

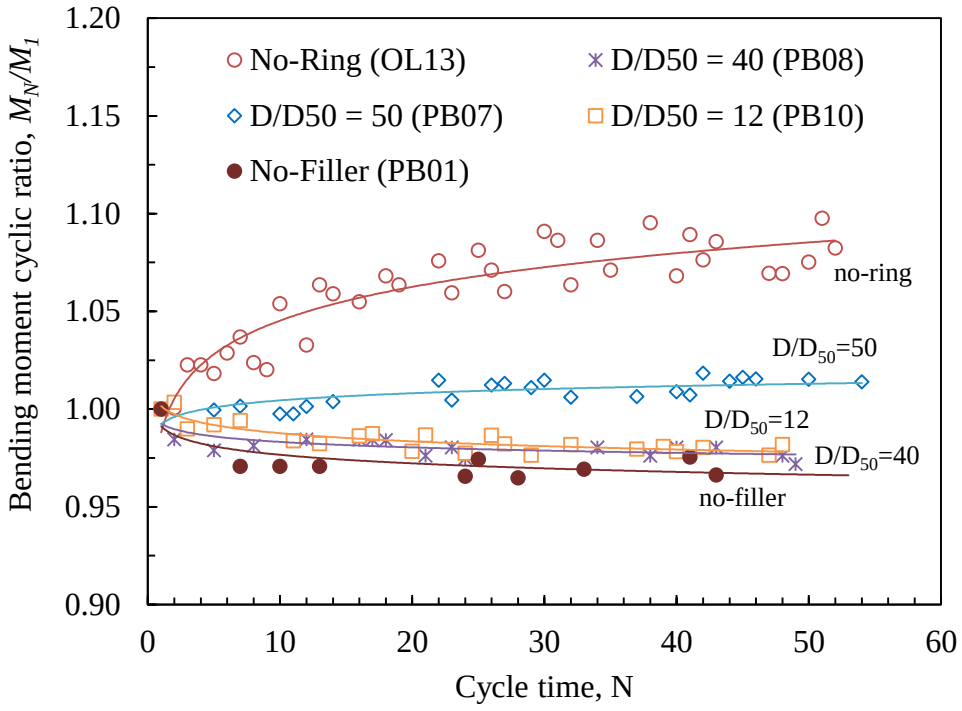

Figure 4-32 Effect of particle diameter on the bending moment of pre-bored pile system under cyclic lateral loading

Based on Figure 4-32, the effect of particle diameter on filler material is not significant. It is relatively providing a stable bending moment during the cyclic loading for all cases with a different particle diameter of filler material. So, the utilization of sandy soil or gravel with uniform particle distribution for filler material in this system are possible. Moreover, utilization of filler material with high permeability coefficient (e.g., uniform gravel) are recommended to avoid the effect of liquefaction inside the pre-bored ring system.

4.6 VALIDATION OF EXPERIMENT USING NUMERICAL ANALYSIS

Numerical analysis using 2D Finite Element Analysis (FEM) was performed on a real scale and model scale condition using scale factor (n = 15), to evaluate the effect of pre-bored ring diameter when lateral loading applied on the pile head. The input properties for FEM analysis is shown in Table 3-4 and Table 4-2. In this numerical analysis, the pile assumes as a continuous wall in plain strain conditions to simplify the boundary conditions and properties of the model. Geometrical idealization used for soil analysis according to equivalent pile stiffness method and soil conditions idealized by the hardening soil model. In this analysis, the wall thickness is same with the pile model width, and the equivalent stiffness of the wall (E_{eq}) is the average of pile and soil stiffness Satibi (2009) as shown in the Equation 4-4.

$$E_{eq} = \frac{E_p A_p + E_s A_s}{A_t} \tag{4-4}$$

Where, E_p, A_p, E_s, A_s, A_t are pile stiffness, pile area, soil stiffness, soil area and the total area of pile and soil. The initial condition of the numerical model using PLAXIS 2D is shown in Figure 4-33. The parameter input is conducted based on the Triaxial consolidated drained (*CD*) laboratory test. The input parameters used in the modeling are shown in Table 4-2.

The result of 2D FEM analysis is shown in Figure 4-34 compared to the experimental test for monotonic loading condition. Based on Figure 4-34, the result of normalized lateral loading, $H/(A_p.E_p)$, for both numerical and experimental test provide a similar relation for the static condition. The potential increase of lateral loading ratio (H_N/H_1) based on 2D FEM analysis are shown in Figure 4-35. The changing of the pre-bored ring diameter results the smaller potential increasing of lateral load, (H_N/H_1), for both experimental (Figure 4-20) and 2D FEM analysis (Figure 4-35) in cyclic lateral loading conditions. The ring diameter ratio

lower than 5 provides a similar result of lateral pile capacity. It indicates that the lateral pile capacity of pile also affected by of pre-bored ring dimension. The gap between 2D FEM analysis (plain strain) and experimental test (1g model) results occurred due to the effect of boundary conditions from each analysis.

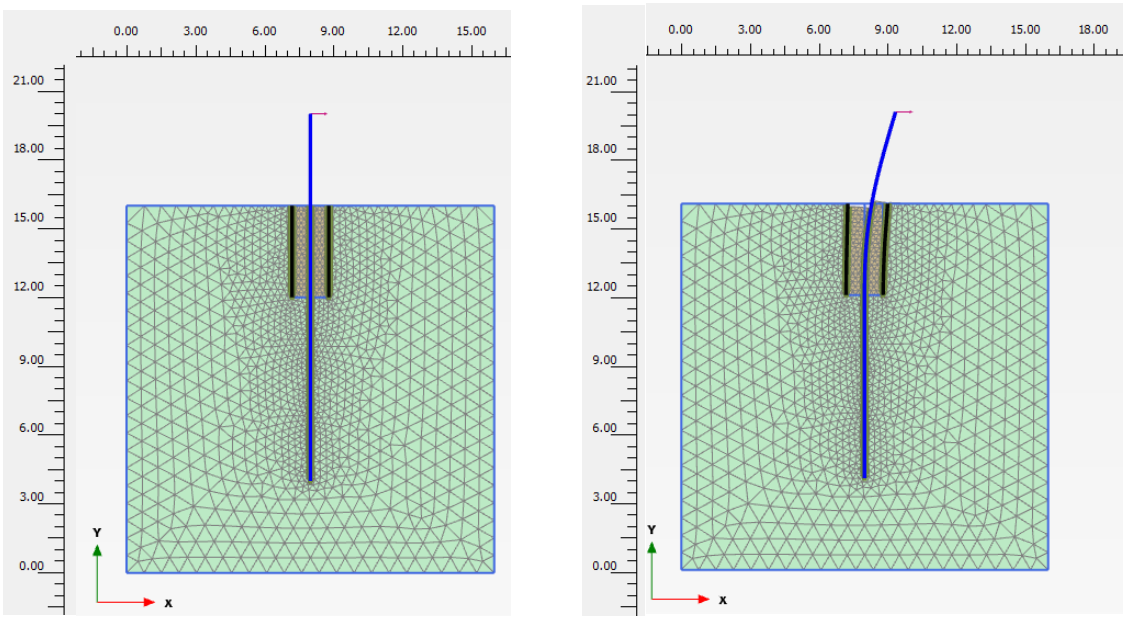

(a) (b)

Figure 4-33 Finite Element Method (2D) analysis: (a) initial condition, (b) after loading

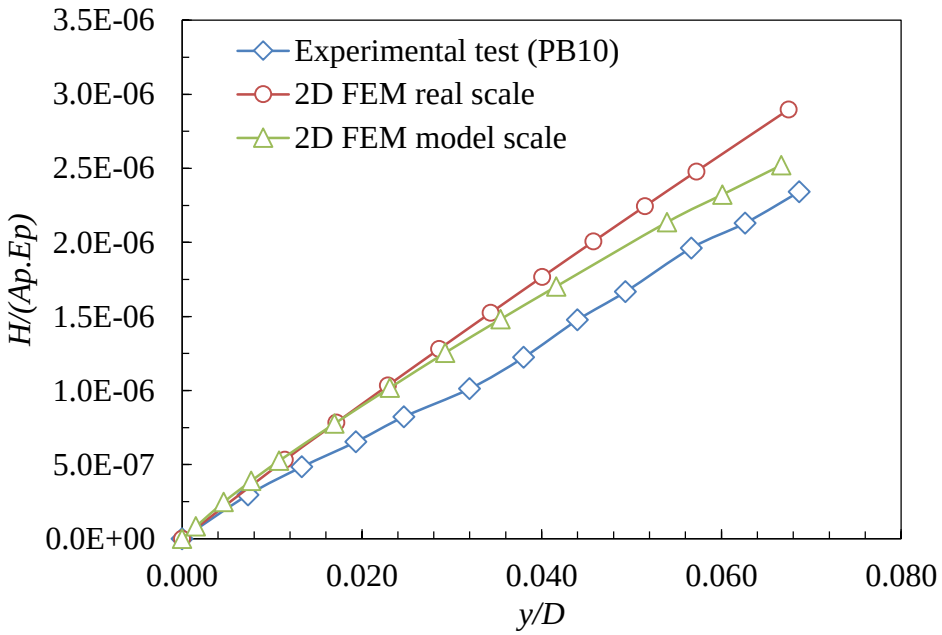

Figure 4-34 Comparison between experimental and 2D numerical analysis

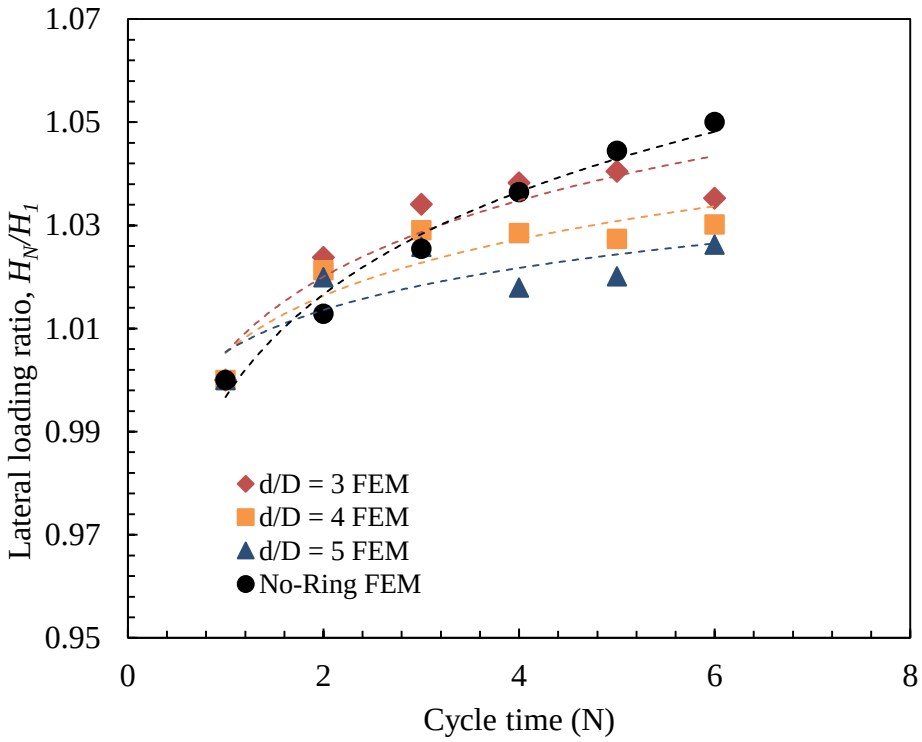

Figure 4-35 Effect of ring diameter on the experimental test and 2D FEM analysis conditions

4.7 SUMMARY

In this chapter, a parametric study was conducted using the laboratory test results to examine the influence of pile slenderness ratio *L/B*, number of cycles *N*, relative density of soil *Dr*, properties of soil material (U_c and D_{50}) and pre-bored ring diameter (*d*) on the behavior of pile behavior including: (1) cyclic lateral capacities of pile, (2) pile bending moment under monotonic and cyclic lateral loading, (3) failure area due to cyclic lateral loading. Conclusions of this study can be summarized as follows:

1. Pile bending moment due to lateral loading is affected by ground soil density, pile slenderness, and soil properties. Increasing the slenderness ratio of the pile will provide a higher bending moment. The higher density of ground soil provides bigger bending moment due to the increase of soil stiffness. The ground soil with lower uniformity coefficient results in a smaller bending moment.
2. Substitution of the topsoil layer using sandy soil with lower uniformity coefficient can reduce the bending moment of the pile. There is no significant reduction of pile

bending moment observed by changing the topsoil layer beyond the layer depth ratio (*x/D*) of 3 for static lateral displacement loading. Bending moment of the pile on the layer depth ratio (*x/D*) of 3 during cyclic loading did not significantly increase until cycle time of 50 due to the plastic deformation occurred on the surface layer and reduced the soil-pile interaction.

3. The diameter of pre-bored ring smaller than the failure zone area can inflict the pre-bored ring movement. In this area, the plastic deformation of the soil occurred during the cyclic lateral displacement, so the friction between soil and ring inflict the movement of the ring.
4. The pre-bored ring with a ring diameter of 3*D* and 4*D* provide similar results and more stable pile bending moment under cyclic loading. On the other hand, the pre-bored ring with wider diameter results in an increasing pile bending moment during the cyclic loading. Based on the results, it indicates that there is an influence of pre-bored ring that can maintain the pile bending moment during cyclic loading. However, the wider ring diameter provides the increasing of pile bending moment during cyclic lateral loading, the similar conditions with the one-layered ground soil test results.
5. The filler material with low uniformity (uniform soil) provides a stable bending moment value during the cyclic loading. On the other hand, the utilization of filler material using non-uniform soil is difficult to maintain the filler properties because the soil hardening has occurred during the cyclic loading. This soil hardening inflicts a plastic deformation on the top area of the pile, and it effected on the soil-pile interaction that reduces the soil resistance on the pile during the lateral cyclic loading.
6. Filler material with low uniformity coefficient and medium or high density provide a stable pile performance during the cyclic loading. So, it can maintain the lateral displacement due to thermal expansion on the integral bridge abutment foundation system. The effective diameter of the ring is recommended more than the plastic deformation area of the soil for a shallow depth of ring to separate the filler material inside the ring and ground soil.
7. The effect of particle diameter on filler material is not so significant. It is relatively provided a stable bending moment during the cyclic loading for all cases with a

different particle diameter of filler material. So, the utilization of sandy soil or gravel with uniform particle distribution for filler material in this system are possible. Moreover, utilization of filler material with high permeability coefficient (e.g., uniform gravel) are recommended to avoid the effect of liquefaction inside the pre-bored ring system.

4.8 **REFERENCES**

Awad-Allah, M.F., and Yasufuku, N., Performance of Pile Foundations in Sandy Soil Under Slow Cyclic Lateral Loading. The 5th International Geotechnical Symposium on Geot. Eng. For Disaster Prevention & Reduction, Incheon, 2013, pp. 291-300.

Awad-Allah M. F., Yasufuku N., and Abdel-Rahman A. H., Factors Controlling the Behavior of Piled Foundations Due to Cyclic Lateral Loading. In Proc.The 6th Japan-Taiwan Joint Workshop on Geotechnical Hazards from Large Earthquakes and Heavy Rainfalls, 2014, pp.555-568.

Awad-Allah M. F., Yasufuku N., and Mandandhar S., Three-dimensional (3D) Failure Pattern of Flexible Pile Due to Lateral Cyclic Loading in Sand. Lowland Technology International, Vol 19, Issue 1, 2017, pp.1-12.

Dunker K. F., and Liu D., Foundations for Integral Abutments. Pract. Period. Struct. Des. Constr., Vol 12, Issue 1, 2007, pp.22-30.

Khodair Y.A., and Hassiotis S., Analysis of Soil–pile Interaction in Integral Abutment. Computers and Geotechnics, Vol 32, 2005, pp.201–209.

Satibi S., Numerical Analysis and Design Criteria of Embankments for Floating Piles. P.A. Vermeer (ed.) Dissertation, DCC Siegmar Kastl e K., 2009, pp.22-24.

Wood D., Crewe A., and Taylor C., Shaking Table Testing of Geotechnical Models. International Journal of Phys Model Geotech, Vol 1, 2002, pp.1–13.

Yang K., and Liang R., Numerical Solution for Laterally Loaded Piles in Two-Layer Soil Profile. J. Geotech. And Geoenviron. Eng. Vol. 132, Issue 11, 2006, pp.1436- 1443.

CHAPTER V

STRESS AND STRAIN DISTRIBUTION ON PRE-BORED PILE FOUNDATION SYSTEM UNDER CYCLIC LATERAL LOADING

5.1 INTRODUCTION

In this chapter, the measurement of soil behavior inside the pre-bored ring, especially on failure pattern and stress-strain distribution of soil on pre-bored ring system are evaluated. The use of Particle Image Velocimetry (PIV) method also explained to measure the soil deformation on an experimental testing model of the laterally loaded pile. The results of soil deformation and strain distribution can explain the failure pattern of the pre-bored pile foundation system under cyclic lateral loading.

Evaluation of soil behavior on a physical model test is critical to describe the accurate measurement of soil deformation. The measurement of soil deformation in the physical model remains some difficulties. Displacement gauges or sensors cannot be placed on the model test to get the soil movement during the lateral cyclic loading. Some techniques have developed to increase the element test measurement into the small-strain range (Scholey et al., 1995). However, the measurement techniques for the geotechnical model are not accurate. Various methods for measure the planar deformation of the geotechnical model test are proposed, such as X-Ray (Rocsoe et al., 1973) and stereo-photogrammetric (Butterfield et al., 1970). Nowadays, the utilization of computer-based image analysis methods become a popular technique to develop using automatic tracking systems (Taylor et al., 1998). In this dissertation, GeoPIV-RG program, which based on Particle Image Velocimetry (PIV) methods were used to measure the deformation of soil due to the lateral cyclic loading on the pile.

5.2 LABORATORY SIMULATION AND TEST CONDITIONS

The failure pattern of the soil inside the pre-bored ring was investigated to determine the point of pile rotation and the soil movement due to the pre-bored ring system. Three different diameters (d) of the pre-bored ring of 45mm, 60mm, and 75mm were used to evaluate the effect of ring dimension on this system. Digital images captured during the cyclic lateral

loading were used as an input on GeoPIV-RG program that performed on MATLAB to analyze the soil deformation pattern. An experimental study using small-scale laboratory model test was conducted in a half size model. Single flexible pile model embedded in sandy soil with the pre-bored ring in a half dimension, which filled with the filler material. Figure 5-1 shows the experimental test setup used in this study and the cross-section of pile and ring model are shown in Figure 5-2. The testing box was made from an acrylic glass panel as an observation area of the pile shaft to monitor the displacement of the pile during the lateral loading. Digital images were used to capture the deformations of the soil and pile foundation during the loading from the side of the testing box. GeoPIV-RG program was used to measure the deformation of soil due to the lateral cyclic loading on the pile. GeoPIV-RG is a new implementation of image-based deformation measurement for geotechnical applications based on Particle Image Velocimetry (PIV) methods (Stainer et al., 2016).

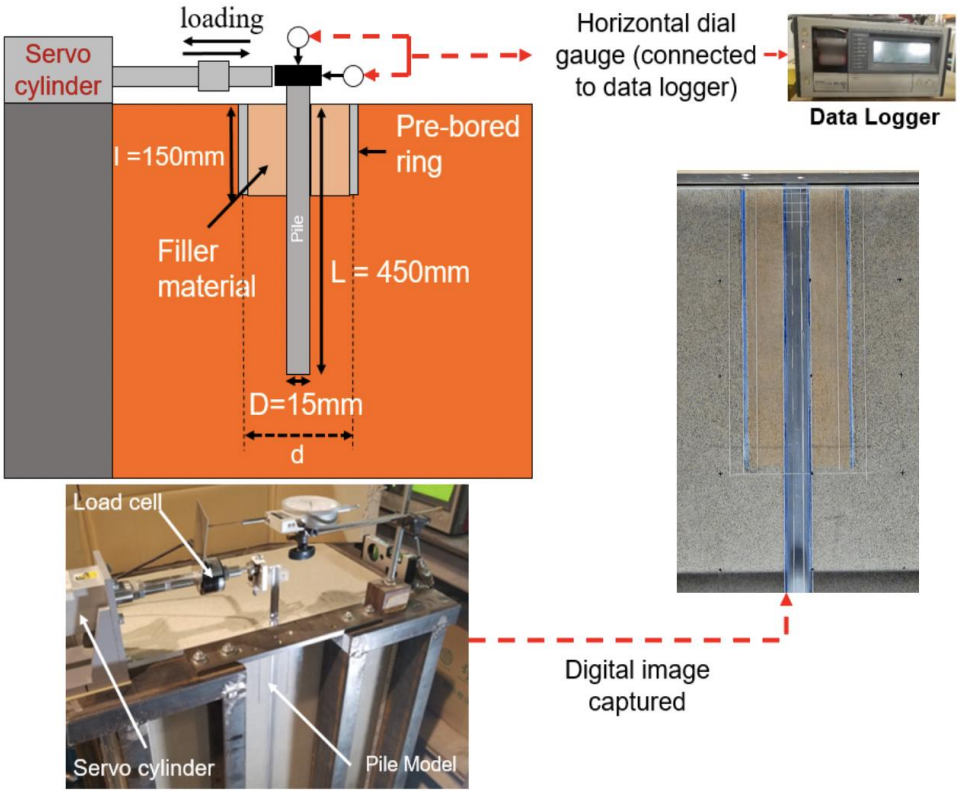

Figure 5-1 Testing scheme of half-size experimental test

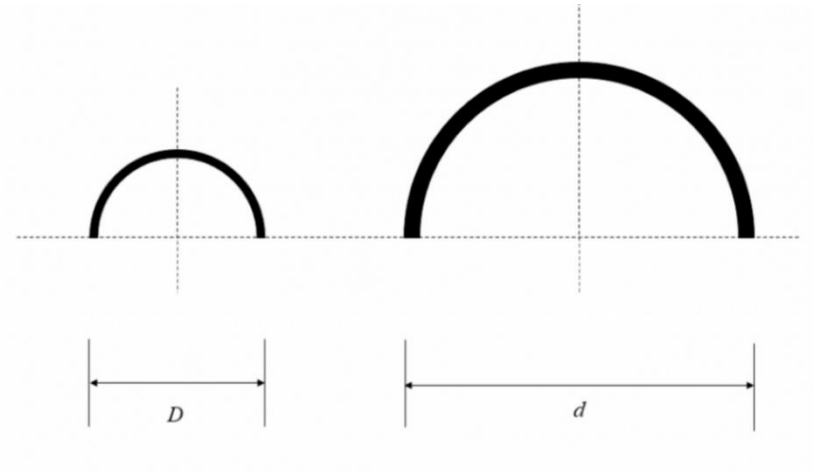

(a) (b)

Figure 5-2 Pile and ring model used in this research: (a) cross-section of the pile model, (b) cross-section of the ring model

5.3 IMAGE ANALYSIS USING PARTICLE IMAGE VELOCIMETRY (PIV) METHOD UNDER CYCLIC LATERAL LOADING

5.3.1 Particle Image Velocimetry (PIV) method

The measurement method of soil deformation explained in this paper conducted by digital images processing, which can be captured by digital cameras. White et al. (2003) described that a monochrome image is a matrix containing the intensity recorded at each pixel on the camera's charge-coupled device (CCD). Color images consist of three intensity matrices, one for each color channel. Most geotechnical physical model and element tests take place sufficiently slowly to be captured by digital cameras. The images analyzed in this paper were captured using a Panasonic Lumix DMC-G85 digital still camera, which has an image resolution of 3840 x 2160 pixels.

Particle Image Velocimetry (PIV) method is a measuring method that was initially developed by Adrian (1991) for the fluid mechanics experimental testing. It is also known as Digital Image Correlation (DIC) proposed by Sutton et al. (1983). This measurement technique is a common technique for investigating the soil deformation on geotechnical experimental model tests. The capabilities of this PIV method have also improved significantly in recent years.

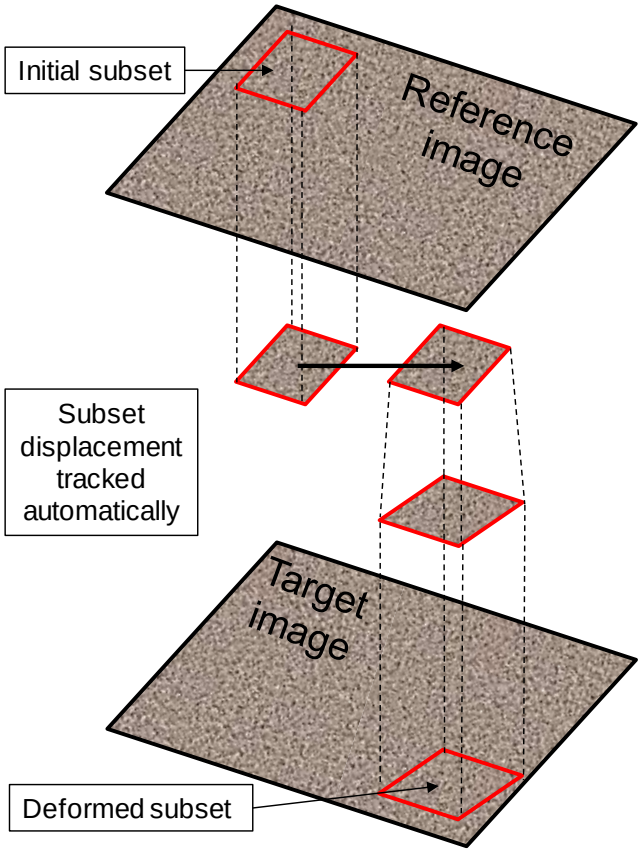

Figure 5-3 General overview of the PIV-DIC method (after Stainer et al., 2016)

The general overview of the PIV-DIC method is shown in Figure 5-3. A modified approach has been developed to implement PIV in geotechnical testing. Fluid requires seeding with particles to create features upon which can operate by image processing, and natural sand has its texture in the form of different-colored grains and the light and shadow formed between adjacent grains when illuminated (White et al., 2003). The image processing conducted by PIV to measure the displacement between a series of digital images. The reference image divided into a grid of test patches, and each patch consists of a matrix image. Measurement of the test patch displacement between reference images and target images, a search patch is extracted from the target images. This search patch extends beyond the test patch by a distance, in the x and y directions. In order to reduce the computational requirement, the correlation operations are conducted in the frequency domain by taking the fast Fourier transform (FFT) of each patch and following the convolution theorem (White et al., 2003). The analysis repeated by comparing the reference image and the next images in the series. To eliminate this possibility, the reference image, in which the test patches are established, is updated at intervals during the analysis.

5.3.2 Image analysis using GeoPIV-RG model in MATLAB

The specific software used for the benchmark cases is referred to as GeoPIV-RG and is an update of the GeoPIV program which represents the typical algorithms currently used in research and described by White et al. (2003). A brief overview of the computational approach is given first. The comparison is then performed using artificial “soil-like” images subjected to various modes of deformation. Lastly, an example application is given that illustrates the impact this improvement in measurement precision can have on the interpretation of a classical geotechnical problem. Digital images captured during a geotechnical model test are usually analyzed in sequence, starting with an initial reference image. If the reference image is retained as the initial image (it is called “leapfrog” scheme), then zero-order subsets can suffer a loss of correlation in regions experiencing large deformations due to a mismatch between the subset shape and the deformation being observed. On the other hand, the reference image is updated after every sequence (it is called “sequential” scheme) to minimize the distortion that would reduce the correlation in the target images, random walk errors are accumulated (White et al. 2003) because the total displacement is measured as the total displacement of many small displacements, which have an associated error for each step.

Stainer et al., 2016 proposed the new version of GeoPIV uses a combination of these two schemes to minimize accumulated random walk errors while maintaining tolerable correlations. The number of increments using the leapfrog scheme before updating the reference image (leapfrog parameter) is user-defined by trial and error depending on the amount of deformation occurring between sequential images. Also, the “search zone” over which the correlation measure is computed for each subset is user-defined. Therefore, the search zone requires trial-and-error refinement to achieve the best results. So, it can avoid the need for trial-and-error refinement of either the leapfrog value or the search zone parameter for each subset. White et al., (2003) conducted seven PIV analysis of the random image, which result the PIV patches size of 50x50 pixel provide the lowest standard error. It was distributed around zero with a standard error of 0·0007 pixels. In this research search patch size of 50x50 pixel was used. The overarching framework controlling the computation process is the reliability-guided (RG) method proposed by Pan (2009), as implemented in MATLAB by Blaber et al. (2015) so the software is referred to as GeoPIV-RG (Stainer et al., 2016).

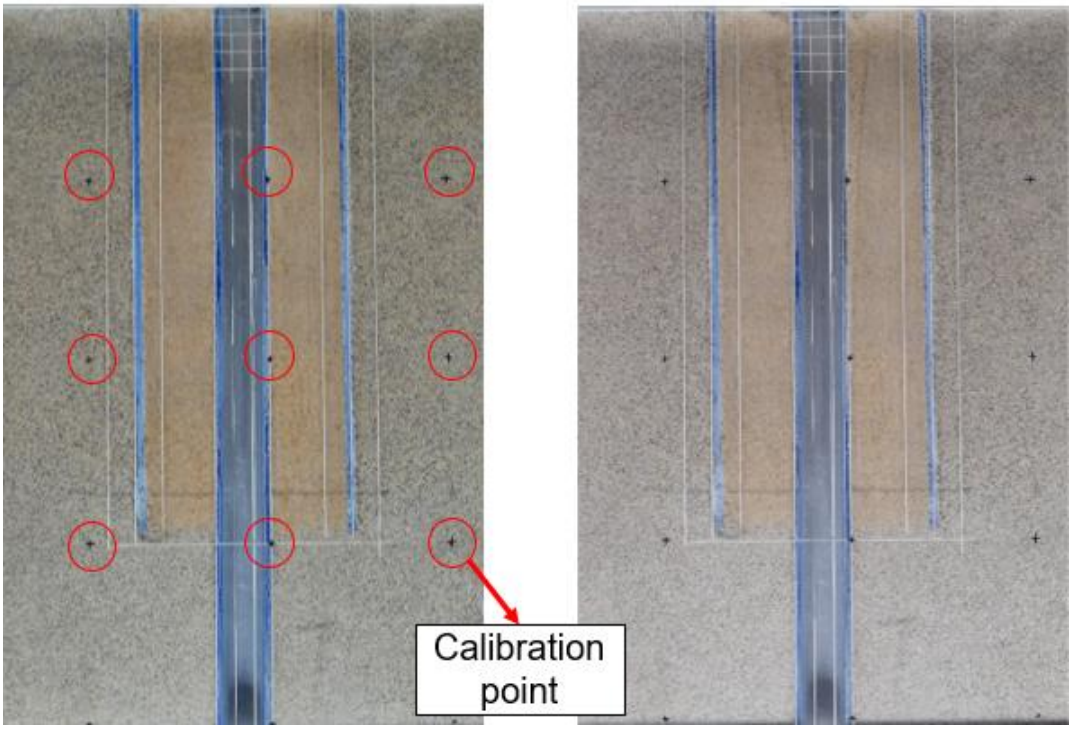

(a) (b)

Figure 5-4 Input image on MATLAB model: (a) reference image (before loading applied) and (b) target image (after 50 times of cyclic loading)

In this research, the reference image is the initial condition before the lateral loading is applied. The target image is the sequence images during the lateral cyclic loading until 50 times of the cycle. Each cycle, the image was captured for four images, so the total target image is 200 target images to get more precision results. The reference subset is allowed to deform using a shape function describing first-order deformations in conjunction with image-intensity interpolation techniques to improve the correlation between the reference and target subsets via optimization (Schreier and Sutton 2002). After an initial subset has been analyzed, the next computations are preconditioned using the results from the previous result of the analyzed subset that has the highest correlation. The reference image is updated when the correlation coefficient of the subsets follows the user-defined boundary. The first-order subset shape function leads to improved precision and reduced random walk errors because correlation is better to allow the reference image to be updated less frequently for the image with low deformations. The procedure of the image processing analysis is summarized by the flowchart shown in Figure 5-5.

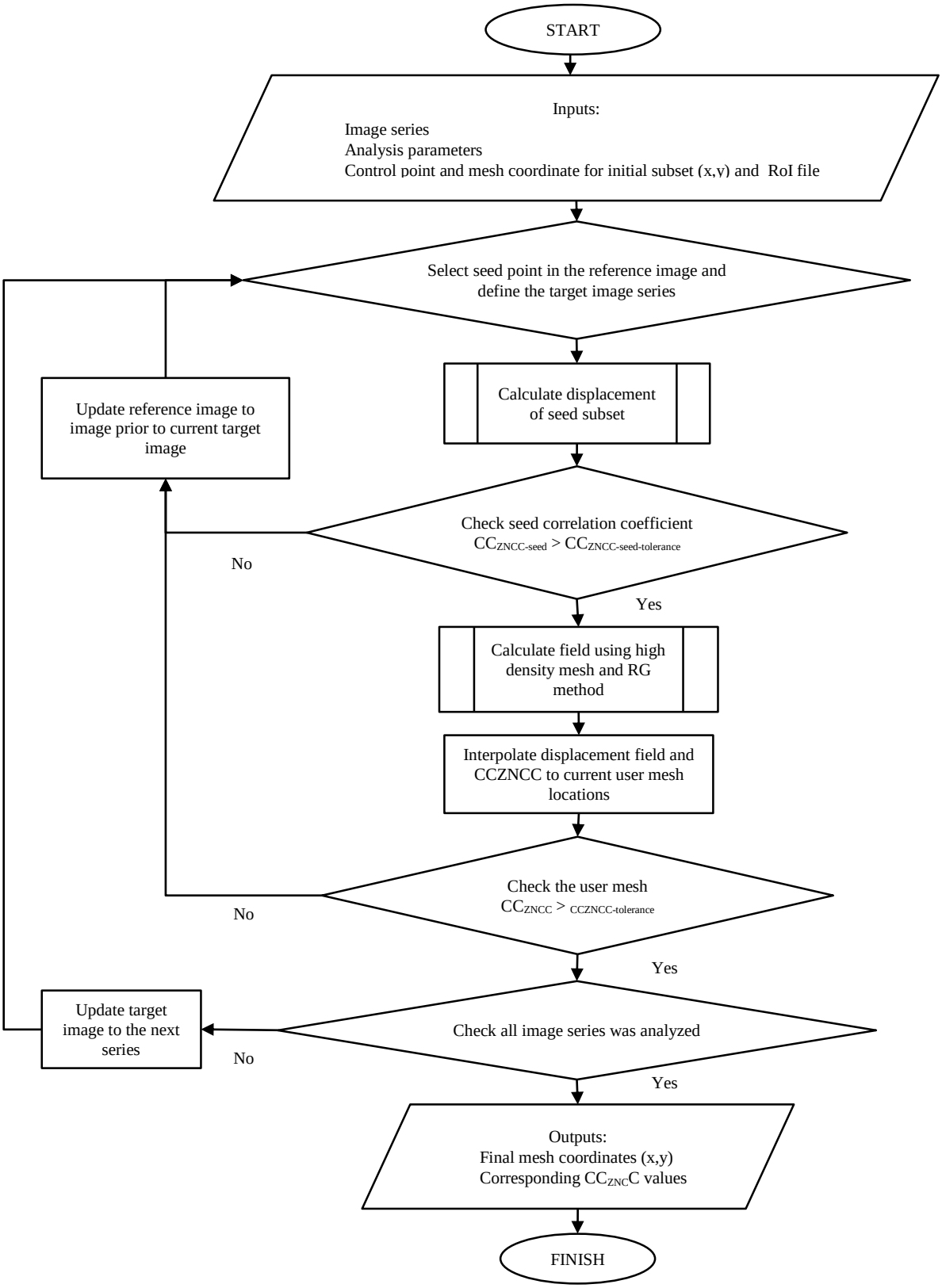

Figure 5-5 Flowchart for GeoPIV-RG analysis (after Stainer et al., 2016)

5.4 STRAIN DISTRIBUTION OF FILLER MATERIAL UNDER CYCLIC LATERAL LOADING

5.4.1 Vector displacement distribution

Figure 5-6 shows the deformation vector of the soil for each case, and resultant displacement is shown in Figure 5-7. It was observed that the soil distribution area was reduced due to the attachment of pre-bored ring with different diameter compared to the one-layered condition. However, on the 45 mm of ring diameter case (3 times of pile diameter, 3*D*), the displacement of soil has occurred in the outside area of the pre-bored ring similar to the no-ring case.

In the case of 60 mm (4*D*) and 75 mm (5*D*) ring diameter, the displacement of soil only occurred inside the ring. It indicates that the ring was displaced during the cyclic loading for the 45 mm pre-bored diameter case which may be associated with the skin friction of soil and ring. This condition can be affected by the performance of the pre-bored ring foundation system because the pre-bored ring might be removed and changes the properties of filler material.

5.4.2 Strain distribution

Figure 5-8 and Figure 5-9 shows the total strain and volumetric strain distribution for each case, respectively. The pre-bored ring with a diameter of 45 mm (3*D*) can reduce the total strain and volumetric strain of soil due to cyclic lateral loading until 50 times of cycle compared with the one-layered case without the ring. Increasing the diameter of the ring also increase the total strain and volumetric strain value.

The failure pattern due to the pre-bored ring attachment also changes for each case. The attachment of pre-bored ring can reduce the failure zone diameter and increase the failure depth, but failure depth (100 mm) still covered inside the pre-bored ring by the ring depth of 150 mm (10*D*). If the diameter of the pre-bored ring is too small, the depth of failure zone increase, so, it needs the deeper embedded pre-bored ring system to accommodate the failure area of filler material due to lateral cyclic loading. PIV methods using GeoPIV-RG can be used to capture the mechanical behavior of soil due to lateral cyclic loading at a uniform loading rate.

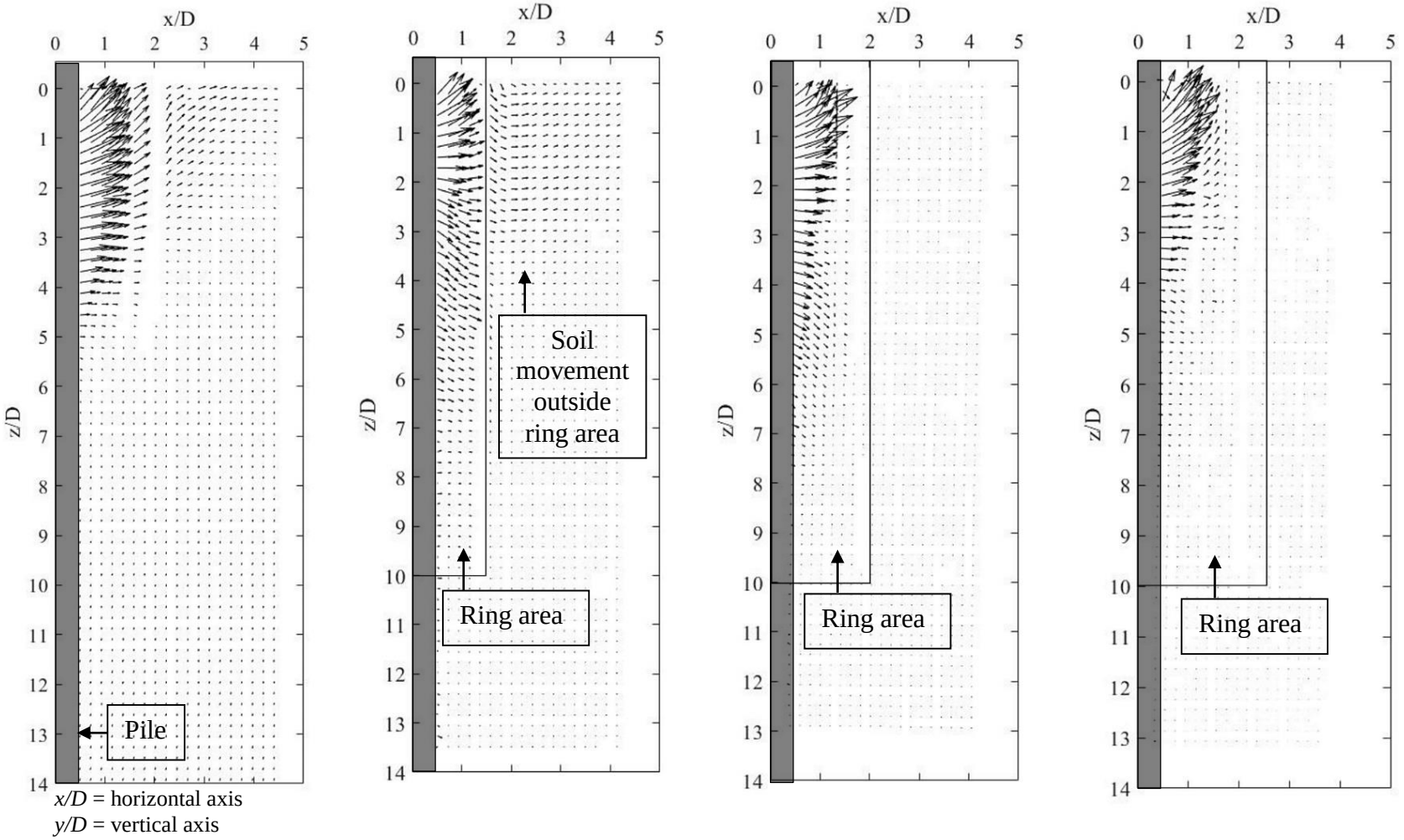

Figure 5-6 Vectoral displacement until 50 times of cyclic loading (a) No-Ring, (b) *d/D* = 3, (c) *d/D* = 4, (d) *d/D* = 5

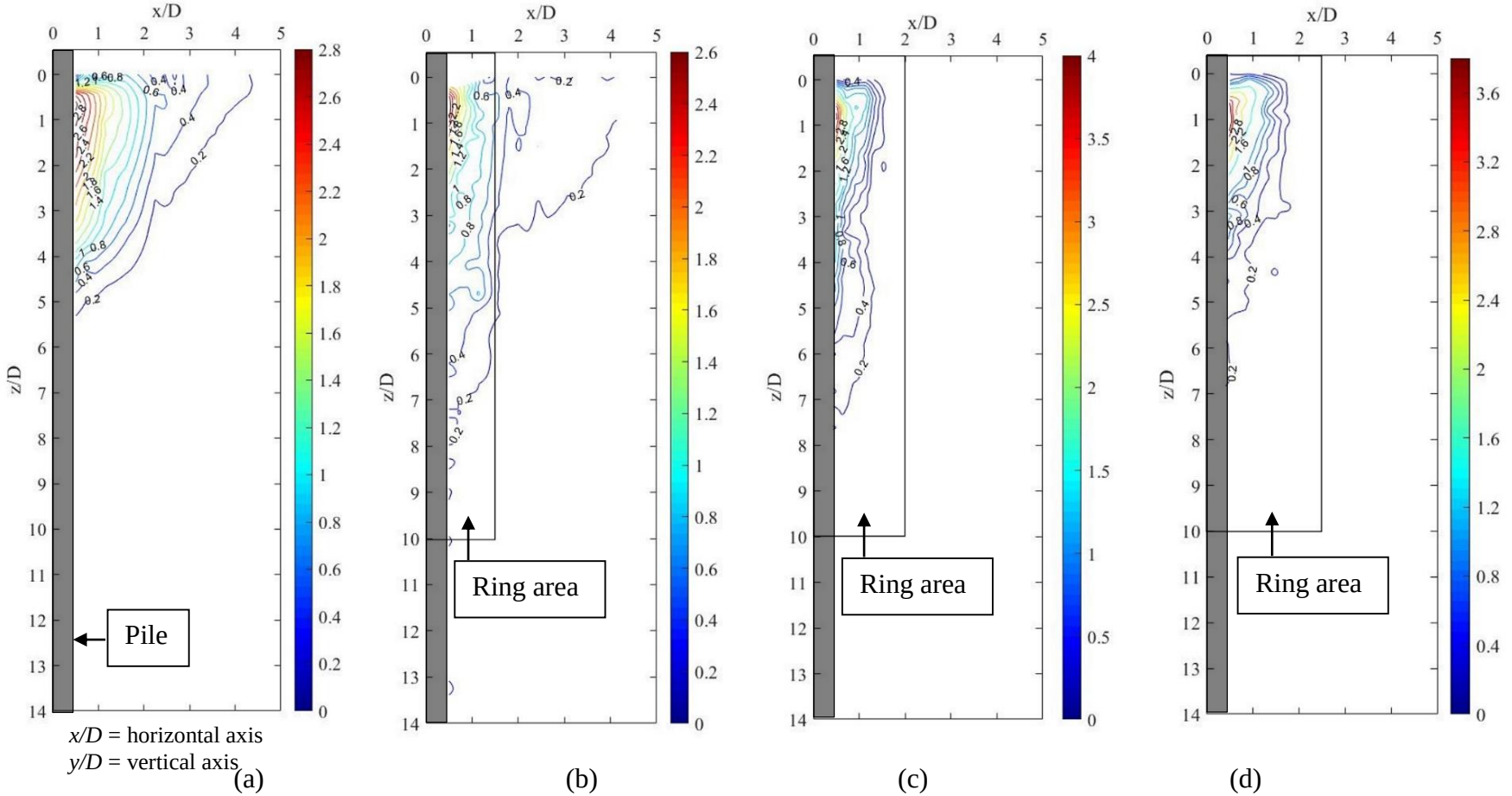

Figure 5-7 Resultant displacement until 50 times of cyclic loading (a) No-Ring, (b) *d/D* = 3, (c) *d/D* = 4, (d) *d/D* = 5

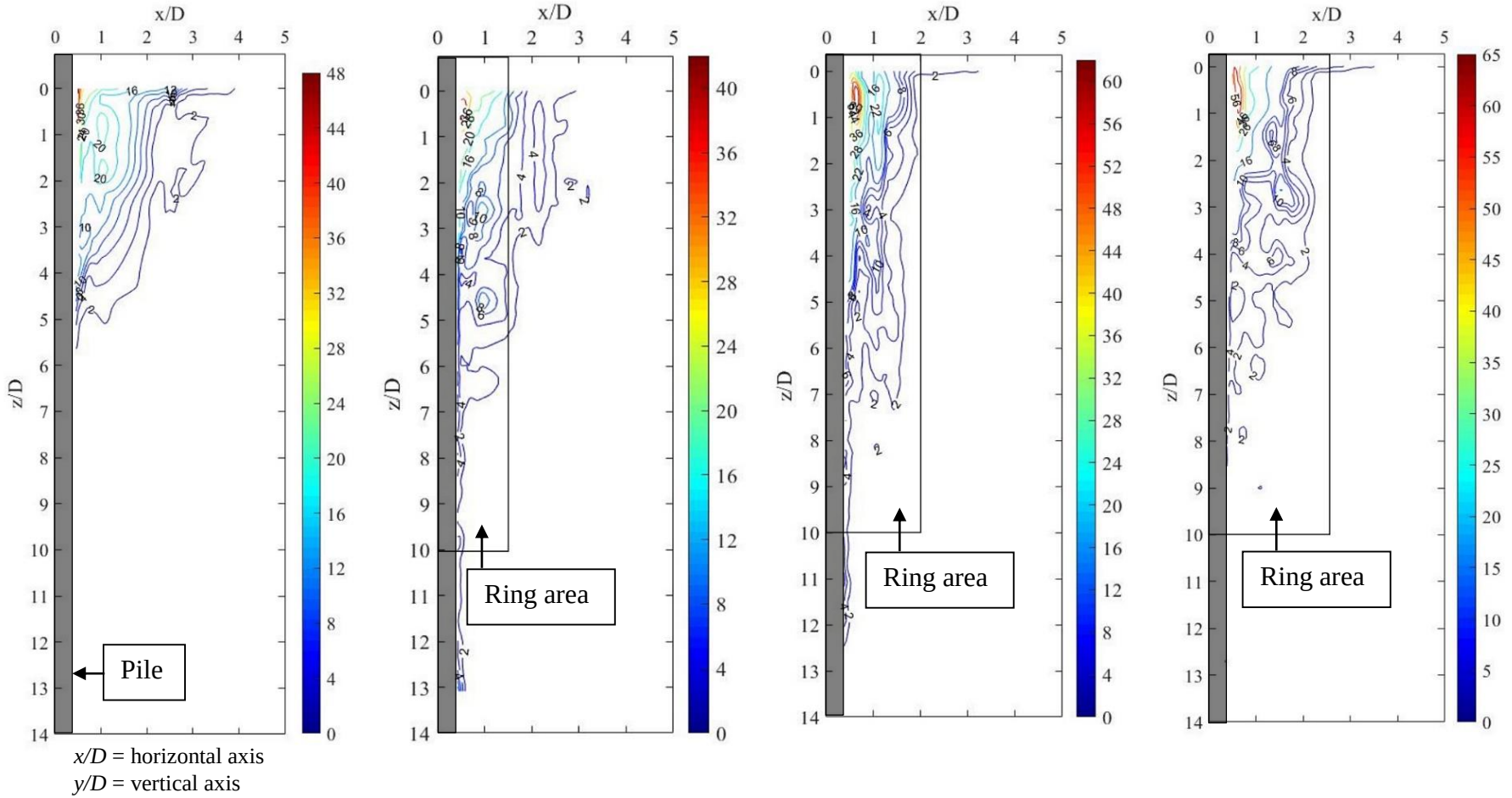

Figure 5-8 Total shear strain distribution until 50 times of cyclic loading (a) No-Ring, (b) *d/D* = 3, (c) *d/D* = 4, (d) *d/D* = 5

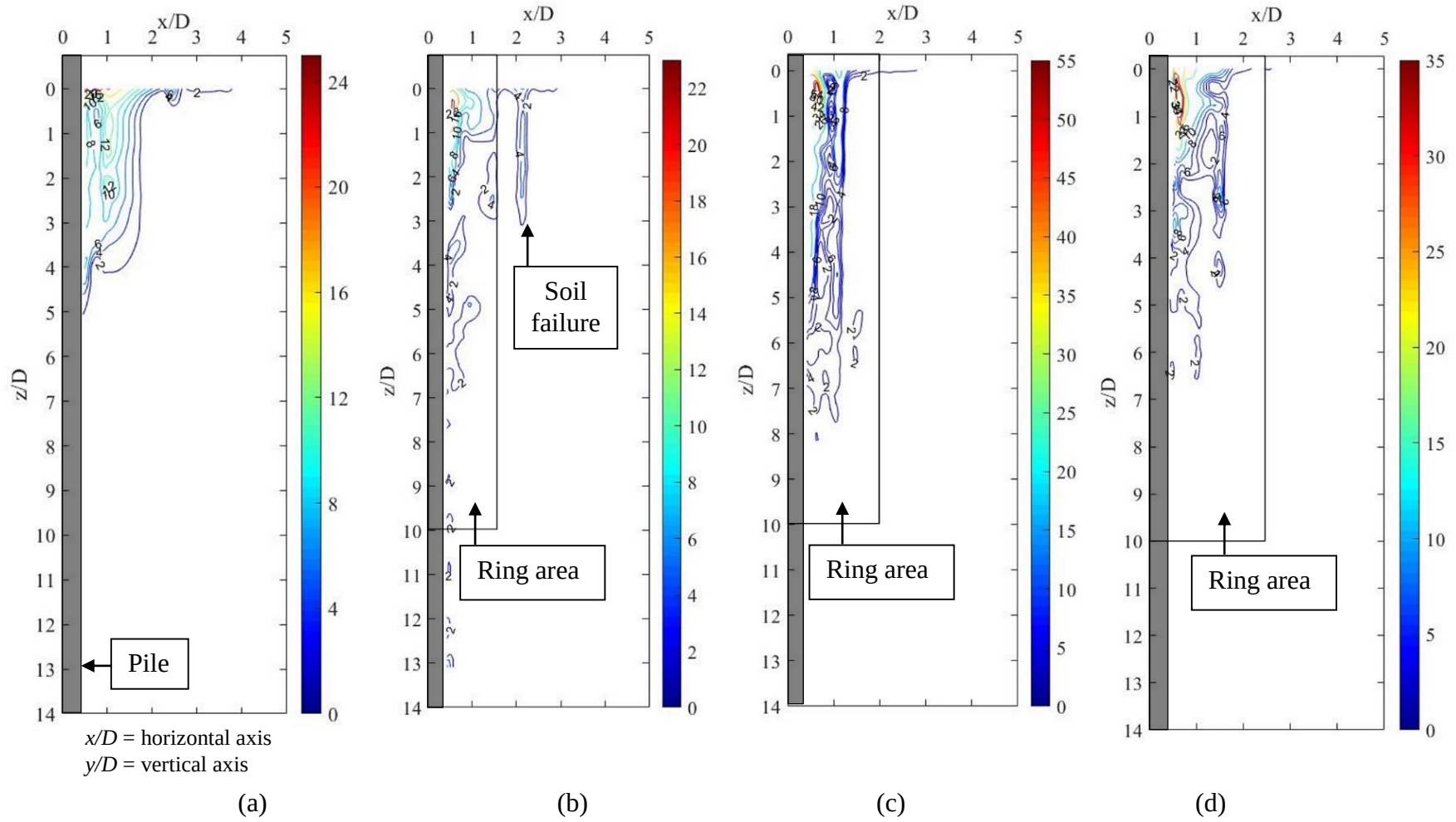

Figure 5-9 Volumetric shear displacement until 50 times of cyclic loading (a) No-Ring, (b) *d/D* = 3, (c) *d/D* = 4, (d) *d/D* = 5

5.5 STRESS DISTRIBUTION OF FILLER MATERIAL UNDER CYCLIC LATERAL LOADING

5.5.1 Measurement of Lateral Earth Pressure

The pressure transducers are attached on the pile body and ring model and monitored using data logger. Four earth pressure transducer sensors were attached at the pile and ring. The location point of pressure transducers attached on the pile and ring is shown in Figure 5-10 to detect the passive earth pressures around the pile body during lateral cyclic load. In this experiment, the pressure transducer type PDA-PB (Figure 5-11) is attached on the pile and on the inside area of the ring to evaluate the stress distribution due to this system.

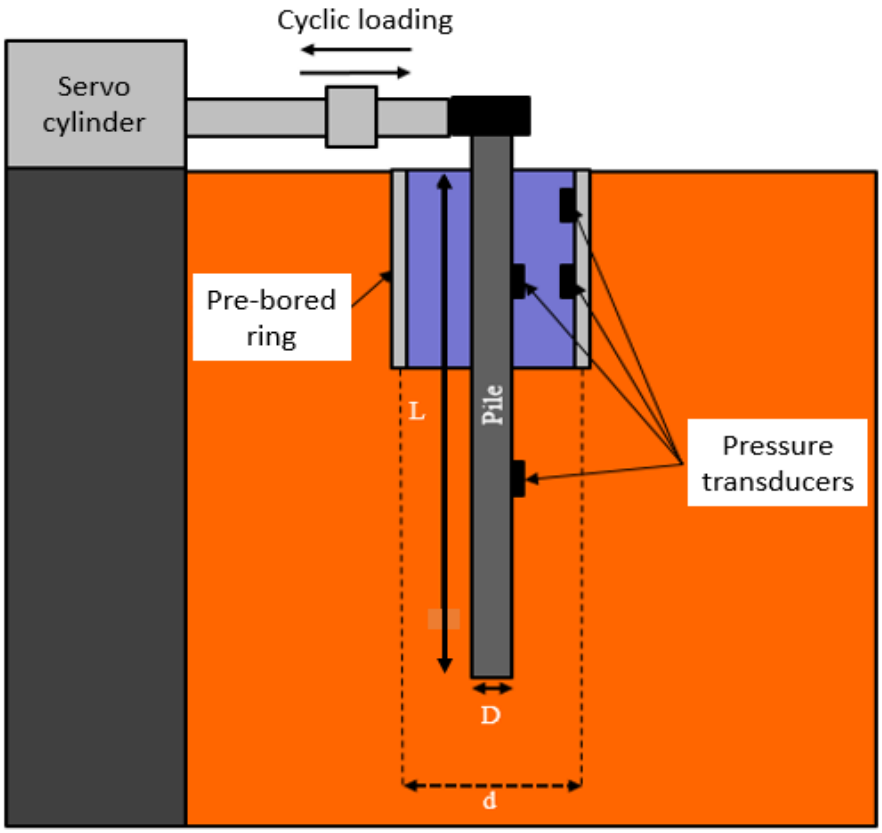

Figure 5-10 Pressure transducer sensor location on the experimental test

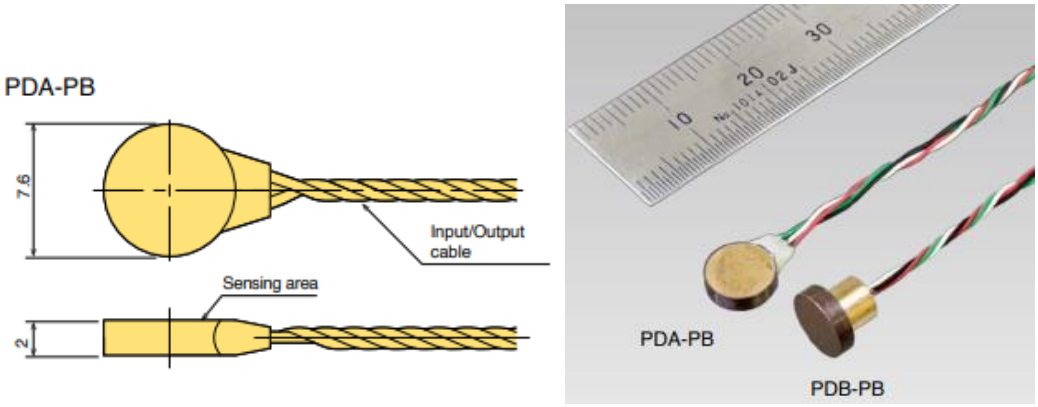

Figure 5-11 Pressure transducer sensor

5.5.2 Pile pressure

Figure 5-12 shows the normalized distributions of the measured earth pressures (P_{max}) with depth z which mobilized on pile body due to lateral loading. Therefore, by dividing the measured P_{max} by $K_p^2\gamma$ and, one can get the distribution of the normalized P_{max} with depth, z. The placement of pre-bored ring induced the increasing of pile pressure inside the ring area, while the piling pressure outside the pre-bored ring area is similar.

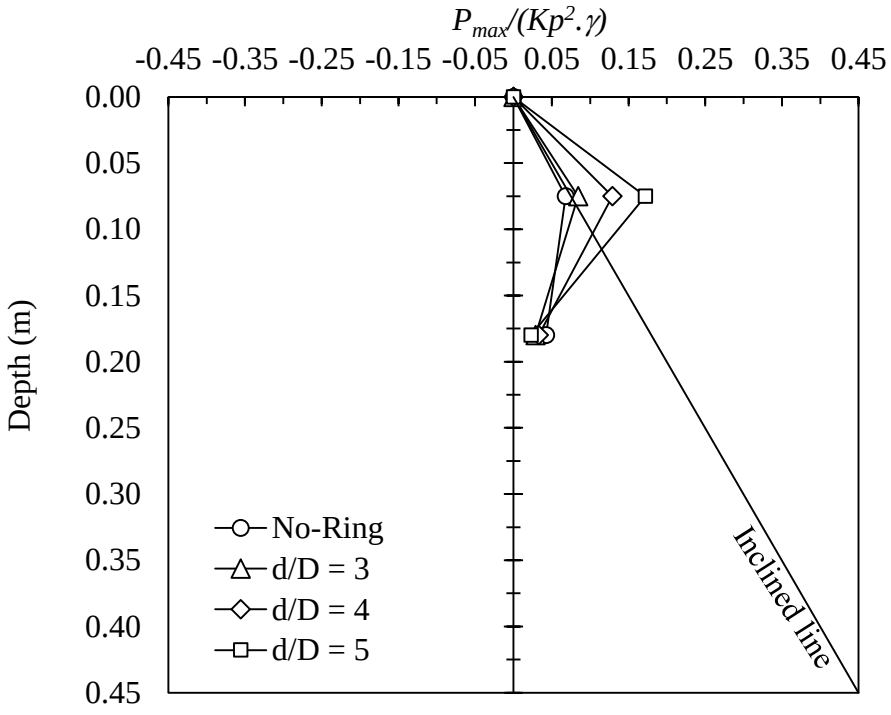

Figure 5-12 Normalized earth pressure distribution, $us/(Kp^2\gamma)$ along pile body

Based on Figure 5-13, placement of pre-bored ring affected the lateral earth pressure on pile foundation during the cyclic loading. At the first cyclic loading, the one-layered soil condition provided the lowest soil pressure. However, during the cyclic loading, it increases significantly. While the soil pressure on the pile using the pre-bored ring provided higher pressure at the first cycle, but it did not increase significantly during the cyclic loading. At 50 times of cyclic loading, the soil pressure on the pile for no-ring condition provide higher value than the pre-bored ring system. It indicates that the pre-bored ring system can reduce the potential increase of passive earth pressure on the pile so that it can reduce the pile stress during the cyclic loading.

The potential increasing of soil pressure on pile can be seen in Figure 5-14. Placement of pre-bored ring system can have reduced the potential increase of pile stress during the cyclic loading until 50 times of the cycle. It can reduce 2-3 times of potential increasing of soil pressure on which can reduce the pressure in the pile body due to lateral cyclic loading. The cracking possibility also can be reduced due to less potential of soil densification under cyclic lateral loading.

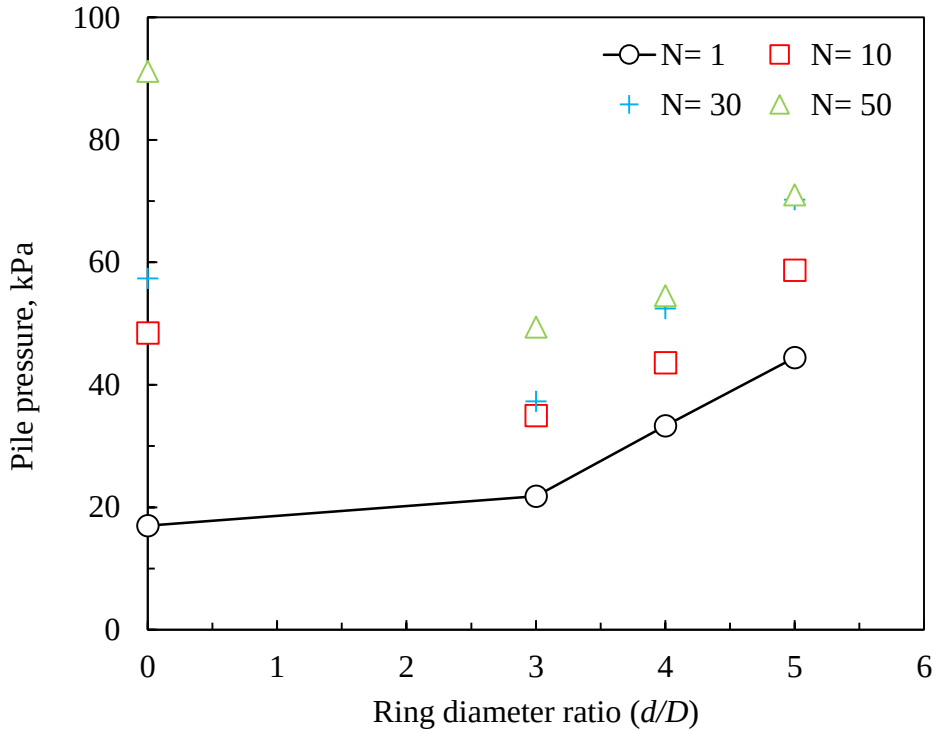

Figure 5-13 Pile pressure occurred during cyclic loading

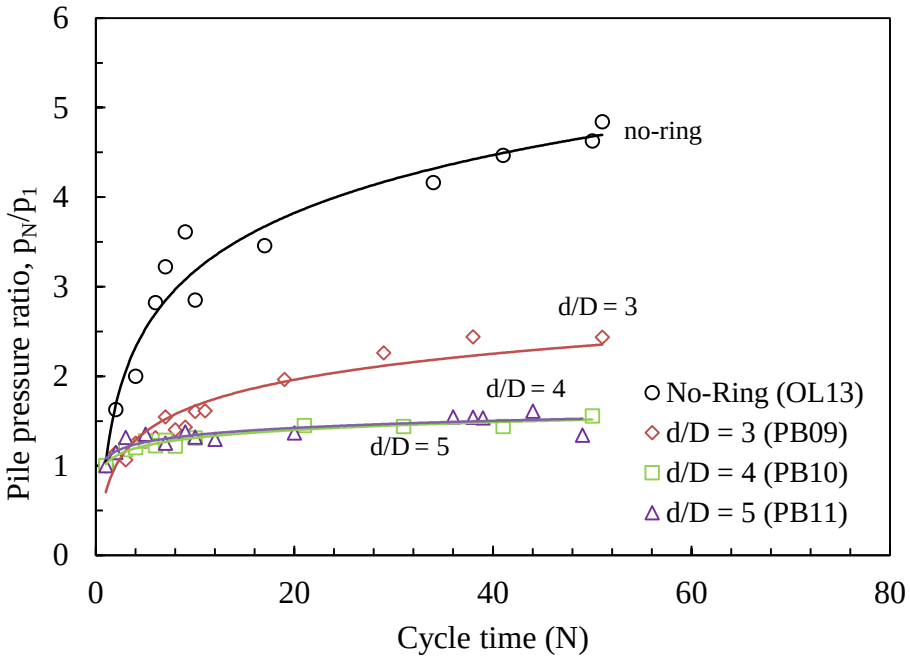

Figure 5-14 Potential increasing of pile pressure during lateral cyclic loading

5.5.3 Inside ring pressure

Measurement of pressure-induced inside the pre-bored ring also conducted to evaluate the effect of lateral displacement on the pile head to the pre-bored ring. The results of ring pressure inside the ring are shown in Figure 5-15. Pre-bored ring with ring diameter ratio (*d/D*) of 3 provides the higher pressure than the other ring diameter. It means the ring was holding the pile and soil displacement due to lateral loading. It is also indicating that there is a possibility of ring movement because of the pressure on the ring still very high almost the same with the piling pressure. This condition is similar to the results of the image analysis that on the ring diameter ratio (*d/D*) of 3 there affected area outside the ring were occurred. Potential increasing of ring pressure is shown in Figure 5-16. The potential increasing of ring pressure is increased with the increasing of ring diameter. The smaller diameter of the ring provides a higher pressure on the ring structure. In the smaller ring, the strain distribution reached the ring area, and the soil movement also occurred in the outside of the ring. It means the cyclic lateral loading affected ring behavior in case of 3D of ring diameter. Reduction of pile stress affected on the increasing of the pressure inside the ring. Influence of pre-bored ring with ring diameter ratio (*d/D*) more than 5 is not significant. Based on these results, the optimum diameter of the ring in between 3 to 5 time of pile diameter that can provide more stable results of pile stress and soil behavior.

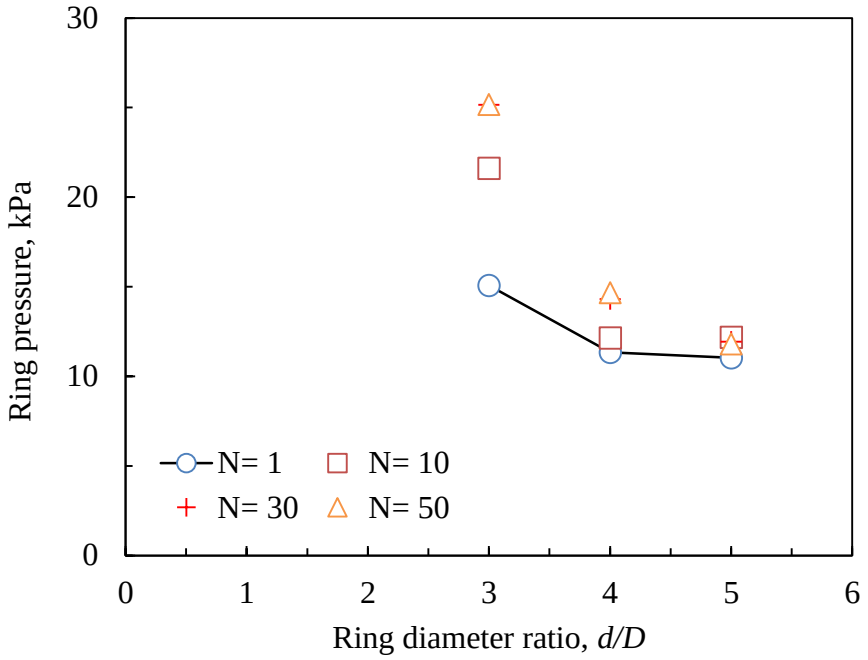

Figure 5-15 Pressure inside the pre-bored ring

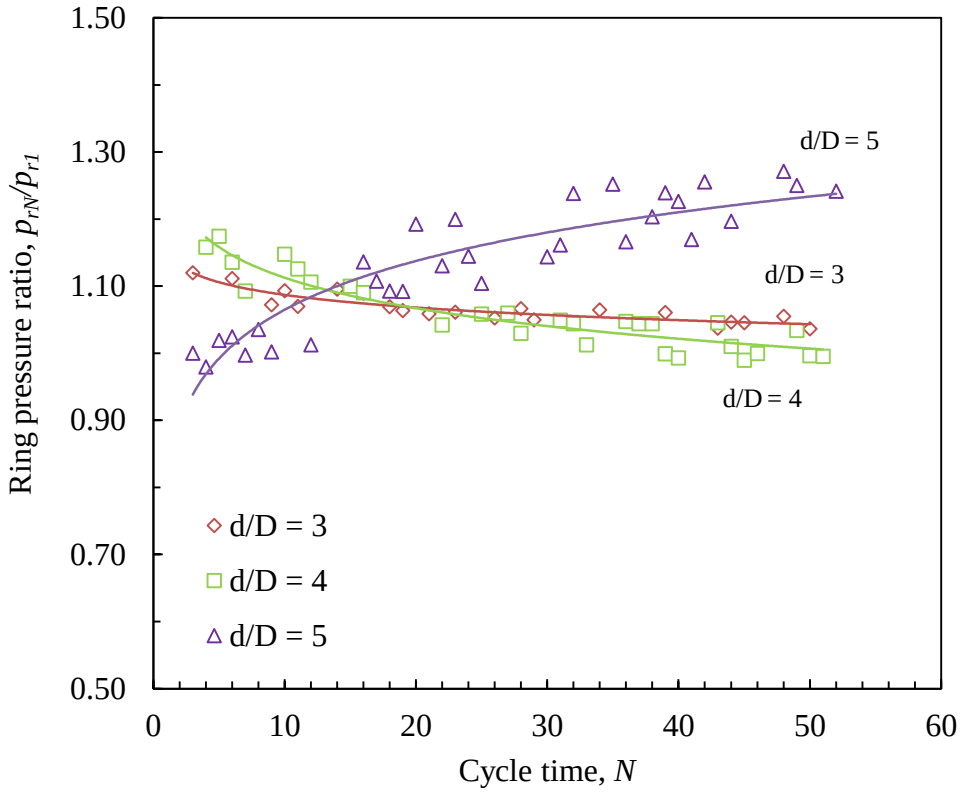

Figure 5-16 Potential increasing of pile pressure during lateral cyclic loading

5.6 SUMMARY

In this chapter, the measurement of soil behavior inside the pre-bored ring, especially on failure pattern and stress-strain distribution of soil on pre-bored ring system are evaluated. The use of Particle Image Velocimetry (PIV) method also explained to measure the soil deformation on an experimental testing model of the laterally loaded pile. The results of soil deformation and strain distribution can explain the failure pattern of the pre-bored pile foundation system under cyclic lateral loading. Conclusions of this study can be summarized as follows.

1. The failure pattern due to the pre-bored ring attachment also changes for each case. The attachment of pre-bored ring can reduce the failure zone diameter and increase the failure depth, but failure depth (100 mm) still covered inside the pre-bored ring by the ring depth of 150 mm (10*D*). If the diameter of the pre-bored ring too small, the depth of failure zone increase, so, it needs the deeper embedded pre-bored ring system to accommodate the failure area of filler material due to lateral cyclic loading. PIV methods using GeoPIV-RG can be used to capture the mechanical behavior of soil due to lateral cyclic loading at a uniform loading rate.
2. The soil deformation area was reduced due to the attachment of pre-bored ring with different diameter compared to the one-layered condition. However, on the 45 mm of ring diameter case (3 times of pile diameter, 3*D*), the displacement of soil has occurred in the outside area of the pre-bored ring. On the wider diameter cases, the displacement of soil only occurred inside the ring.
3. Attachment of pre-bored ring with different diameter changes the failure pattern of soil on the pre-bored ring system due to lateral cyclic loading. Pre-bored ring with a diameter of less than 60 mm (4*D*) can reduce the total strain of soil and the failure diameter due to cyclic loading. However, if the pre-bored ring diameter is too small, it might be affected in the long term condition of the pre-bored ring and filler material properties which associated with the skin friction of soil and ring. This condition can be affected by the performance of the pre-bored ring foundation system because the pre-bored ring might be removed in case of shallow ring depth and changes the properties of filler material.
4. Placement of pre-bored ring system can reduce the potential increase of pile stress during the cyclic loading until 50 times of the cycle. It can reduce 2-3 times of

potential increasing of soil pressure on which can reduce the pressure in the pile body due to lateral cyclic loading. The cracking possibility also can be reduced due to less potential of soil densification under cyclic lateral loading.

5. The pressure occurred on the ring is reduced with the increasing of ring diameter. The smaller diameter of the ring provides a higher pressure on the ring structure. In the smaller ring, the strain distribution reached the ring area, and the soil movement also occurred in the outside of the ring. It means the cyclic lateral loading affected ring behavior in case of 3*D* of ring diameter. Reduction of pile stress affected on the increasing of the pressure inside the ring. Influence of pre-bored ring with ring diameter ratio (*d/D*) more than 5 is not significant. Based on these results, the optimum diameter of the ring is between 3 to 5 time of pile diameter that can provide more stable results of pile stress and soil behavior.

5.7 **REFERENCES**

Adrian, R.J., 1991. Particle-imaging techniques for experimental fluid mechanics. Annual Review of Fluid Mechanics, 23: 261–304.

Blaber, J., Adair, B., and Antoniou, A., 2015. Ncorr: open-source 2D digital image correlation MATLAB software. Experimental Mechanics, 55(6): 1105–1122.

Pan, B., 2009. Reliability-guided digital image correlation for image deformation measurement. Applied Optics, 48(8): 1535–1542.

Schreier, H.W., and Sutton, M.A., 2002. Systematic errors in digital image correlation due to under matched subset shape functions. Experimental Mechanics, 42(3): 303–310.

Stanier, S.A., and White, D.J., 2013. Improved image-based deformation measurement in the centrifuge environment. Geotechnical Testing Journal, 36(6): 1–14.

Stainer, S.A., Blaber, J., Take, W.A., and White, D.J. Improved image-based deformation measurement for geotechnical applications. Can. Geotech. J. Vol 53. 2016. pp. 727-739.

Sutton, M.A., Wolters, W.J., Peters, W.H., Ranson, W.F., and McNeill, S.F. 1983. Determination of displacements using an improved digital correlation method. Image and Vision Computing, 1(3): 133–139.

Taylor, Z.J., Gurka, R., Kopp, G.A., and Liberzon, A. 2010. Long-duration time-resolved PIV to study unsteady aerodynamics. IEEE Transactions on Instrumentation and Measurement, 59(12): 3262–3269.

The Mathworks (2006): MATLAB software reference.

White, D.J., Take, W., and Bolton, M. 2003. Soil deformation measurement using Particle Image Velocimetry (PIV) and photogrammetry. Géotechnique, 53(7):619–631.

CHAPTER VI

SIMPLIFIED MODEL FOR DESIGN OF PRE-BORED PILE FOUNDATION SYSTEM

6.1 INTRODUCTION

In this Chapter, a simplified model for predicting the lateral response of pile foundations in a homogenous cohesionless soil describes by assuming a perfect plastic response of soil using differential equation based on the ultimate lateral strength mechanism. Comparison study between the proposed method and previous methods was evaluated to determine the best method for predicting the ultimate lateral pile capacity. The predicted lateral load also compared with the measured value based on an experimental laboratory test. In this research, 30 data from an experimental model test conducted in the laboratory test have been evaluated as a database for statistical analysis.

Previous researchers have published the prediction method for ultimate lateral resistance of piles in cohesionless soil (e.g., Brinch Hansen, 1961; Broms 1964; Meyerhoff et al. 1981; Petrasovits and Award, 1972; Prasad and Chari, 1999; Zhang et al., 2002; Awad-Allah and Yasufuku, 2013). The main parameter between those methods is the different assumption of lateral soil resistance on pile due to lateral loading. Each method provided a different value of lateral soil resistance; thus, the lateral load of the pile also different. So, in this research, the main parameter to evaluate in design method is lateral soil resistance of pile that occurred due to lateral pile loading. The behavior of the pile due to lateral loading can be analyzed using the beam on an elastic foundation theory or Winkler's model following this equation.

$$EI\frac{d^4y}{dz^4} + P = 0 \qquad (6\text{-}1)$$

where:

E = elastic modulus of the pile

I = inertia moment of pile section

P = lateral resistance per unit length of the pile

The general distribution of pile deflection, pile slope variation, bending moment, shear force and lateral soil reaction along the pile body due to lateral load and moment applied on the pile head are shown in Figure 6-1 (Reese and Matlock, 1956). The change of pile deflection, pile slope variation, bending moment, shear force, and lateral soil reaction with depth defined by the principle of structural mechanics followed the Winkler's model.

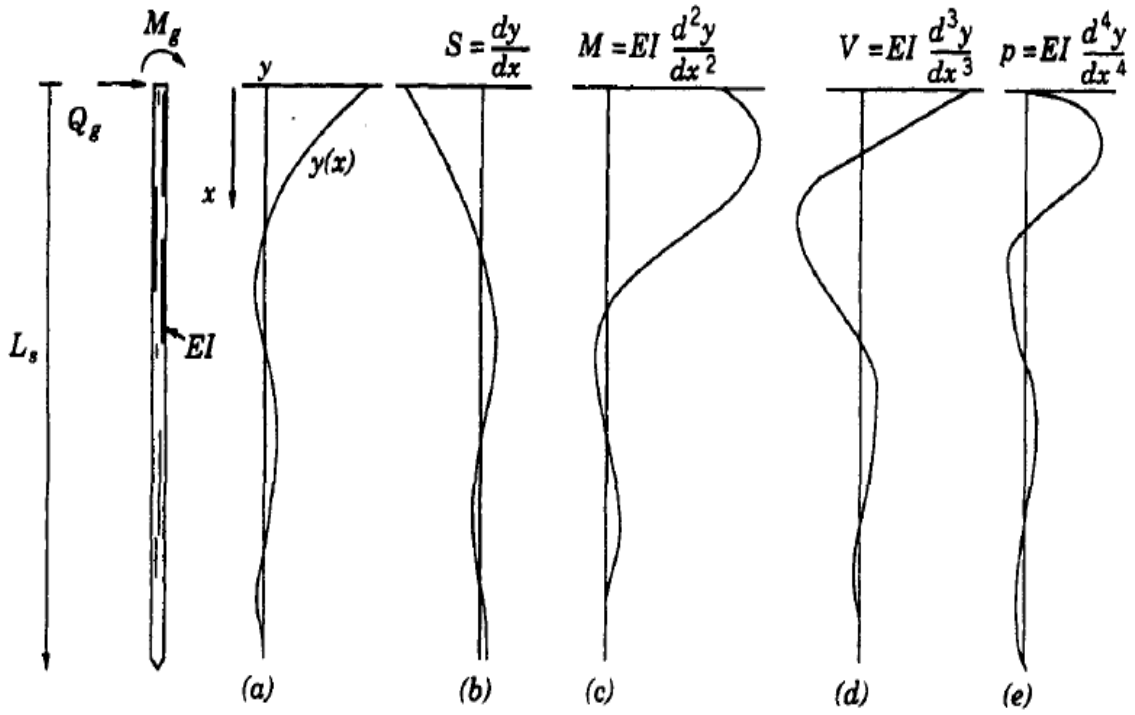

Figure 6-1 Pile foundation acted by lateral load and bending moment (Reese and Matlock, 1956)

The change in deflection, slope, moment, shear, and soil reaction with depth is defined by the principles of structural mechanics as follows:

$$S = \frac{dy}{dz} \tag{6-2}$$

$$M = EI\frac{dS}{dz} = EI\frac{d^2y}{dz^2} \tag{6-3}$$

$$V = EI\frac{dM}{dz} = EI\frac{d^3y}{dz^3} \tag{6-4}$$

$$P = EI\frac{dV}{dz} = EI\frac{d^4y}{dz^4} \tag{6-5}$$

where:

y = lateral displacement of the pile

S = slope of the pile

M = bending moment of the pile

V = shear force of the pile

P = lateral resistance per unit length of the pile

z = pile depth

EI = stiffness of the pile

Reese (1977) proposed the well-known 'p–y method' based on the differential equation to solve the laterally loaded pile problem, and it can be used for both free-and fixed-head single piles.

6.2 DIFFERENTIAL EQUATION FOR ESTIMATING PILE ULTIMATE LATERAL LOADING

The proposed analytical solution is based mainly on a fourth-order differential equation (beam on elastic foundation theorem). Therefore, the differential equation of the problem of a single laterally loaded pile will be formulated based on a beam on an elastic foundation technique (Winker's model). The differential equation of laterally loaded piles in cohesionless soil is given as the following formula.

$$EI\frac{d^4y}{dz^4} + p_u z = 0 \tag{6-6}$$

The general solution for the above differential equation is obtained as the following equation.

$$V = EI\frac{d^3y}{dz^3} = -\frac{p_u z^2}{2} + C \tag{6-7}$$

C is the unknown constant of integration results that can be obtained using the boundary conditions of the problem, as mention in Equation 6-8 and 6-9.

$$z = 0 \rightarrow \quad V = C = H_u \tag{6-8}$$

$$z = z_0 \rightarrow \quad V = 0 \tag{6-9}$$

So, the general equation for estimating the lateral capacity for flexible pile (L/D > 10) is obtained by the following equation.

$$H_u = \frac{P_u z_0^2}{2} \tag{6-10}$$

In case of rigid pile with $L/D \leq 10$ the general equation for estimating the lateral capacity is calculated by the following equation (Zhang et al., 2002).

$$H_u = \alpha p u z \tag{6-11}$$

where:

$$\alpha = 0.3(2.7z - 1.7L) \tag{6-12}$$

$$z = [-(0.567L + 2.7e) + (5.307L^2 + 7.29e^2 + 10.541eL)^{0.5}]/2.1196 \tag{6-13}$$

where:

H_u = ultimate lateral pile capacity

p_u = ultimate lateral soil pressure

z_0 = depth of pressure point

z = rotation point of the rigid pile

L = pile embedment length

e = eccentricity of loading on the pile

6.3 INFLUENCE OF EARTH PRESSURE AND SHEAR RESISTANCE

Most of the previous methods ignore the effect of side shear resistance as well as active earth pressure to predict the ultimate lateral capacity of pile. Recently published literature (Briaud and Smith, 1983; Smith, 1987; Zhang et al., 2002 and Awad-Allah and Yasufuku, 2013) has shown that the lateral pile-soil resistance can be expressed in two components: (1) the maximum earth pressure reaction, N_u, and (2) the maximum side shear reaction, T_u, as shown in Figure 6-2. The ultimate lateral resistance per unit length of pile (P_u) that can be calculated by two soil resistance components (i.e., N_u and T_u) against the pile, as follows.

$$P_u = N_u + T_u \tag{6-14}$$

where,

$$N_u = \eta p_{\max} z \tag{6-15}$$

$$T_u = \varsigma \tau_{\max} z \tag{6-16}$$

where:

P_u = ultimate lateral resistance per unit length of the pile

N_u = ultimate frontal soil resistance

T_u = ultimate side shear resistance

p_{max} = maximum frontal earth pressure

τ_{max} = maximum side shear pressure

z = depth of pressure point

η = shape factor for frontal soil pressure

ζ = shape factor for side shear resistance

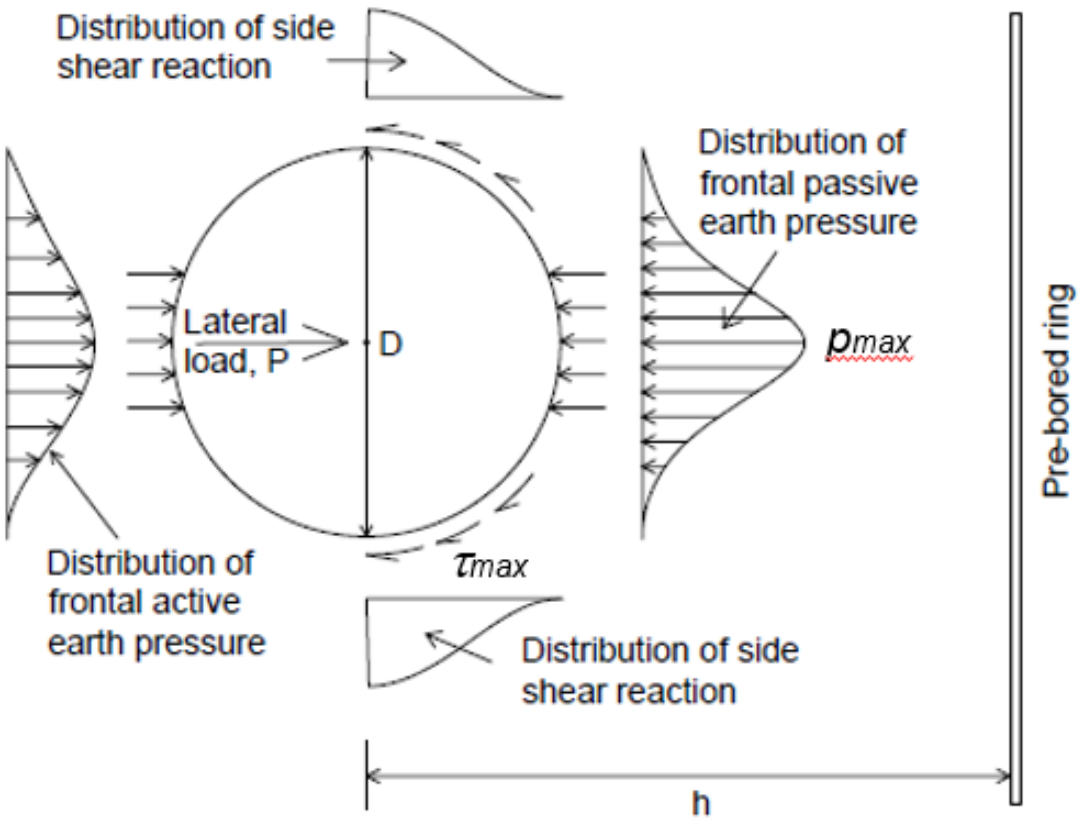

Figure 6-2 Distribution of side shear resistance and total earth pressure around the pile due to lateral loading

6.4 BOUNDARY CONDITIONS OF THE PROPOSED MODEL

1. Full active and passive earth pressure is mobilized due to lateral displacement on the pile head

The load applied on the pile head assume as a pinned connection on the superstructure. The pile is deflected towards the one side by the applied lateral loading. Thus, passive earth pressure is created in front of the pile, while active earth pressure is created on the other side. Relatively similar patterns of earth pressure distributions were primarily introduced by Meyerhof et al. (1981); Broms (1964); and Brinch Hansen (1961), but they ignored the effect of active (rear) earth pressure.

2. Soil behavior is perfectly plastic

The assumption for the response of the soil due to lateral loading is an elastic-plastic response. Since the lateral displacement in the elastic range is very small (almost equal zero), the soil response can be assumed to be a perfect plastic. As soon as there is a lateral deflection, the response is at its maximum or its minimum conditions. So, the total lateral resistance for each unit length of the pile is as given by the following formula for cohesionless soil (c=0).

$$P = \gamma' Dz(K_p - K_a) \tag{6-17}$$

where:

P = lateral resistance per unit length of the pile
γ’ = unit weight of soil
D = pile diameter
z = depth of pressure point
D = pile diameter
K_p = coefficient of passive earth pressure
K_a = coefficient of active earth pressure

3. Rotation point of the pile due to lateral loading

Lateral soil resistance and deformation of the pile are affected by soil type and slenderness of pile (L/D). These parameters also effected on pile rotation point due to lateral loading. Abbas et al. (2017) described the pile with slenderness ratio (L/D) of 10 or rigid pile, the

rotation point of pile located in (1/5) *L* from the pile base. While the pile with slenderness ratio (*L/D*) of 15 and 20, the rotation point location is (1/2) *L* and (3/5) *L* from pile base, respectively. Pile with L/D of 25 or flexible pile; the rotation point location is (7/10) *L* from pile base. Awad-Allah and Yasufuku (2013) expressed the pile rotation is around the plastic hinge, which is in a range between 9*D* to 9.5*D* below the soil surface (transition zone) for the flexible pile.

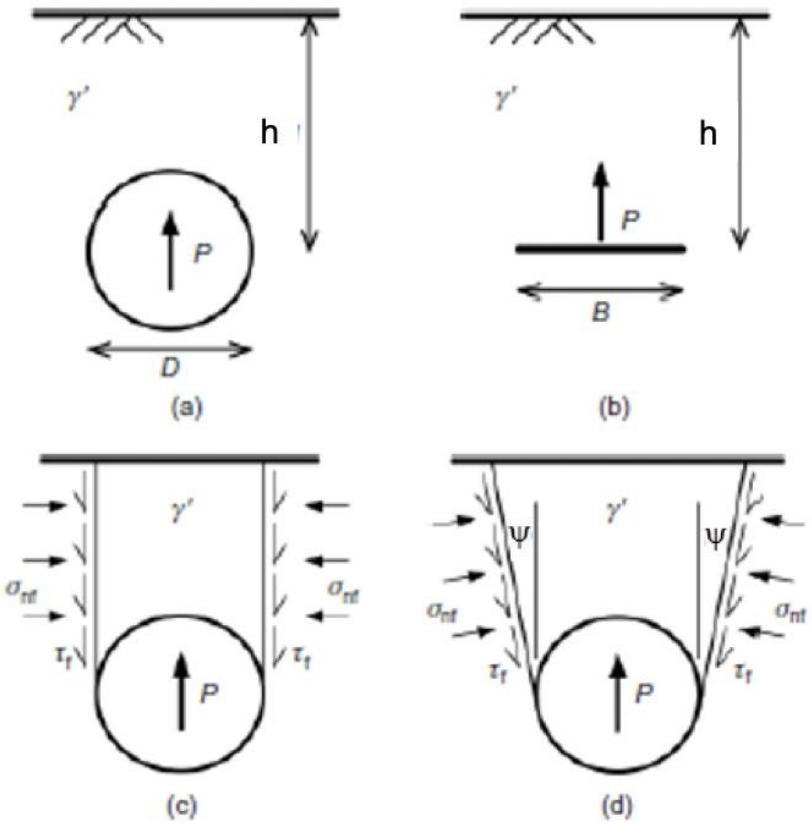

Figure 6-3 Failure mechanism of uplift pipe (a) pipe geometry; (b) strip geometry; (c) vertical slip mechanism; (d) inclined slip mechanism (White et al., 2008)

4. Effect of ring diameter on the pre-bored ring

The general solution for ring effect on the system is adopted from the buried pipe in a certain depth proposed by White et al. (2008). These solutions can be broadly classified into two categories: limit equilibrium and plasticity solutions. The limit equilibrium approach does not impose any particular flow rule but instead allows the equilibrium of any assumed failure mechanism to be assessed. It is necessary to assume the stress distribution in the soil, so this

assumption must be realistic if an accurate solution is to be reached. The boundary value problem is defined in Figure 6-3(a), a pipe with a diameter of *D*, and in Figure 6-3(b) for a strip anchor of breadth *B*. The cover depth *h* is measured to the waist of the pipe, and the uplift resistance per unit length is denoted *P*.

6.5 ULTIMATE LATERAL SOIL PRESSURE

6.5.1 Idealization from uplift resistance of buried pipe (White et al., 2008)

By idealizing the pile as a flat horizontal element, a small additional volume of soil is considered, occupying the space that is filled by the top half of the pile. At a small distance (low *h/D*), the circular surface of the pile should be accounted on the equation. In the case of buried pipe, the uplift resistance is equal to the weight of the lifted soil block plus the shear resistance along the two inclined failure surfaces. Calculation of the weight of the block is straightforward, but an assumption regarding the distribution of normal stress (and hence shear resistance) along the slip planes must be made. This failure mechanism is similar to the laterally loaded pile using the pre-bored ring system. It can be used to predict the behavior of laterally loaded pile using a pre-bored ring system. The ratio of the distance of ring from the center of the pile, *h*, and diameter of pile, *D* effect is similar to the effect of trapezoidal failure mechanism in a buried pipe.

It assumed that the normal stress on the sliding planes is equal to the in-situ value inferred from *K*, which is 1.5 times of K_0 (Awad-Allah and Yasufuku, 2013). It follows the condition using the small Mohr's circle shown in Figure 6-4. As a result, a realistic increase in vertical stress ahead of the pipe is permitted, as shown by the larger Mohr's circle representing the conditions at peak resistance. From the geometry of these two Mohr's circles, the peak mobilized shear stress along the slip surface can be calculated as:

$$\tau = \gamma' z \tan \varphi_{peak} \left[\frac{1+K}{2} - \frac{(1+K)\cos 2\psi}{2} \right] \tag{6-18}$$

By integrating along the slip planes and equating the vertical forces acting on the sliding block, the peak uplift resistance per unit length, *P*, is calculated as:

$$P = \gamma' hD \left(1 - \frac{\pi D}{8h} + F \frac{h}{D} \right) \tag{6-19}$$

$$F = \tan\psi + (\tan\varphi - \tan\psi)\left[\frac{1+K}{2} - \frac{(1+K)\cos 2\psi}{2}\right] \quad (6\text{-}20)$$

where:

P = lateral resistance per unit length of the pile

τ = side shear pressure

F = slip factor

γ' = unit weight of soil

D = pile diameter

z = depth of pressure point

D = pile diameter

h = distance from the center of the pile to the ring

ψ = soil dilatancy angle

φ = soil internal friction angle

K_0 = coefficient of lateral earth pressure at rest (1-sin φ)

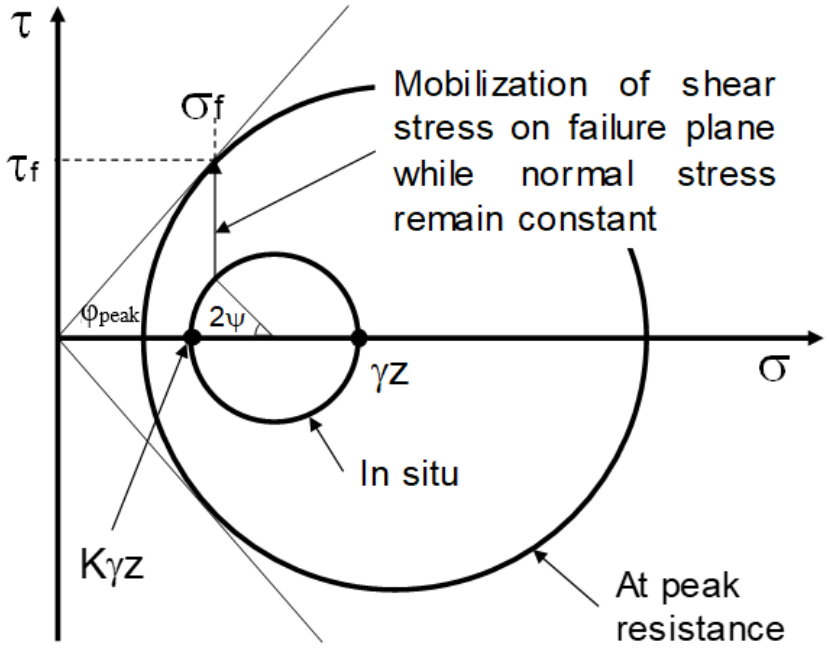

Figure 6-4 Mohr's circle in situ and peak resistance

6.5.2 Maximum Frontal Earth Pressure

The simplifying assumption that ultimate frontal soil resistance equal to three times of the value (K_p) is based on empirical evidence from comparisons between predicted and observed

ultimate loads made by Broms (Poulos and Davis, 1980). However, when the pile head moves laterally by displacement in a range of 20% of pile diameter, the effect of active earth pressure rear of the pile must be considered in the calculation. Figure 6-2 illustrates the proposed distribution of net lateral earth pressure distribution, taking into account the effect of active earth pressure. Consequently, maximum net earth pressure proposed by Awad-Allah and Yasufuku (2013), p_{max}, can be given by Equation 6-21.

$$p_{\max} = \left(K_p^2 - K_a\right)\gamma D \tag{6-21}$$

6.5.3 Maximum Side Shear Resistance

Maximum side shear resistance, τ_{max}, can be computed the same as the ultimate vertical shear resistance of piles estimated divided by three conditions: (1) rigid pile, (2) flexible pile without a pre-bored ring, and (3) flexible pile with a pre-bored ring with the following equation.

$$\tau_{\max} = \left(F\frac{h}{D}\right)\gamma D \tag{6-22}$$

For the case without a pre-bored ring, the ring diameter ratio (h/D) is equal to 1. The values of lateral coefficient (F) can be calculated using Equation 6-20. In this research, the value for K is $1.5K_0$.

So, the ultimate lateral soil pressure can be predicted by considering the maximum frontal earth pressure and maximum side shear pressure for $h/D \leq 2.5$ using the following equation.

$$p_u = \left(1-\frac{\pi D}{8h}\right)\left(K_p^2 - K_a\right)\gamma D + \left(\left(\tan\psi + \left(\tan\varphi - \tan\psi\right)\left[\frac{1+K}{2} - \frac{\left(1+K\right)\cos 2\psi}{2}\right]\right)\frac{h}{D}\right)\gamma D \tag{6-23}$$

where:

p_u = ultimate lateral soil pressure
D = pile diameter
h = distance from the center of the pile to the ring
K_p = coefficient of passive earth pressure
K_a = coefficient of active earth pressure
γ = unit weight of soil

ψ = soil dilatancy angle

φ = soil internal friction angle

K_0 = coefficient of lateral earth pressure at rest (1-sin φ)

Detail procedure for developing the proposed approach to estimate the ultimate lateral capacity of the pile foundation is illustrated in Figure 6-5.

6.6 COMPARISON BETWEEN PREDICTED AND MEASURED ULTIMATE LATERAL LOAD

Table 6-1 shows the proposed, and previous researchers closed-form equation models for predicting lateral soil pressure, p_u, as a comparison study. A comparison study is carried out to evaluate the accuracy of each method compared to the measured ultimate loads which are obtained from the experimental results case studies collected from other researchers.

Table 6-1 Predicting methods of lateral soil pressure on the pile

Method	Equation of p_u
Prasad and Chari (1999)	$p_u=10^{(1.3\tan\phi+0.3)}\gamma 0.6z$
Zhang et. al. (2002)	$p_u=\eta p_{max}+\zeta\tau_{max}$
Awad-Allah and Yasufuku (2013)	$p_u=\eta[(K_p^2-K_a)+\zeta K_s \tan\delta]\gamma B$
Proposed model	$p_u=[\eta (K_p^2-K_a)+\zeta F(h/D)]\gamma B$

6.6.1 Database and Case Studies from Previous Results

In this study, 27 case studies of laterally loaded pile tests are evaluated. Eight (8) of those tests were obtained from experimental tests conducted by the authors. Nineteen (19) tests were collected from similar laboratory pile lateral load-displacement tests carried out by other researchers. The database was selected on condition that the ultimate lateral load was measured at maximum lateral displacement less than 20% of pile diameter at pile head and pile still in an elastic condition so that comparison criterion can be unified. Table 6-2 show parameters of each case studies which have been carried out by the authors and previous researchers in laboratory test for laterally loaded pile in cohesionless soil.

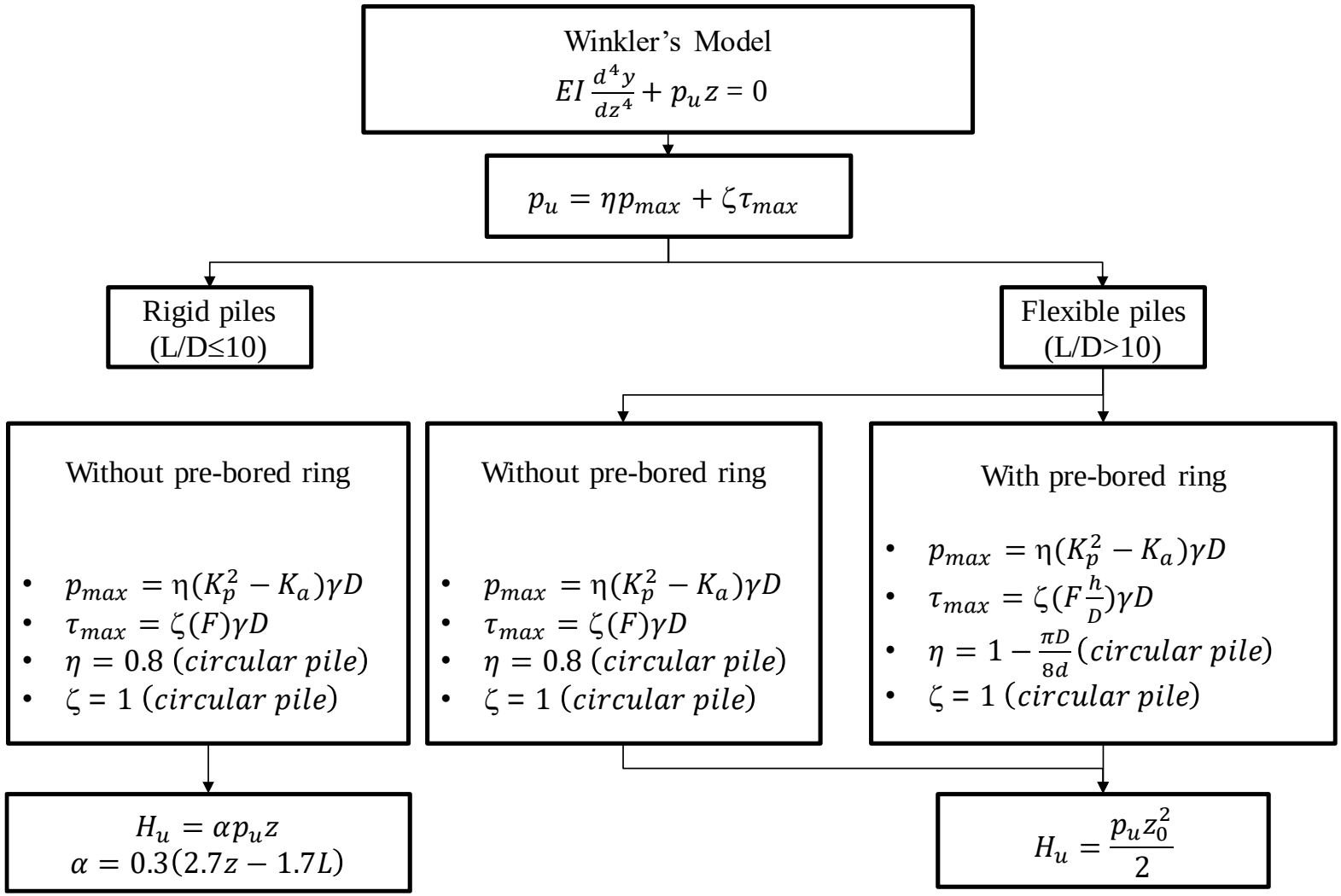

Figure 6-5 Flowchart of the proposed design procedure

Table 6-2 Comparison data for each case studies of the laterally loaded pile

	Case no.	D (m)	L (m)	L/D	γ (kN/m^3)	ϕ (°)
Adams and Radhakrishna (1973)	1	0.1016	0.4445	4.38	15.70	31.00
	2	0.1016	0.4445	4.38	17.60	45.00
	3	0.0762	0.4445	5.83	17.60	45.00
	4	0.0508	0.4445	8.75	17.60	45.00
Meyerhoff et. al. (1981)	5	0.0125	0.2000	16.00	15.20	50.00
	6	0.0125	0.2000	16.00	14.00	35.00
Chari and Meyerhoff (1983)	7	0.0750	0.9910	13.21	15.00	46.00
Joo (1985)	8	0.0730	0.7300	10.00	14.60	40.00
	9	0.1020	0.9000	8.82	14.60	40.00
Meyerhoff and Sastry (1985)	10	0.0740	0.9500	12.84	13.60	35.00
Prasad and Chari (1999)	11	0.1020	0.6120	6.00	16.50	35.00
	12	0.1020	0.6120	6.00	17.30	41.00
	13	0.1020	0.6120	6.00	18.30	45.50
Awad-Allah and Yasufuku (2013)	14	0.0150	0.1500	10.00	15.65	41.00
	15	0.0150	0.1500	10.00	14.45	36.50
	16	0.0150	0.3000	20.00	15.65	41.00
	17	0.0150	0.3000	20.00	14.45	36.50
	18	0.0150	0.4500	30.00	15.65	41.00
	19	0.0150	0.4500	30.00	14.45	36.50
Proposed	20	0.0150	0.4500	30.00	14.96	37.73
	21	0.0150	0.4500	30.00	14.96	37.73
	22	0.0150	0.4500	30.00	14.96	37.73
	23	0.0150	0.4500	30.00	13.93	35.20
	24	0.0150	0.4500	30.00	14.72	36.67
	25	0.0150	0.4500	30.00	15.21	39.59
	26	0.0150	0.4500	30.00	15.01	36.18
	27	0.0150	0.4500	30.00	14.13	37.73

6.6.2 Percentage of Error

The results of predicting the lateral capacity of the pile for all methods are shown in Table 6-3 in conjunction with the percentage of average error obtained from each method. In order to evaluate the results, the average error of the predictability is calculated to control the accuracy of the predicted methods. Percentage of average error obtained from each method of design can be calculated using Equation 6-24 and Equation 6-25.

$$error(\%) = \frac{(H_u)_p - (H_u)_m}{(H_u)_m} x100 \quad (6\text{-}24)$$

$$\text{Average of cumulative error} = \sqrt{\sum_{i=1}^{n} (error^2)} \quad (6\text{-}25)$$

where:

$(H_u)_p$ = ultimate predicted lateral pile capacity

$(H_u)_m$ = ultimate measured lateral pile capacity

The negative average error indicates that this method is under-predicting the values of ultimate lateral pile capacities, which means that it is a conservative method. On the other, the positive sign indicates that this method is over-predicting the values of ultimate lateral pile capacities, which means that it is an un-conservative method. So the proposed predicted method can be used as a design method for laterally loaded pile, which provide the lower value compared to experimental test.

Based on Table 6-3, it can be seen that the proposed closed-form solution can reduce average error percentages compared to values resulted from other methods. It can be noted that the distance of the ring to the pile on the side shear resistance, which is created at the maximum lateral movement of the pile head, can be represented using the proposed equation. The key parameter is the rotation point of each case. The rotation point for the rigid and flexible pile is different, and it also provides a different maximum pressure on the pile. The previous estimation methods are limited for the rigid pile conditions. Estimation of lateral pile resistance for both rigid and flexible pile can be represented using the proposed method.

Table 6-3 Comparison data for predicted and measured lateral pile capacity for each case studies

Authors	Case no.	$(H)_m$ (kN)	Proposed		Awad-Allah and Yasufuku (2013)		Zhang et. al. (2002)		Prasad and Chari (1999)	
			$(H_u)_p$ (kN)	error (%)	$(H_u)_p$ (kN)	error (%)	$(H_u)_p$ (kN)	error (%)	$(H_u)_p$ (kN)	error (%)
Adams and Radhakrishna (1973)	1	0.1520	0.1853	21.912	0.107	-29.333	0.128	-15.719	0.151	-0.802
	2	0.5400	0.7145	32.321	0.414	-23.299	0.483	-10.566	0.558	3.382
	3	0.4100	0.5359	30.707	0.311	-24.235	0.362	-11.656	0.419	2.122
	4	0.3400	0.3573	5.078	0.207	-39.091	0.241	-28.979	0.279	-17.902
Meyerhoff et. al. (1981)	5	0.0400	0.0186	-53.490	0.036	-9.395	0.036	-10.736	0.044	9.873
	6	0.0110	0.0042	-62.242	0.008	-26.445	0.008	-26.548	0.009	-15.505
Chari and Meyerhoff (1983)	7	2.0500	2.7923	36.211	3.068	49.649	3.101	51.256	3.614	76.281
Joo (1985)	8	0.7600	0.7188	-5.419	0.709	-6.744	0.752	-0.991	0.855	12.543
	9	1.4000	1.5266	9.045	1.358	-2.971	1.471	5.051	1.672	19.410
Meyerhoff and Sastry (1985)	10	1.3000	0.8420	-35.227	1.050	-19.243	1.048	-19.355	1.206	-7.232
Prasad and Chari (1999)	11	0.6200	0.5161	-16.752	0.501	-19.266	0.537	-13.342	0.618	-0.315
	12	1.0400	0.9159	-11.930	0.888	-14.589	0.945	-9.125	1.075	3.361
	13	1.7900	1.4851	-17.034	1.440	-19.539	1.528	-14.662	1.773	-0.972
Awad-Allah and Yasufuku (2013)	14	0.0190	0.0073	-61.319	0.004	-78.045	0.005	-74.250	0.006	-70.712
	15	0.0160	0.0046	-71.265	0.003	-83.839	0.003	-80.933	0.003	-78.195
	16	0.0290	0.0213	-26.542	0.024	-16.099	0.027	-8.078	0.030	4.552
	17	0.0250	0.0133	-46.695	0.015	-39.672	0.017	-33.512	0.019	-23.964

Table 6-3 Comparison data for predicted and measured lateral pile capacity for each case studies (continued)

Authors	Case no.	$(H)_m$ (kN)	$(H_u)_p$ (kN)	error (%)	$(H_u)_p$ (kN)	error (%)	$(H_u)_p$ (kN)	error (%)	$(H_u)_p$ (kN)	error (%)
Awad-Allah and Yasufuku (2013)	18	0.0410	0.0270	-34.240	0.064	55.965	0.068	65.914	0.077	88.710
	19	0.0280	0.0169	-39.764	0.040	41.562	0.042	51.487	0.049	73.241
Proposed	20	0.0206	0.0184	-10.610	0.047	128.429	0.050	142.549	0.057	176.425
	21	0.0214	0.0204	-4.780	0.047	120.044	0.050	133.645	0.057	166.277
	22	0.0217	0.0217	-0.209	0.047	116.356	0.050	129.729	0.057	161.814
	23	0.0197	0.0151	-23.093	0.035	79.112	0.038	91.030	0.043	119.555
	24	0.0201	0.0183	-9.246	0.042	109.736	0.045	123.078	0.051	154.976
	25	0.0248	0.0243	-1.839	0.056	127.413	0.060	140.879	0.068	173.825
	26	0.0243	0.0176	-27.325	0.041	70.017	0.044	80.987	0.050	107.208
	27	0.0219	0.0191	-12.948	0.044	102.457	0.047	114.971	0.054	144.996
Average of error (%)				-16.174		20.331		28.597		47.517
Average of $\sqrt{\sum_i^n (error^2)}$				32.634		67.317		73.024		89.863

6.7 STATISTICAL ANALYSIS

The statistical analysis data is carried out to evaluate the accuracy of the prediction method. The ratio between predicted and measured ultimate pile capacity, which is equal to $(H_u)_p/(H_u)_m$, is a key parameter in this analysis. An evaluation scheme using three criteria was considered for sorting the methods based on their accuracy, as follows:

1. The best fit line of $(H_u)_p/(H_u)_m$, with a coefficient of determination, r^2 (R_1).
2. Cumulative probability at 50% and 90% of $(H_u)_p/(H_u)_m$, (R_2).
3. Statistical parameter criterion for $(H_u)_p/(H_u)_m$, (R_3).

An overall rank, R, is defined as the average of total ranking values obtained from the three criteria ($R=R_1+R_2+R_3$). The lower the ranking index is, the better the performance of the method is, i.e., accuracy and predictability (Titi and Abu-Farasakh, 1999).

6.7.1 Best Fit Line Criterion (R_1)

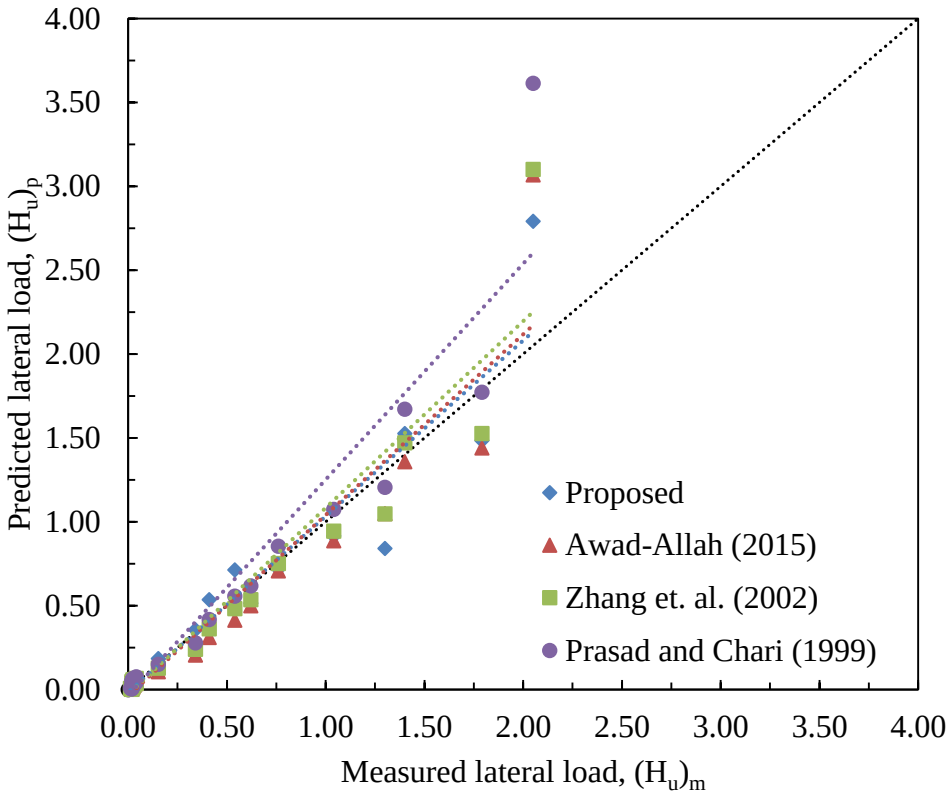

Figure 6-6 Correlation between measured and predicted the lateral capacity of piles

Table 6-4 Best fit calculation for lateral loading assessment

Estimation method	r^2	r	Best fit calculations	R
Proposed	0.9179	0.9581	y = 1.0487x - 0.0168	1
Awad-Allah and Yasufuku (2013)	0.8966	0.9469	y = 1.0767x - 0.0372	4
Zhang (2002)	0.9097	0.9538	y = 1.1126x - 0.0302	2
Prasad and Chari (1999)	0.9060	0.9518	y = 1.287x - 0.0366	3

Linear best fit using regression analysis was performed for each method, and the coefficient of determination (r^2) was determined. The best-predicted method is the method that has the corresponding coefficient of determination (r^2) close to 1. Figure 6-6 shows the best-fit line analysis for the measured and the predicted lateral loading for the experimental test results. Table 6-4 shows the best-fit equations with the coefficient of determination, r^2, of the experimental test results for all methods. All the methods result in an excellent coefficient of determination (r^2). The proposed method gives a best-fit line that is much closer to the line of 45°, and it comes in the first order. On the other hand, the method of Prasad and Chari (1999) provides the highest slope of the best-fit equations line, and its trend lines also are far from the line of 45°. It means that this method is over-predicting to estimate the values of ultimate lateral capacity.

6.7.2 Cumulative Probability Criterion (R_2)

The cumulative probability criterion is used to calculate the accuracy of the predicted methods to estimate the lateral pile capacity. The first step for this criterion is sorting the ratio of $(H_u)_p/(H_u)_m$ for each case in ascending order. The smallest value is given $i = 1$, and the largest one is given number $i = n$, where n is the number of the case studies. The cumulative probability value, CP_i, is given in Equation 6-26.

$$CP_i = \frac{i}{n+1} \tag{6-26}$$

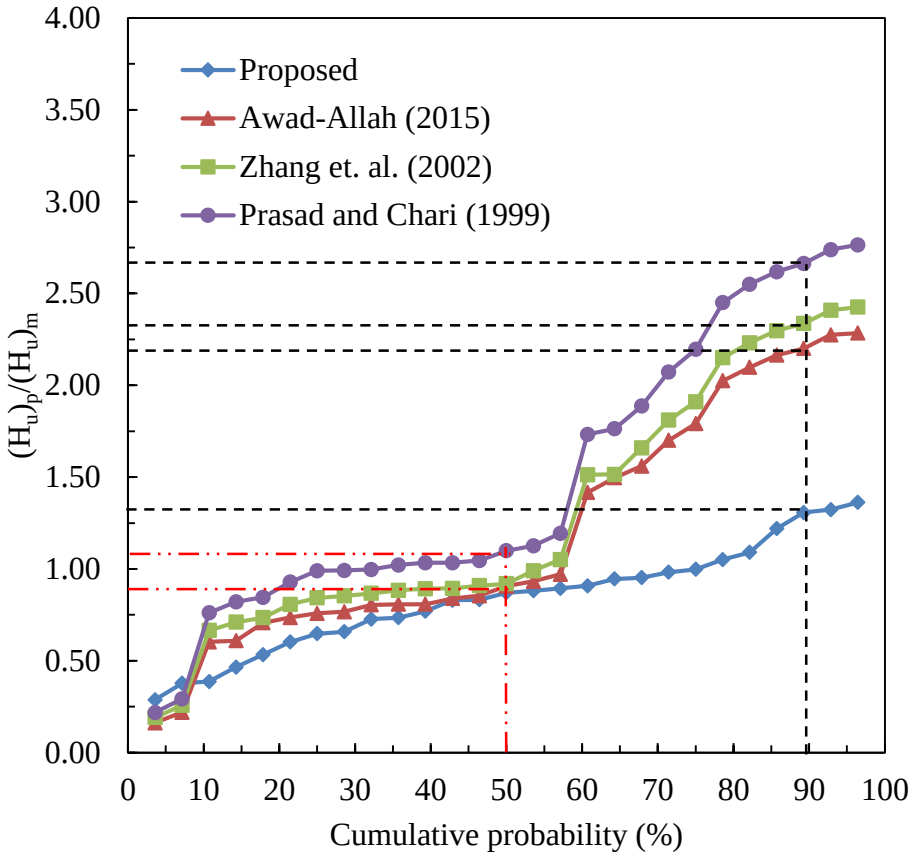

Figure 6-7 Cumulative probability analysis results for the estimation method

Table 6-5 Summary of cumulative probability analysis results for the all method

Estimation method	P_{50}	P_{90}	P_{90}-P_{50}	R
Proposed	0.87	1.31	0.44	1
Awad-Allah and Yasufuku (2013)	0.88	2.20	1.32	2
Zhang (2002)	0.92	2.34	1.42	3
Prasad and Chari (1999)	1.10	2.66	1.56	4

Figure 6-7 illustrates the cumulative probability curves for all methods of estimation of ultimate lateral static pile capacity, H_u. The values of $(H_u)p/(H_u)m$ at 50% and 90% cumulative probability are measured on the graph ($P50$ and $P90$). The predicting method, which gives $P50$ value that is closest to 1 and the lowest difference between $P50$ and $P90$

value (P_{90}-P_{50}) is considered the best method (Titi and Abu-Farasakh, 1999). Figure 6-7 illustrates the cumulative probability curves for all methods of estimation of ultimate lateral static pile capacity, H_u. Table 6-5 summarizes the results of P_{50} and P_{90} and ranking for all methods. It can be noticed that the proposed method provides the best result, based on the lowest value of (P_{90}-P_{50}). Other methods of estimation are ranked as follows: Awad-Allah and Yasufuku (2013) are in the second rank, Zhang et al. (2002) are in the third rank, and Prasad and Chari (1999) are in the last rank with the highest value of (P_{90}-P_{50}).

6.7.3 Statistical Parameter Criterion (R_3)

The accuracy of each method can be evaluated by measuring the mean value (μ) and standard deviation value (s) for the ratio of $(H_u)_p/(H_u)_m$. Calculation of coefficient of variation (COV), which is equal to s, divided by μ. The most accurate method provides the value of μ equal to 1, and COV is close to 0. The summarizes of s, μ, and COV values for each case are shown in Table 6-6. It can be seen the most accurate method is proposed method with mean value, μ of 0.838 and COV value of 0.345, and the second rank is Awad-Allah and Yasufuku (2013) with mean value, μ of 1.203 and COV value of 0.543, Zhang et al. (2005) with mean value μ of 1.286 and COV value of 0.532. The method of Prasad and Chari (1999) in the last rank with μ and COV values equal to 1.475 and 0.527, respectively.

Table 6-6 Statistical parameters for assessment of the predicted model

Estimation method	μ	s	COV	R
Proposed	0.838	0.289	0.345	1
Awad-Allah and Yasufuku (2013)	1.203	0.654	0.543	2
Zhang (2002)	1.286	0.654	0.532	3
Prasad and Chari (1999)	1.475	0.777	0.527	4

6.7.4 Overall Ranking Index (R)

Table 6-7 shows the summary of the final ranking for all methods evaluated using the statistical study. The proposed method for estimating the lateral static pile capacity, which considering the consideration the effect of net frontal earth pressure, side shear resistance of

soil around the pile, the pile slenderness and pre-bored ring effect due to lateral displacement of the pile, provides the lowest overall ranking index (R=3). On the other hand, Awad-Allah and Yasufuku (2013) and Zhang et al. (2005) are in the second-ranking with indexes of (R=8), and Prasad and Chari (1999) is the last rank (R=11).

Table 6-7 Summary of final ranking for the simplified model for predicting the lateral load

Estimation method	R_1	R_2	R_3	R_{total}	R
Proposed	1	1	1	3	1
Awad-Allah and Yasufuku (2013)	4	2	2	8	2
Zhang (2002)	2	3	3	8	2
Prasad and Chari (1999)	3	4	4	11	4

6.8 **SUMMARY**

In this Chapter, a simplified model for predicting the lateral response of pile foundations in a homogenous cohesionless soil describes by assuming a perfect plastic response of soil using differential equation based on the ultimate lateral strength mechanism. Comparison study between the proposed method and previous methods was evaluated to determine the best method for predicting the ultimate lateral pile capacity. Furthermore, the proposed approach is evaluated against the previous researcher's prediction method for ultimate lateral resistance of piles in cohesionless soil (e.g. Brinch Hansen, 1961; Broms 1964; Meyerhoff et. al. 1981; Petrasovits and Award, 1972; Prasad and Chari, 1999; Zhang et. al., 2002; Awad-Allah and Yasufuku, 2013). Besides, the average error percentage obtained from each method has been calculated.

1. The proposed closed-form solution can reduce average error percentages compared to values resulted from other methods. It can be noted that the distance of the ring to the pile on the side shear resistance, which is created at the maximum lateral movement of the pile head, can be represented using the proposed equation. The key parameter is the rotation point of each case. The rotation point for the rigid and flexible pile is different, and it also provides a different maximum pressure on the

pile. The previous estimation methods are limited for the rigid pile conditions. Estimation of lateral pile resistance for both rigid and flexible pile can be represented using the proposed method.

2. The proposed method for estimating the lateral static pile capacity, which considering the consideration the effect of net frontal earth pressure, side shear resistance of soil around the pile, the pile slenderness and pre-bored ring effect due to lateral displacement of the pile, provides the lowest overall ranking index (R=3). On the other hand, Awad-Allah and Yasufuku (2013) and Zhang et al. (2005) are in the second-ranking with indexes of (R=8), and Prasad and Chari (1999) is the last rank (R=11).
3. The proposed predicted method can be used as a design method for laterally loaded pile, which provide a lower value compared to the experimental test. Further evaluation of the rotation point and effect of eccentricity need to be considered to obtain more accurate predicted result.

6.9 **REFERENCES**

Awad-Allah, M.F., and Yasufuku, N. Comparative Study between the Methods Used for Estimating Ultimate Lateral Load of Piles in Sandy Soil. Proceedings of the 5th International Young Geotechnical Engineers' Conference, Paris, France., 2013, pp. 165-168.

Adams, J. I., and Radhakrishna, H. S. (1973): The lateral capacity of deep augured footings, Proc., 8th Int. Conf. Soil Mechanics Foundation Engineering, Vol. 2, Moscow, pp. 1–8.

Briaud, J.-L., and Smith, T. D. (1983): Using the pressuremeter curve to design laterally loaded piles, Proc., 15th Offshore Technology Conf., Houston, Paper No. 4501, pp. 495–502.

Brinch Hansen, J. (1961): The ultimate resistance of rigid piles against transversal forces, Bulletin No. 12, Danish Geotechnical Institute, Copenhagen, Denmark, pp. 5–9.

Broms, B. B. (1964): Lateral resistance piles on cohesionless soils. Journal of Soil Mechanics and Foundation Division, ASCE, (SM3), 123–156.

Chari, T. R., and Meyerhof, G. G. (1983): Ultimate capacity of single piles under inclined loads in sand, Can. Geotech. J., 20, pp. 849–854.

Joo, J. S. (1985): Behavior of large scale rigid model piles under inclined loads in sand, Ms Engineering thesis, Memorial Univ. of Newfoundland, St. John's, Newfoundland, Canada.

Meyerhof, G. G., Mathur, S. K., and Valsangkar, A. J. (1981): Lateral resistance and deflection of rigid wall and piles in layered soils, Can. Geotech. J., Vol. 18, pp.159–170.

Meyerhof, G. G., and Sastry, V. V. R. N. (1985): Bearing capacity of rigid piles under eccentric and inclined loads, Can. Geotech. J., Vol. 22, pp. 267–276.

Poulos, H. G., and Davis, E. H. (1980): Pile foundation analysis and design, Wiley, New York.

Prasad, Y. V. S. N., and Chari, T. R. (1999): Lateral capacity of model rigid piles in cohesionless soils, Soils Found., Vol. 39, No. 2, pp. 21–29.

Reese, L. C., Cox, W. R., and Koop, F. D. (1974): Analysis of laterally loaded piles in sand, Proc., 6th Offshore Technology Conf., Vol. 2, Houston, pp. 473–483.

Reese, L. C. (1977): Lateral loaded pile: program documentation, Int. Geotch. Eng. Div., ASCE, 103(GT4), pp. 287-305.

Zhang, L., Silva, F., Grismala, R. (2005): Ultimate lateral resistance to piles in cohesionless soils, Journal of Geotechnical and Geoenvironmental Engineering, Vol. 131, No. 1, pp. 78-83.

CHAPTER VII

CONCLUSIONS AND FUTURE WORKS

7.1 CONCLUSIONS

The main objective of this research is to investigate the influence of pre-bored ring and filler material on the pre-bored pile foundation system under cyclic lateral loading based on geotechnical point of view. In order to understand the fundamental mechanism of soil-structure interaction and pre-bored ring system related to laterally loaded piles, experimental test (1g model condition) and theoretical approaches has been carried out in this research. The main conclusion can be described as follows:

1. A small-scale lateral static and cyclic test setup (1g laboratory model) has been developed to evaluate the behavior of pre-bored pile foundation system which consists of testing box, LDVT, lateral loading servo cylinder, strain gauges, earth pressure sensors, and data acquisition system.
2. The pre-bored pile foundation system filled with filler material can reduce the stresses on pile foundation due to the lateral movement of the bridge superstructure. Filler material with low uniformity coefficient (uniform soil) and medium or high relative density provide a stable pile performance during the cyclic loading. So, it can maintain the lateral displacement due to thermal expansion on the integral bridge abutment foundation system. The effective diameter of the ring is recommended more than the plastic deformation area of the soil for a shallow depth of ring to separate the filler material inside the ring and ground soil.
3. The effect of particle diameter on filler material is not significant. It relatively provides a stable bending moment during the cyclic loading for all cases with a different particle diameter of filler material. So, the utilization of sandy soil or gravel with uniform particle distribution for filler material in this system are possible. Moreover, utilization of filler material with high permeability coefficient (e.g., uniformly graded of gravel) is recommended to avoid the effect of liquefaction inside the pre-bored ring system.

4. Attachment of pre-bored ring with different diameter changes the failure pattern of soil on the pre-bored ring system due to lateral cyclic loading. Pre-bored ring with a diameter of less than 60 mm (4*D*) can reduce the total strain of soil and the failure diameter due to cyclic loading. However, if the pre-bored ring diameter is too small, it affected the long term condition of the pre-bored ring and filler material properties which associated with the skin friction of soil and ring. This condition can be affected by the performance of the pre-bored ring foundation system because the pre-bored ring might be removed in case of shallow ring depth and changes the properties of filler material.
5. The proposed simplified equation model can reduce average error percentages compared to values resulted from other methods. It can be noted that the distance of the ring to the pile on the side shear resistance, which is created at the maximum lateral movement of the pile head, can be represented using the proposed equation. The key parameter is the rotation point of each case. The rotation point for the rigid and flexible pile is different, and it also provides a different maximum pressure on the pile. The previous estimation methods are limited for the rigid pile conditions. Estimation of lateral pile resistance for both rigid and flexible pile can be represented using the proposed method. The advantages of this approach over the previous methods are that it considers the influence of:
    a. Pile geometry, including pile slenderness ratio (*L/D*) and rotation point (*z*).
    b. Effect of attachment of the pre-bored ring

7.2 **FUTURE WORKS**

This research presented has shed some lights on understanding and modeling the response of pre-bored pile foundation system by considering the soil-pile structure interaction during lateral loading; moreover, the objectives stated in Chapter 1 have been accomplished. However, additional detailed studies would be necessary to be done in the coming future. The following suggestions are provided for coming research on wind turbine pile foundations, and further development on the proposed models:

1. Influence of degree of saturation (S_r) in terms of the potential liquefaction occurrence around pre-bored pile foundation system due to cyclic lateral loading should be investigated. Degree of saturation of filler material inside the pre-bored ring might

induce the liquefaction potential, and attached filter material between the filler material and ground soil should be done in a cyclic loading scheme.

2. The load applied on the pile head in this research assume as a pinned head connection on the superstructure. The evaluation of the pinned head connection revealed a good agreement with the experimental and analytical results. A further experimental study using the fixed head connection on the pile is needed to generalize the model on the various connection type that can be applied by the bridge engineer.
3. The failure mechanism on the *x*-*z* direction has been established to describe the effect of pre-bored ring on laterally loaded pile foundation. Failure pattern on the *x*-*y* direction is needed to evaluate the displacement of filler material during the cyclic loading so that it can generalize the three-dimensional soil displacement due to cyclic lateral loading. Distribution of soil also can be measured in the *x*-*y* direction using the image analysis method.
4. Based on the results, if the pre-bored ring diameter is too small, it will affect in the long term condition of the pre-bored ring and filler material properties which associated with the skin friction of soil and ring. This condition can be affected by the performance of the pre-bored ring foundation system because the pre-bored ring might be removed in case of shallow ring depth and changes the properties of filler material. So, for further research, it can be developed the deep ring condition with a small diameter of the ring. In order to reduce the ring movement, the roughness of the ring surface can be increased by using a spiral ring surface to increase the interaction between ring and soil.